Understanding Hydrologic Alteration of Mediterranean-Climate Streams Using a Functional Flows Approach

By

NOELLE KATHLEEN PATTERSON
DISSERTATION

Submitted in partial satisfaction of the requirements for the degree of

DOCTOR OF PHILOSOPHY

in

Hydrologic Sciences

in the

OFFICE OF GRADUATE STUDIES

of the

UNIVERSITY OF CALIFORNIA

DAVIS

Approved:

Samuel Sandoval Solis, Chair

Belize A. Lane

Gregory B. Pasternack

Xiaoli Dong

Committee in Charge

2022

Abstract

Rivers have a fundamental importance to human civilization and are considered the primary source of renewable freshwater supply for societies worldwide. Human prosperity depends heavily on surface water and the groundwater it replenishes, but this growth often comes with a heavy cost to river health. Rivers worldwide and particularly in arid climates have experienced profound levels of human alterations, particularly through damming, that affect flow patterns, channel form, and species composition. Functional flows theory offers a promising method to characterize ecologically-important aspects of flow and how changes to flow patterns may affect ecosystems. The goal of this dissertation is to quantify and understand hydrologic alteration of rivers and its ecological effects using a functional flows approach. This work validates functional flows as an effective strategy for ecological streamflow analysis with evidence that they can be used to differentiate California's natural flow regimes, quantify streamflow response to climate change, and reveal the links between flow management and riparian forest health. Chapter 1 describes creation of a novel tool to quantify functional flow metrics for Mediterranean streamflow patterns using time series analysis methods. Chapter 2 characterizes climate-caused changes to streamflow in snowmelt-dependent regions of California, highlighting the importance of both temperature increase on functional flow change and human emissions levels on potential outcomes. Chapter 3 describes an ecohydrologic field

study linking riparian cottonwood growth to functional flows and offers promising evidence that environmental flows can lead to measurable improvement in riparian forest productivity. This dissertation advances river science through the creation and implementation of new tools that can be used to balance human and ecological needs of streamflow.

Acknowledgements

This dissertation would not have been possible without all the people who have supported me in my endeavors over the past five years. Writing this dissertation did not happen in a vacuum, but instead involved contributions from so many mentors, colleagues, classmates, and friends. I thank you all for your contributions large and small.

Sam, I am so grateful for your generous mentoring, guidance, and friendship. You never once doubted me, but have given me the confidence to believe in myself. Your wonderful lab community and productive collaborations are a testament to your compassion and dedication. Thank you for nurturing me to become a better scientist and person.

Belle, I have learned so much from you since moving into your old desk space five years ago when I entered grad school. You have been a role model to aspire to, and with your guidance I have become a more thoughtful and capable scientist. The dedication and effort you give your students is impressive and I am proud to be your first graduating PhD.

Sam and Belle, you make a great team. I credit you both for everything I have learned and accomplished along this journey.

I am grateful to my Dissertation and Qualifying Exam committee members for their guidance and expertise. Thank you Greg Pasternack, Xiaoli Dong, and Mark Grismer, for the helpful and motivating discussions I've shared with each of you along the way. Thank you also to my coauthors Sarah Yarnell and Geeta Persad for being great collaborators and role models.

Building up a dendrochronology field project from scratch was aided tremendously by the generous guidance of several mentors. I am so grateful to Stew Rood for answering my cold call several years ago that opened the door to my scientific exploration of the Truckee River. It

has been such a privilege to receive guidance from you on this wonderful study system. To Adam Csank I owe a mountain of gratitude for freely offering dendrochronology equipment, laboratory space, and expert guidance. I am humbled by your kindness and I hope I can someday pay it forward. To Kameron Morgan, Aaron Bill, and the great staff at Pyramid Lake Paiute Tribe Natural Resources, I am incredibly grateful for your partnership, knowledge, and companionship in the field. I thank the good folks at the Nature Conservancy including Chris Sega, Laurel Saito, Sarah Byer, and Mickey Hazelwood for your partnership and for all you do in the Truckee River watershed.

To the fantastic folks in the Water Management Lab and the Hydrologic Sciences Graduate Group, I thank you all for the camaraderie, support, and impressive shared knowledge. Special thanks to Hervé Guillon for sharing wisdom of all kinds. Another special thanks to Claire Kouba for your relentless advocacy for your fellow students and the extremely cathartic conversations we've shared. Many more thanks go particularly to Pablo Ortiz-Partida, Laura Garza, Alyssa DeVincentis, Sloane Rice, Helaine Berris, Ramon Saiz, Grace Gomez Quiroga, Paulina Rojas, Sam Winter, Jason Weiner, Rich Pauloo, Steve Maples, Katie Markovich, Marina Mautner, Nusrat Molla, Paige Kouba, Kira Waldman, and the exemplary volunteers of UC Davis GOALS.

A special shout-out and thank you goes to the "Reno crew" for the overflowing friendship, community, and great many adventures we've shared over the past three years. Thank you especially to Marlene and Simon for showing me what it means to have friends like family.

To my family, I am so grateful for a lifetime of support. And to Leo, my partner in life, you are my everything. Thank you for the love and support that made this journey possible.

Table of Contents

List of Figures

List of Tables

Introduction

Background and Motivation

Rivers act as arteries of the landscape, sustaining freshwater-dependent ecosystems and many scales of geomorphic work as they transport water and sediment from headwater slopes to oceans and sinks. Riparian and instream habitats support high diversity and provide many ecosystem services, such as water supply, nutrient cycling, recreation, and maintenance of floodplain water tables (Postel and Richter 2003). Rivers also have a fundamental importance to human civilization and culture, and are considered the primary source of renewable freshwater supply for societies worldwide (UNESCO 2009; Vorosmarty et al. 2005). Growth of populations and economies depends heavily on surface water and the groundwater it replenishes, but this growth often comes with a heavy cost to river health (Grill et al. 2019; Vorosmarty et al. 2010).

Rivers are naturally dynamic systems, integrating rainfall and snowmelt into a terrestrial response representing surface runoff characteristic of a watershed. In naturally variable climates such as Mediterranean climates with distinct wet and dry periods, rivers are especially dynamic (Kondolf, Podolak, and Grantham 2013). Freshwater species living in and around these dynamic systems are adapted to seasons of high and low streamflow through their behavior and life history (Gasith and Resh 1999; Lytle and Poff 2004). Human societies today and historically have sought to gain control over rivers, using technology such as dams, diversions, and canals to tame unpredictable rivers into conduits of stable flow (Grill et al. 2019; Postel and Richter 2003).

In many cases dams have allowed human populations to flourish and grow, by providing predictable access to surface water and controlling floods. As a result of intensive river damming over the past century, 60% of the world's large rivers are now dammed (Grill et al. 2019). Consequently, the effects of river impoundments have been felt at a global scale. Des (2012) estimates that the influence of dams is large enough to significantly influence global sediment budgets by the trapping of sediment behind dams. Increasingly, free-flowing rivers are a threatened component of the landscape, found most abundantly in high-elevation headwaters regions with low human populations.

The ecological effects of altering natural flow regimes are widespread (S. E. Bunn and Arthington 2002; Palmer and Ruhi 2019; Vorosmarty et al. 2010). More than 50% of the world's rivers are reported to have suffered declines in fish biodiversity, with much of this damage concentrated in temperate climate rivers (Su et al. 2021). Riparian forests support high biodiversity, but their reliance on natural flow patterns has caused significant decline of riparian ecosystems (Shafroth et al. 2017). Apart from disruption of flow patterns, dams also create disturbances in sediment and chemical regimes, which come at a high cost to freshwater biodiversity. In the U.S. and Australia for example, cold outflows from the bottom of dams introduce water at temperatures below the preferred threshold of native fish, favoring the proliferation of invasive fish species (Sherman et al. 2007; Zarri et al. 2019). The physical barrier of a dam also prevents passage, disrupting fish spawning and survival. Even where fish passage facilities are constructed, fish fitness may be reduced following passage over dams (Burnett et al. 2017).

Rivers are vastly complex systems integrating water chemistry, sediment fluxes, hydraulics, nutrient cycling, biotic interactions, and other processes (N Leroy Poff and Ward

1990; Wohl et al. 2015). While streamflow analysis alone cannot guarantee understanding of all these facets of a river, it serves well as a controlling variable of river processes (Poff et al. 1997). Changes to natural streamflow patterns are often associated with alteration of these other processes (Ahearn et al. 2004; Yarnell et al. 2015). Much like the pulse of a living organism, the flowing pulse of a stream can indicate the well-being of its component parts.

Functional flows theory offers a promising method to characterize ecologically-important aspects of flow and how changes to these patterns may affect ecosystems. Functional flows refer to sub-annual aspects of the flow regime that support key ecological, geomorphic, or biogeochemical processes in river systems (Escobar-Arias and Pasternack 2010; Yarnell et al. 2015). For rainfall-snowmelt flow regimes typical of California, five functional flow components have been identified that each provide distinct ecological functions, further described in the following chapters (Yarnell et al. 2020). These functional flows can be quantified with metrics describing the magnitude, timing, duration, and rate of change of each functional flow component (Poff et al. 1997). Functional flows can serve as the building blocks of an environmental flows program since they target aspects of flow most critical for ecosystem needs, which can prioritize limited flow in impacted basins. Functional flows are currently being used to guide environmental flow efforts across the state of California (Carlisle et al. 2017) and in the Rio Grande Basin of the southwestern U.S. The three studies in this dissertation rest on the concept of functional flows, and using them to understand alterations to natural flow regimes.

The ability of societies to thrive in the next century hinges on effective management of water resources in a changing world. Climate change has been associated with increasingly variable weather, resulting in less secure surface water resources in some regions such as the Western U.S. (Dettinger 2016). Warming temperatures cause a higher fraction of precipitation to

fall as rain instead of snow, reducing the amount of slow-releasing snowmelt historically relied on in regions such as California or the Front Range in Colorado (Lundquist et al. 2009; Pepin et al. 2015). On top of this, human population pressures already strain water resources in many parts of the world (Donnenfeld et al. 2018, Martinez et al. 2015, Ortiz-Partida et al. 2019). Effective solutions in water resources must consider river management strategies that preserve essential ecological functioning in the context of human need and climate change.

Research Objectives

The goal of this dissertation is to quantify and understand hydrologic alteration of rivers and its ecologic effects by characterizing streamflow, using a functional flows approach. The dissertation is organized into three chapters of research, addressing different angles of the overarching research objective. Each chapter stands alone as an independent study, so that each chapter includes a separate abstract, introduction, methodology, results, discussion, and conclusion.

Chapter 1 describes creation of a novel tool to quantify functional flow metrics for Mediterranean streamflow patterns using time series analysis methods of iterative smoothing, feature detection, and windowing. This tool is then tested using highly variable natural flow regimes of California, U.S., along with a quantitative assessment of error. An important contribution of this work is the ability to identify the timing of seasonal components of flow unique to each water year in a time series, an ecologically-important yet previously overlooked component of streamflow analysis. The following two chapters use the tool developed in Chapter

1 to perform state-of-the-art time series analysis on streamflow, with particular focus on climate change and ecological response to streamflow.

Chapter 2 of this dissertation seeks to characterize climate-caused changes in streamflow in snowmelt-dependent regions of California, using functional flows to quantify change. Climate change will compound water resources challenges in the western U.S., where freshwater ecosystems are already strained due to human pressure (Dettinger 2016), making this research subject especially timely.

Chapter 3 describes an ecohydrologic field study linking riparian cottonwood growth to functional flows, with a particular emphasis on streamflow alterations caused by river diversions. A fundamental assumption of functional flows theory is that the target functional flow metrics have real links to aquatic ecosystem functioning. Chapter 3 helps confirm these flow-ecology relationships while revealing the response of cottonwood forests to streamflow in a river system with a legacy of heavy management.

In summary, this dissertation tackles applied river science through creation of a functional flows analysis tool, followed by applications related to climate change and ecohydrology. Throughout this research is a recognition of both human and ecological needs of surface water, and the balance that must be achieved to meet both. It is a grand challenge, and this dissertation advances progress towards this goal through the creation and implementation of new tools for quantitative river science.

Chapter 1

A hydrologic feature detection algorithm to quantify seasonal components of flow regimes[1]

1.1 Abstract

Seasonal flow transitions between wet and dry conditions are a primary control on river conditions, including biogeochemical processes and aquatic life-history strategies. In regions like California with highly seasonal flow patterns and immense interannual variability, a rigorous

[1] This chapter has been published: Patterson, N. K., Lane, B. A., Sandoval-Solis, S., Pasternack, G. B., Yarnell, S. M., & Qiu, Y. (2020). A hydrologic feature detection algorithm to quantify seasonal components of flow regimes. *Journal of Hydrology*, *585*, 1–12. https://doi.org/10.1016/j.jhydrol.2020.124787

approach is needed to accurately identify and quantify seasonal flow transitions from the annual flow regime. Drawing on signal processing theory, this study develops a transferable approach to detect the timing of seasonal flow transitions from daily streamflow time series using an iterative smoothing, feature detection, and windowing methodology. The approach is shown to accurately identify and characterize seasonal flows across highly variable natural flow regimes in California. A quantitative error assessment validated the accuracy of the approach, finding that inaccuracies in seasonal timing identification did not exceed 10%, with infrequent exceptions. Results for seasonal timing were also used to highlight the statistically distinct timing found across streams with varying climatic drivers in California. The proposed approach improves understanding of spatial and temporal trends in hydrologic processes and climate conditions across complex landscapes and informs environmental water management efforts by delineating timing of seasonal flows.

1.2 Introduction

Streams and rivers in semi-arid/Mediterranean climates are physically, chemically, and biologically driven by predictable, seasonal periods of wet and dry conditions over an annual cycle (Gasith and Resh, 1999). Seasonal flow regimes support predictable river processes such as disturbance regimes (Rood et al. 2005), seasonal habitat provision (Aadland 1993; Booker and Acreman 2007; Jacobson 2013), and native species life-history cues (Yarnell et al., 2010). While streamflow characteristics including magnitude, duration, frequency, and rate of change are useful for describing components of the flow regime (Poff et al., 1997), the timing of seasonal flow transitions within the annual flow regime is particularly important for understanding

seasonally-adapted ecological processes such as migration, spawning, or vegetation recruitment (Cambray 1991; Greet, Webb, and Cousens 2011; N. Leroy Poff and Zimmerman 2010). It is critical to identify these distinct wet and dry conditions and when they occur across different flow regimes to improve understanding of physical climate and watershed controls on these seasonal transitions and their sensitivity to change.

Numerical descriptors of the flow regime, known as flow metrics, are routinely quantified from daily streamflow time series to link streamflow patterns to river processes (Buttle 2011; N. LeRoy Poff and Ward 1989) and biological response (Mazor et al. 2017; Olden and Poff 2003). Existing flow metrics used to identify and quantify the timing of seasonal flow transitions are limited, especially across large regions and in hydrologically variable settings. These measurements of timing are often simplified by calculating flow metrics within predetermined timing windows instead of identifying the occurrence of seasonal transitions and key events based on annual flow patterns. The Hydroecological Integrity Assessment Process (Henriksen et al. 2006) and the Indicators of Hydrologic Alteration (Richter et al. 1996) incorporate timing through calculations such as monthly average flows or the date of annual minimum and maximum flow. However, in variable flow regimes such as flashy rain-sourced streams, the timing of seasonal flow transitions varies significantly between water years and hydroclimatic settings (Lane et al., 2018). This wide inter-annual variability suggests that metrics describing a particular aspect of seasonal flow, such as dry season flow magnitude, cannot be accurately quantified based on the same months in each water year. Calculation of the annual maximum or minimum similarly may oversimplify understanding of seasonal flow components, because these calculations do not account for annual or seasonal patterns of flow or events other than the most extreme conditions (Déry et al. 2009).

To better quantify flow regimes based on variable seasonal patterns, signal processing techniques can be used to identify sub-annual hydrologic patterns from daily flow time series. Signal processing theory provides well-established techniques, such as data smoothing, peak detection, and time windowing, that have been applied in hydrology (Kusche et al. 2009; Mann 2004) and can be used to detect features from a time series of daily streamflow data. Time series smoothing is used to enhance certain frequencies (i.e., the signal) while attenuating others (i.e., the noise), and many smoothing techniques are available such as moving average, exponential moving average, empirical mode decomposition, regression smoothing (e.g. LOESS, (Cleaveland and Loader 1996)), wavelet, and splines (Janert 2010). Smoothing functions generate fitted curves to time series data that emphasize different frequency signals depending on the function and level of smoothing (Pollock 1999). Feature detection is used to extract peaks or valleys of interest from the smoothed data and can depend on attributes such as magnitude or slope (Schneider 2011; Scholkmann, Boss, and Wolf 2012). Dynamic windowing around a detected feature constrains further analysis to a particular period of interest and allows for increased resolution of subsequent analysis (Palshikar 2009).

In previous work, signal processing techniques have been applied to hydrologic time series for applications such as detecting long-term trends (Letcher et al. 2001), modeling hydrologic processes (Zhang et al. 2016), and predicting future trends (Adamowski and Sun 2010; Cannas et al. 2006). Common techniques such as harmonic analysis using Fourier or wavelet transform methods can be effective in analyzing hydrologic time series characteristics, such as periodicity, trends, coherence and cross-phase among deriving and response variables, or complexity determined by wavelet entropy (Pasternack and Hinnov 2003; Sang 2013). Additionally, many techniques have been developed to identify baseflow recession (Hall 1968);

recent attempts include identifying a consecutive number of days of negative slope in the hydrograph (Bart and Hope 2014), combining requirements of negative slope with a percentile-based magnitude threshold (Sawaske and Freyberg 2014), or automatic identification of recession curves based on parameters balancing accuracy and coverage (Smith and Schwartz 2017). While some methods share similarities with components of the proposed method, to the authors' knowledge there has not yet been a method developed to automatically isolate and quantify all major seasonal flow transitions from annual streamflow time series.

To identify ecologically significant flow transitions from the annual hydrograph, this study applied signal processing methods to identify functional flows found in the highly seasonal Mediterranean streams of California, USA. Functional flows refer to sub-annual aspects of the flow regime that support key ecological, geomorphic or biogeochemical processes in riverine systems (Escobar-Arias and Pasternack, 2010, Yarnell et al., 2015). Yarnell et al. (2015) aggregated flow ecology literature to identify four functional flow components relevant to Mediterranean streams with a distinct wet and dry season: wet-season initiation flows, peak magnitude flows, spring recession flows, and dry-season low flows. Building on those efforts and more recent work highlighting key functional flows specific to California (Yarnell et al., 2020), this study identifies the timing of four functional flow components applicable to California's natural streamflow regimes: fall pulse flow, wet season flow (encompassing both wet season baseflow and peak flow conditions), spring recession, and dry season baseflow (Figure 1-1). Once the timings of functional flow transitions are identified from the annual hydrograph, each functional flow component can be further quantified using additional flow metrics such as magnitude, timing, frequency, duration, or rate of change, and can be used to design functional flow regimes in managed river systems (Yarnell et al., 2020).

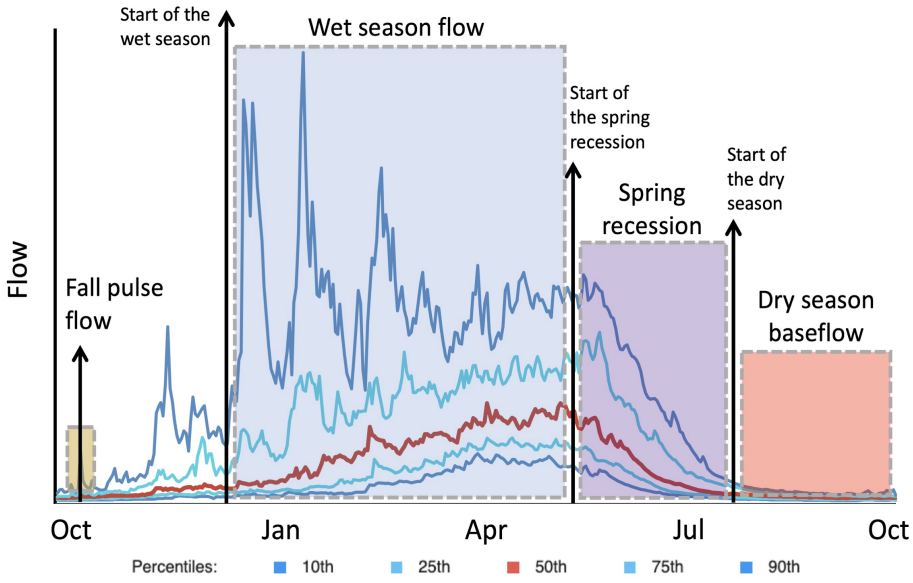

Figure 1-1. Identification of the start timing of four functional flows identified for California (Yarnell et al., 2020) using the proposed signal processing algorithm. The timing of flow transitions identified by the algorithm are marked with arrows. Hydrographs indicate the 10th, 25th, 50th, 75th, and 90th percentiles of flow in a mixed rain-snow river system (modified from Yarnell et al., 2020). A water year in California is defined as October 1 to September 30.

Drawing on signal processing theory, this study develops an algorithm in the open-source Python programming language to calculate the timing of seasonal flow transitions from daily flow time series, allowing for improved characterization of seasonal flows. This research addresses the following questions: (1) is it possible to automatically identify timing of seasonal streamflow components from annual hydrographs, and if so what is the level of error?; and (2) does the timing of seasonal flow components calculated through this study reveal distinctions among streams with varying climatic drivers? Using data from the highly seasonal streams of California

as a testbed, this study assesses the accuracy and limitations of the algorithm for quantifying functional flows across a wide range of natural flow regimes and climate conditions, including flow regimes exhibiting snowmelt, rain, or mixed rain and snowmelt signatures. To further achieve confidence in the results, algorithm outputs are analyzed in the context of California hydrology and tested for the extent that results align with expectations for regional hydrologic regimes.

1.3 Methods

The study design describes development, calibration, and performance assessment of the algorithm for detecting the timing of functional flow transitions from daily streamflow time series, with algorithm steps summarized in Figure 1-4. Six general steps of the SFDA use data smoothing, windowing, and feature detection to identify seasonal flow transitions from daily streamflow data.

1.3.1 Study Region

California has a Mediterranean climate with pronounced wet and dry seasons, as well as high interannual variability and spatial heterogeneity (Dettinger et al. 2011; Liu et al. 2018) . Much of this variability stems from California's wide latitudinal extent (800 km) and physiographic diversity, with multiple mountain ranges and valleys of different sizes, shapes, and relief (Abatzoglou, Redmond, and Edwards 2009; Ladochy, Medina, and Patzert 2007). California rainfall is characterized by the capability of a limited number of high intensity storm events to contribute to the majority of annual precipitation; Dettinger et al. (2011) found that 20–

50% of California's long-term rainfall average derives from these high precipitation storm events. California's rivers and streams reflect the state's climatic and physiographic diversity, ranging from small, intermittent streams in the southwest deserts to larger snowmelt-fed rivers draining the western slopes of the Sierra Nevada mountain range (Lane et al. 2018; Mount 1995).

For this study, nine natural hydrologic classes previously identified for California by Lane et al. (2018) were aggregated into three dominant stream types recognized throughout the state (Mount, 1995): snowmelt-, rainfall-, and mixed snowmelt and rain-sourced streams (Figure 1-2). Snowmelt-sourced flow regimes are largely controlled by the timing and rate of snowmelt, which are driven by seasonal patterns of precipitation and temperature. Rain-sourced flow regimes are controlled by the intensity of winter rainfall and characteristics of individual storm events. Mixed-source streams experience both rain-driven flows in the winter and a snowmelt pulse in the spring, or they occur in large drainages that receive both snowmelt and rainfall contributions from upstream.

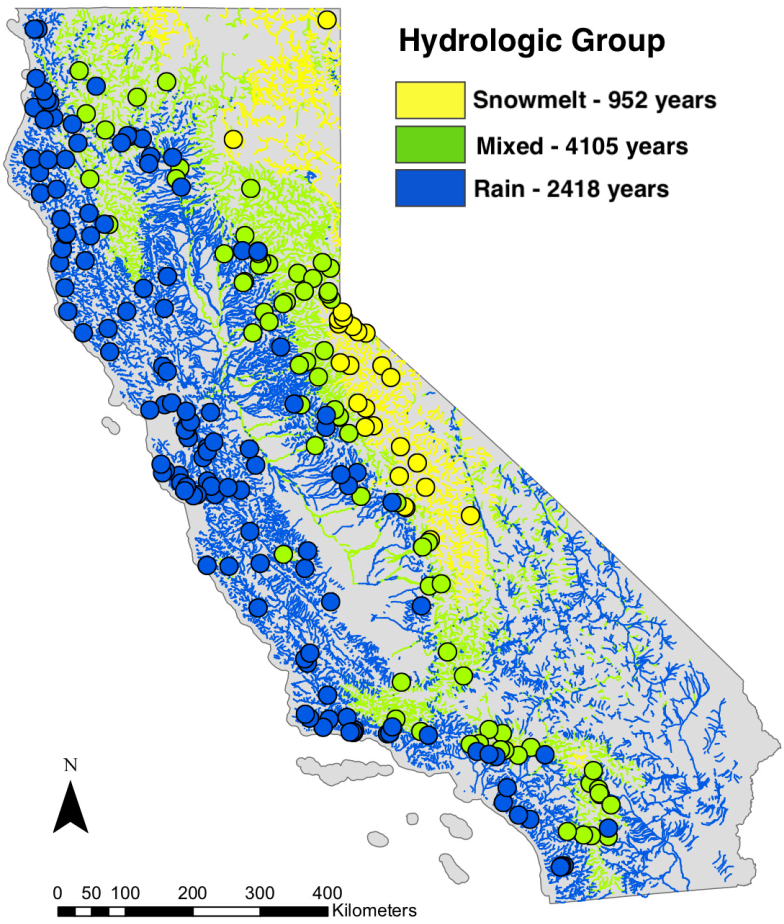

Figure 1-2. The three dominant stream types in California based on aggregated natural hydrologic classes developed by Lane et al. (2018): snowmelt (yellow), mixed snow and rain (green), and rain (blue). Reference streamflow gages used in this study are shown as circles, and the number of total water years of data in each stream type are shown. (For interpretation of the references to colour in this figure legend, the reader is referred to the web version of this article.)

1.3.2 Data

Streamflow data used for this analysis come from 223 gage stations with unimpaired or naturalized daily streamflow records in California (refer to Kennard et al. (2010) for definitions of unimpaired and naturalized streamflow) (Figure 1-2). Unimpaired gage data was sourced from

the dataset compiled by Zimmerman et al. (2017), who followed a 3-step protocol to obtain unimpaired daily streamflow. Their process designated gage stations as unimpaired based on: (1) designation as a "least disturbed" site from a U.S. Geological Survey database of watershed attributes (Falcone et al. 2010) (2) status of unimpairment based on annual gage station reports and appearance of natural conditions from satellite imagery, and (3) historical flow records that pre-date anthropogenic disturbance such as dams and urbanization. Seven gages with simulated unimpaired (i.e., naturalized) daily streamflow data were also added to the dataset to cover the Central Valley region of California (CDWR 2007), which was otherwise poorly represented by unimpaired gage stations. A final screening of the annual hydrographs of the resulting dataset was performed, and several gages were removed from the analysis that had flow patterns appearing irregular, impaired, or too low to exhibit seasonal patterns. The resulting dataset of 223 reference gages includes periods of record as early as 1891 and as recent as 2015, with an average period of record of 34 years and a range of 6 to 65 years.

1.3.3 Seasonal flow detection algorithm development

The following sections provide the theory and rationale for the Seasonal Flow Detection Algorithm (SFDA), explain the signal processing methods applied, and describe individual calculation steps. Additional description of signal processing methods is described in the Supplemental Materials.

1.3.3.1 Data Smoothing

Data smoothing is a type of filtering in which low-frequency components are retained while high-frequency components are attenuated, enabling detection of features of interest at different frequencies or time-scales(Press and Teukolsky 1990) . Common finite-difference smoothing techniques include simple running averages, weighted moving averages, and exponential filters (Janert, 2010). In this study, a Gaussian weighted moving average filter was used to generate a smoothed time series using the function gaussian_filter1d from the SciPy Image Processing package (Verveer 2003) in Python. This smoothing method was selected for its ability to retain local maxima in the output function, while avoiding abrupt distortions in the filtered data. The Gaussian filter sets the weighting factors of the smoothing window w_j according to a Gaussian normal distribution

$$f(x,\sigma) = \frac{1}{\sqrt{2\pi\sigma^2}}\, exp\left(-\frac{1}{2}\left(\frac{x}{\sigma}\right)^2\right) \qquad [1]$$

such that any new streamflow observation that enters the smoothing window is only gradually added to the moving average and then gradually removed. The standard deviation of the Gaussian function (σ) dictates the width of the distribution and consequently the degree of smoothing applied. In this study, low and high levels of streamflow data smoothing were associated with $\sigma < 5$ and $\sigma > 8$, respectively. For example, a daily streamflow time series smoothed with a high standard deviation Gaussian filter ($\sigma = 12$, Figure 1-3) will dampen daily to weekly hydrologic variability while preserving major seasonal patterns. Alternatively, a low standard deviation Gaussian filter ($\sigma = 4$, Figure 1-3) will preserve storm events occurring on

weekly scales. High levels of smoothing are often applied first in the algorithm to identify coarse resolution temporal patterns such as the distinction between the annual wet and dry season, while removing the signal noise caused by individual storm events. Increasingly lower levels of smoothing are then applied to identify hydrologic features on finer temporal scales.

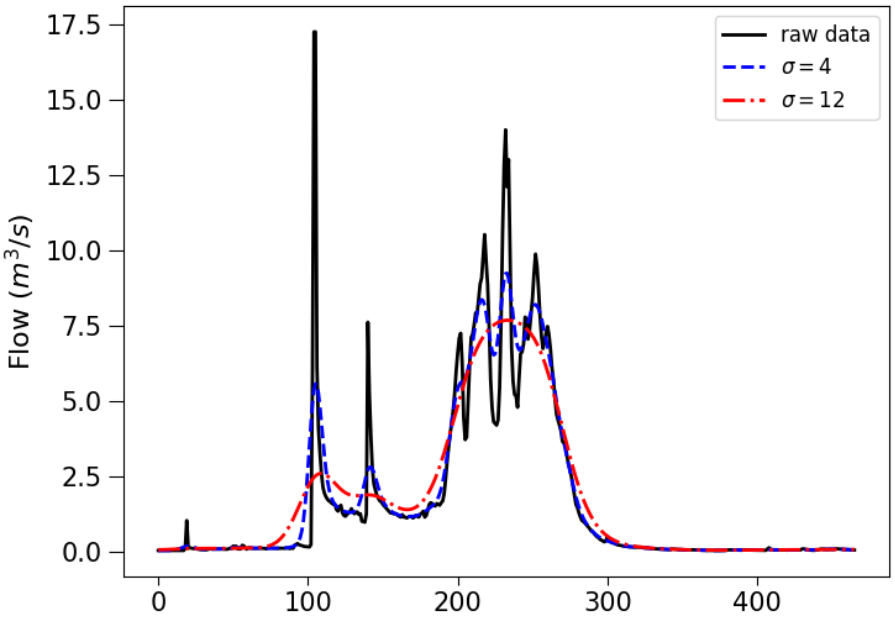

Figure 1-3. Daily streamflow time series (black) plotted for one water year (Oct. 1–Sept. 30) with two levels of filters using Gaussian weighted moving averages with different σ parameter values.

1.3.3.2 Splines

Splines are functions constructed from segments of polynomials between each time series observation that are constrained to be smooth at the junctions (Letcher et al. 2001). Splines, which are used in the SFDA for derivative estimation of smoothed streamflow, have been shown to generate nearly optimal derivative estimates of noisy data such as streamflow time series due to low interpolation error (Craven and Wahba 1979; Ragozin 1983; Thomas, Vogel, and

Famiglietti 2015). The SFDA employs a cubic spline function (three degrees of freedom) for derivative estimates, which is generally considered an optimal interpolation function for large time series (Carter and Signorino 2010; Kimball 1976; Wahba 1978). For further explanation on spline fitting, refer to Hastie and Tibshirani (1990). In this study, derivative estimation using a cubic spline was performed on smoothed and windowed streamflow time series using the one-dimensional univariate spline fitting function available from the SciPy library in Python (Jones, Oliphant, and Peterson 2001).

1.3.4 Seasonal flow detection algorithm (SFDA) general steps

The SFDA consists of six general steps used to detect seasonal flow transitions, although some applications may require either a subset of these steps or multiple iterations (Figure 1-4). Steps are applied to each water year in a dataset, which in California is defined as October 1 to September 30. Step 1 (Figure 1-4.a): A high standard deviation Gaussian filter (G1) is applied to the observed daily streamflow time series to detect dominant peaks, valleys, or trends in the annual hydrograph. Depending on the level of smoothing, different frequency patterns (e.g., seasonal, sub-seasonal) are attenuated or left intact. Step 2 (Figure 1-4.b): A hydrologic feature of interest is identified from G1, such as annual peak flow. Step 3 (Figure 1-4.b): A localized search window is set around the feature of interest to constrain subsequent analysis to a hydrologically relevant period (e.g., 30 days before and after the feature of interest). Step 4 (Figure 1-4.c): Within the search window, a low standard deviation Gaussian filter (G2) is applied to the observed daily time series to extract high-resolution hydrologic patterns (e.g., individual storm events). Step 5 (Figure 1-4.d): A spline curve is fitted to smoothed data G2, and

the derivative is taken to identify the slope of the hydrograph (S1′). Step 6 (Figure 1-4.d): A feature of interest is characterized in one of two ways: i) directly from G2 using relevant flow characteristics (i.e. magnitude), or ii) using the derivative of the spline curve (S1′) to detect peaks or valleys of interest based on slope or sign change (triangles represent peak features of interest, and the black diamond is the final selected feature).

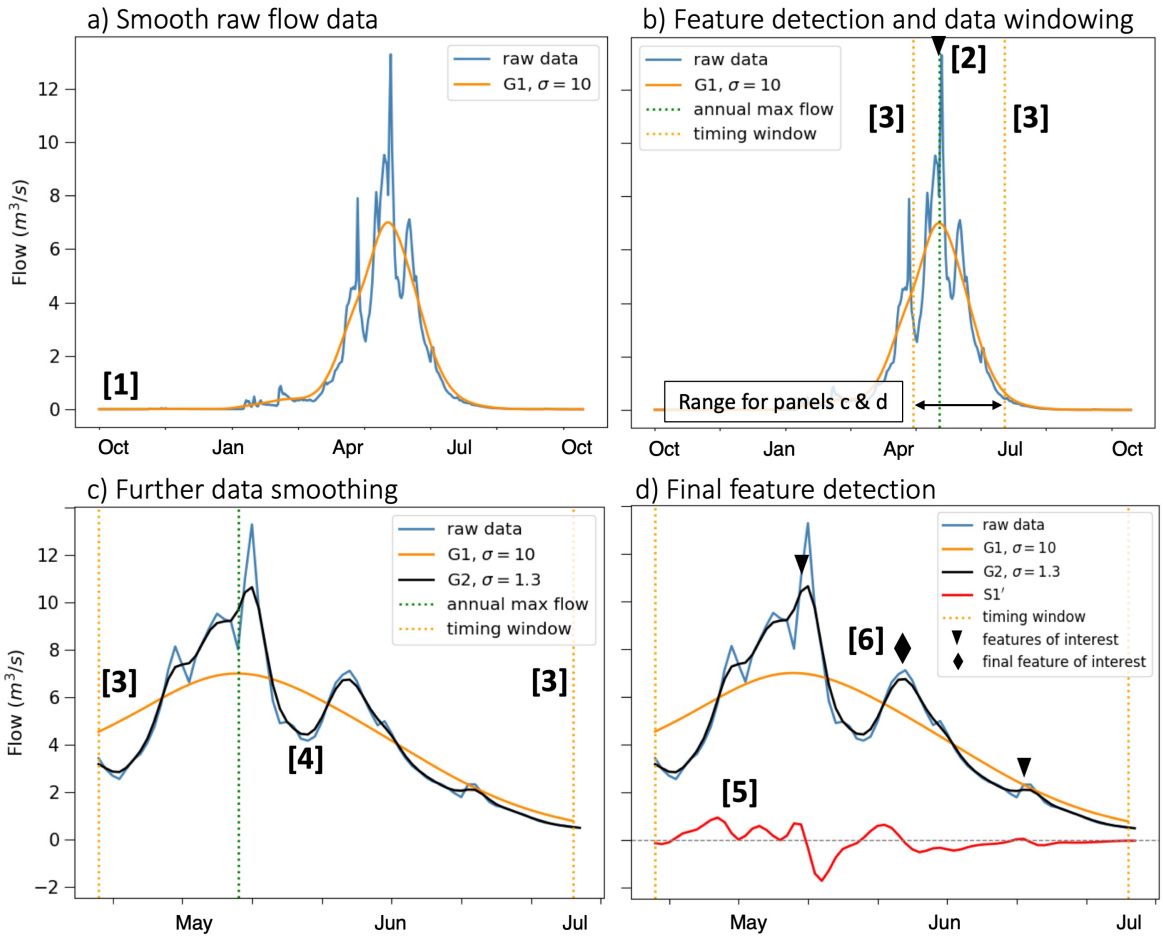

Figure 1-4. Six general steps of the SFDA use data smoothing, windowing, and feature detection to identify seasonal flow transitions from daily streamflow data.

The SFDA steps are iterative and can be repeated multiple times to consistently and accurately identify flow transitions across water years and stream types. For example, the calculation of spring recession requires three iterations of smoothing and feature detection, while the calculation for dry season start timing only requires one iteration. The parameter values (e.g., smoothing parameter σ, window size, or magnitude thresholds) can be adjusted to suit the needs of particular flow regimes or hydrologic features of interest. For example, in flashy rain-driven streams the start of the dry season is generally indicated by the last significant storm event of the

water year, which can be found using a low standard deviation Gaussian filter that closely fits daily streamflow data. Meanwhile, the start of the dry season in a snowmelt-driven stream may be better identified by the general trend of flow reduction representing catchment drainage, which is best represented with a high standard deviation Gaussian filter to capture broader trends.

To contextualize the parameterization process, the algorithm for the dry season start timing may be considered. The dry season start timing is identified in the receding limb of the annual hydrograph through a combination of relative magnitude and slope, which are determined by parameterization. The start timing will be identified later in the water year, for example, if the relative magnitude threshold is reduced (requiring lower magnitude) or if the slope threshold is reduced (requiring a flatter slope), essentially creating more stringent hydrologic requirements. Further, the degree of smoothing applied to raw daily streamflow dampens fluctuations in flow and can allow a stabilized slope to be detected earlier in the water year as the level of smoothing is increased. The combinations of parameters for each algorithm were determined by expert opinion of the co-authors to best achieve timing of the functional flows illustrated conceptually in Figure 1-1 across a diversity of hydrologic inputs, and this parameterization is available as default values in the SFDA code.

1.3.5 Application of the SFDA to functional flows in California

Four distinct applications of the SFDA were used to calculate the timing of functional flow component transitions based on reference-condition California streamflow gages (Figure 1-2). In these applications, the SFDA steps were repeated up to three times to accurately identify functional flow transitions across the variety of stream types found in California. The parameter

values (e.g., smoothing parameter σ or window size) were determined heuristically by the co-authors for each functional flow component to achieve timing results aligning with the conceptual timing of functional flow transitions illustrated in Figure 1-1 and described in Yarnell et al. (2020). In the calibration process, parameters for each functional flow identification algorithm were empirically and incrementally adjusted to achieve hydrologically meaningful results; for example, the parameters for spring recession start timing (smoothing parameter σ, window sizes, and magnitude thresholds) were adjusted so that the timing would occur after wet season high flows, but before flows had receded to baseflow conditions. Supplemental Materials and associated online resources provide more information about the calculation of each functional flow timing metric, how to download the SFDA code, and how to modify algorithm parameters to achieve desired results. To demonstrate SFDA application to a specific functional flow component, the calculation of wet season start timing is described in Section 1.3.5.1.

The timing metrics from the SFDA can be used to calculate additional functional flow metrics describing the magnitude, duration, frequency, and rate of change of flow within each functional flow component (e.g., baseflow magnitude or duration of the dry season) (Yarnell et al., 2020). The full suite of SFDA-based functional flow metrics can be visualized and downloaded at *eFlows.ucdavis.edu*, a website developed to view and interact with California's natural hydrology.

1.3.5.1 Functional flow calculation for wet season start timing

Wet season start timing delineates the portion of the water year during which streams receive the greatest inputs from storm runoff or snowmelt, and flows are elevated above dry season baseflow levels (Yarnell et al., 2020). The calculation for wet season start timing is presented as an example of the SFDA application to California functional flows. This calculation

uses one iteration of the SFDA steps (Figure 1-5). Within each water year, a high standard deviation Gaussian filter (G1, $\sigma = 10$) is applied (Fig. 5, Step 1) to detect the water year's global peak (P1) and preceding global valley (V1) (Figure 1-5, Step 2). A relative magnitude threshold M1 is then set based on the magnitude of P1 and V1 as an upper limit (M1 = γ*(P1-V1), where $\gamma = 0.2$), to ensure that the wet season start timing is not set after flows have already increased during the water year (Figure 1-5, Step 3). A spline curve is fit to G1 so that its derivative can be used as a hydrologic requirement in the final feature detection step. Finally, searching backwards in time from P1, the date that discharge first falls below M1 and below a rate of change equaling (δ*P1, where $\delta = 0.002$) is selected as the wet season start timing (Figure 1-5, Step 4). The values for γ and δ were adjusted for California reference streamflow based on the co-authors' expert opinions to achieve identification of the functional flows described conceptually in Figure 1-1 and Yarnell et al. (2020).

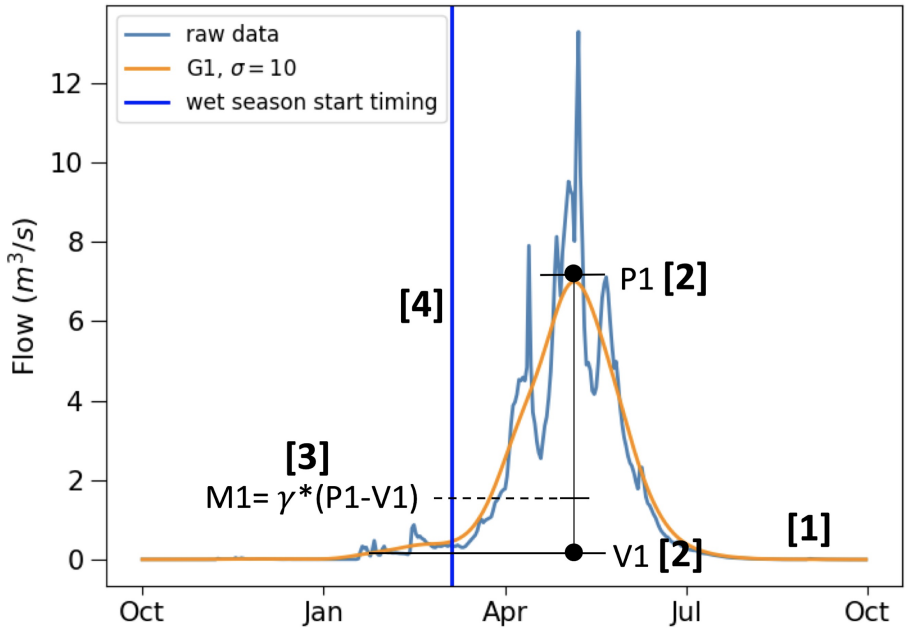

Figure 1-5. SFDA steps to calculate the wet season start timing metric using data smoothing and feature detection based on magnitude and rate of change requirements.

1.3.6 Performance assessment

The calibrated SFDA was evaluated based on its ability to accurately determine the timing of functional flow transitions across all years in the California unimpaired streamflow dataset. The analyzed results consist of four flow timing metrics calculated annually for each gage (6–65 years per gage). Performance assessment included: 1) a comparison of results across stream types, 2) visual inspection of results, and 3) calculation of assessment indices to quantify issues in algorithm performance.

1.3.6.1 Comparison of functional flow timing results across stream types

Results were grouped by stream type (rain-, snowmelt-, or mixed rain and snowmelt-sourced) and visualized with violin plots, which use a rotated kernel density plot to depict the distribution of results. Distinct letters above the violin plots denote groups with statistically distinct mean values based on Tukey's Honestly Significant Difference statistical test with a confidence level of 95% (Abdi and Williams 2010). Groups with no statistical difference share the same letter above the violin plot. Results were interpreted according to the co-authors' expert knowledge of California streamflow hydrology and supported where possible with relevant region-specific literature.

1.3.6.2 Visual performance assessment

Visual inspection of functional flow timing results was performed as a preliminary step to inform quantitative inspection (Section 1.3.6.3). The four annual flow timing metrics were reviewed for each water year in the dataset (n = 7475 years), yielding 29,900 visual inspections.

Accuracy was visually assessed based on the authors' knowledge of California seasonal flow components and when they were expected to occur across a range of water year types. Results that appeared incorrect were tabulated, grouped according to functional flow component and stream type, and reviewed by multiple experts in California hydrology from the co-author team to ensure consistency. After performing the 29,900 visual inspections of the four timing metrics, issues were characterized based on the bias in timing (e.g., early or late timing) and the stream type in which it occurred.

1.3.6.3 Quantitative analysis with assessment indices

The purpose of this analysis was to quantify issues in algorithm performance observed during visual assessment. The issues characterized during visual assessment were quantified using programmed rules defined to identify occurrence of each issue across the dataset. For example, one rule identified years in rain-sourced streams in which dry season start timing was set after August 1. This was based on repeated observation that flow magnitude and slope generally decrease to baseflow levels in this stream type before August 1, and dry season start timing set after August 1 was usually inaccurate. The developed rules were quantified across relevant stream types and resulting values were termed assessment indices. Many of the assessment indices attempt to quantify cases in which functional flow timing was either earlier or later than expected for a given water year, and these issues with timing were often stream type-specific. For example, seasonal timing metrics tend to occur later in the water year for snowmelt-sourced streams than rain-sourced streams, so a dry season timing metric of March 1 could be considered anomalously early in snowmelt streams but normal in rain streams. Early or late occurrence was defined either through an empirical, evidence-based cut-off point (such as Aug.

1) or if possible through a relative hydrologic relationship, such as the number of high-flow events that occur before or after a particular timing metric is set. Other assessment indices quantify water year features that make characterization with the SFDA difficult, such as dry water years in which only one or two peak flow events occur. Table 1-1 lists performance assessment indices used to quantify issues in algorithm timing calculations, based on final results from the SFDA.

1.4 Results and Discussion

The SFDA was found to consistently identify functional flow components across a wide range of hydrologic input data, enabling quantitative differentiation across stream types based on the timing of seasonal functional flows. Example SFDA timing results are presented in Figure 1-6 for individual water years spanning a range of stream types (rain-, mixed-, and snowmelt-sourced streams) and water year types (dry, moderate, and wet years) across a variety of watersheds, illustrating the ability of the SFDA to capture the timing of functional flow transitions in California across a diversity of hydrologic regimes.

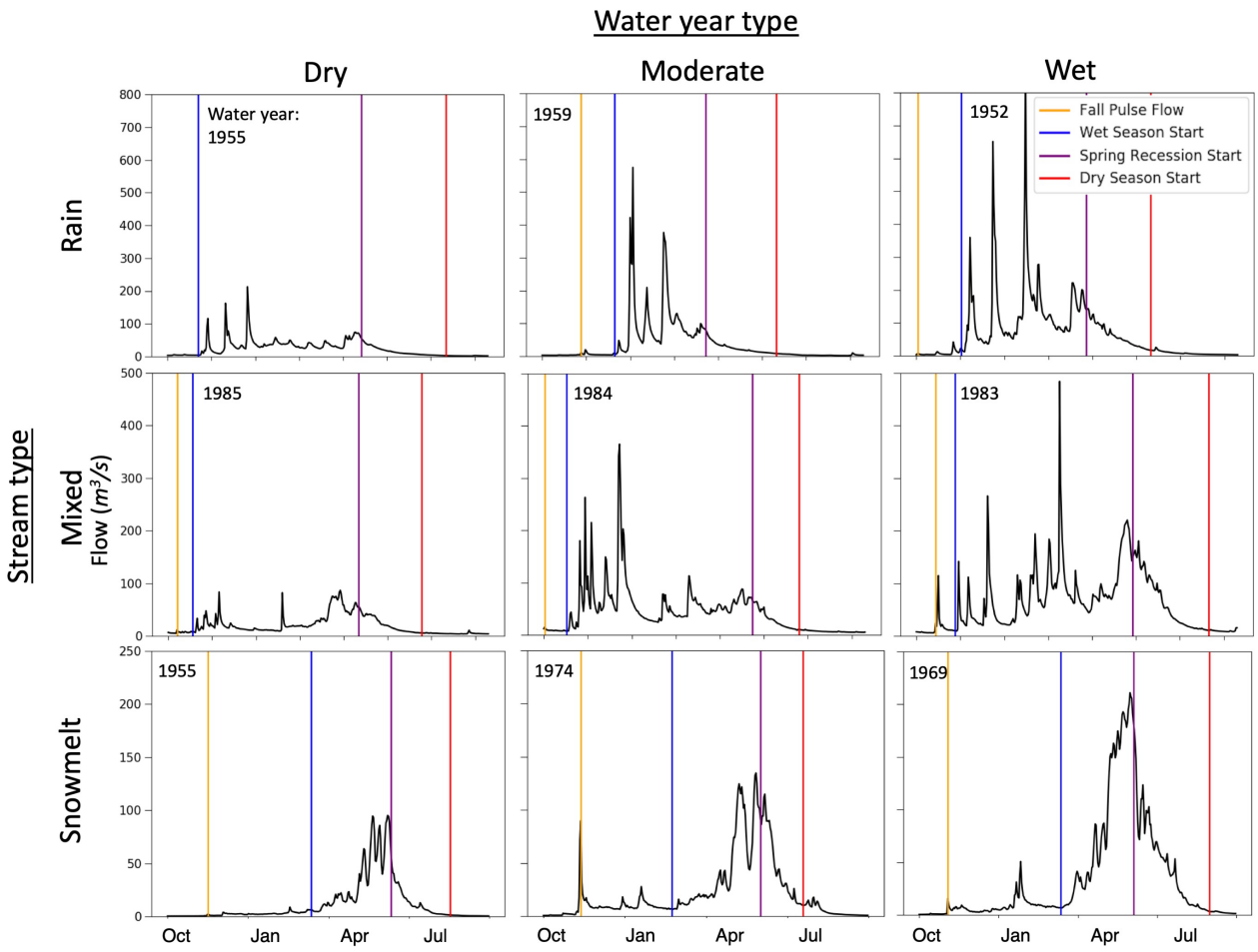

Figure 1-6. Select SFDA results for the timing of functional flow transitions across three stream types (rain, mixed rain and snow, and snowmelt) and three water year types in California (dry, moderate, and wet). Individual hydrographs are from USGS gages 11529000 (rain), 11413100 (mixed rain and snow), and 11266500 (snowmelt).

1.4.1 Comparison of results across stream types

1.4.1.1 Fall pulse flow timing

The timing of the fall pulse flow marks the first peak flow of the water year when magnitude surpasses baseflow in a distinct pulse. Unlike the other functional flow components, the fall pulse flow is constrained to only occur during a subset time of the water year (Oct. 1-

Dec. 15) when hydrologic requirements for relative magnitude and duration are met, and it does not necessarily occur in each water year. A fall pulse flow was identified in 60–65% of water years across all stream types. Although there were significant differences in event timing ($p < 0.05$) between snowmelt streams and other stream types, wide overlap exists across all stream types (Figure 1-7.A). This is due in part to large-scale temperature and precipitation patterns that affect California streamflow. Early in the water year (Oct.-Nov.), temperatures across the state including the Sierra Nevada mountains are often above freezing, causing precipitation to fall as rain or rapidly melting snow (Lundquist et al. 2008; Serreze et al. 1999). Additionally, atmospheric river events can cause correlated streamflow patterns across much of the state (Cayan and Peterson 1989), which are most pronounced when all precipitation is falling as rain. Therefore, a high degree of similarity is expected in the timing of fall pulse flows across all stream types. Further reason for the limited distinction among stream classes stems from the algorithm itself, which detects events over a narrow search window of 75 days (Oct.1-Dec. 15) considered ecologically significant for California streams (Yarnell et al., 2015). The upper and lower bounds of the violin plots span nearly the entire available time window of 75 days (Figure 1-7.A), indicating that fall pulse flow varies widely across all stream types. These results broadly align with Ahearn et al. (2004), who state that the season of flushing flows in California typically begins in November.

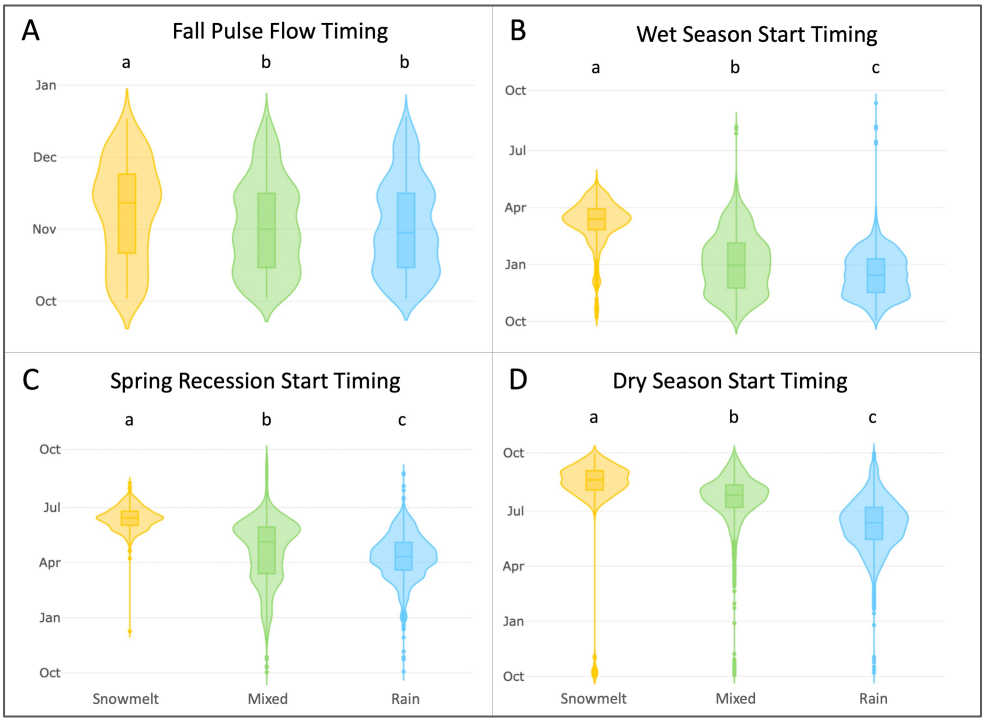

Figure 1-7. Functional flow timing distributions across all stream types of California unimpaired streamflow. Letters above violin plots indicate statistical significance. The y-axis spans the California water year (Oct.-Sept. 31) for all components except the fall pulse flow, which is constrained from October 1-December 15.

1.4.1.2 Wet season start timing

Wet season start timing is the date that the water year begins to experience consistently elevated flows from either rainfall or snowmelt (Yarnell et al., 2020). The differences in these values were statistically significant ($p < 0.05$) across the three stream types (Figure 1-7.B). The timing occurred three to four months later in snowmelt-sourced streams (average Mar. 4) than rain-sourced streams (average Dec. 12), and timing from mixed-source streams occurred across a wide range of values whose mean (Dec. 30) closely resembles rain-sourced streams. These differences were expected due to differing geographic and climatic drivers of wet season flow across California. In rain-sourced streams, the timing of wet season flow closely reflects patterns

of winter precipitation, which occurs primarily during the winter months (Dec.-Feb.), although these peak flows also experience high interannual variability in timing (Cayan and Peterson, 1989, Dettinger, 2011). In high elevation snowmelt-sourced streams, peak flows are initiated by the snowmelt pulse as air temperatures warm enough to melt snowpack in the spring. In mixed-source streams, wet season start timing may be cued by either winter storms or a snowmelt pulse, resulting in a wide range of possible values driven either by precipitation timing or temperature-driven snowmelt (Figure 1-8). The proportion of streamflow driven by rain versus snow is an important consideration in mid- and high-elevation basins, as runoff is expected to shift towards more rain-driven flow with warming climate in the western United States (Hamlet et al. 2005; Stewart et al. 2015; Sultana and Choi 2018).

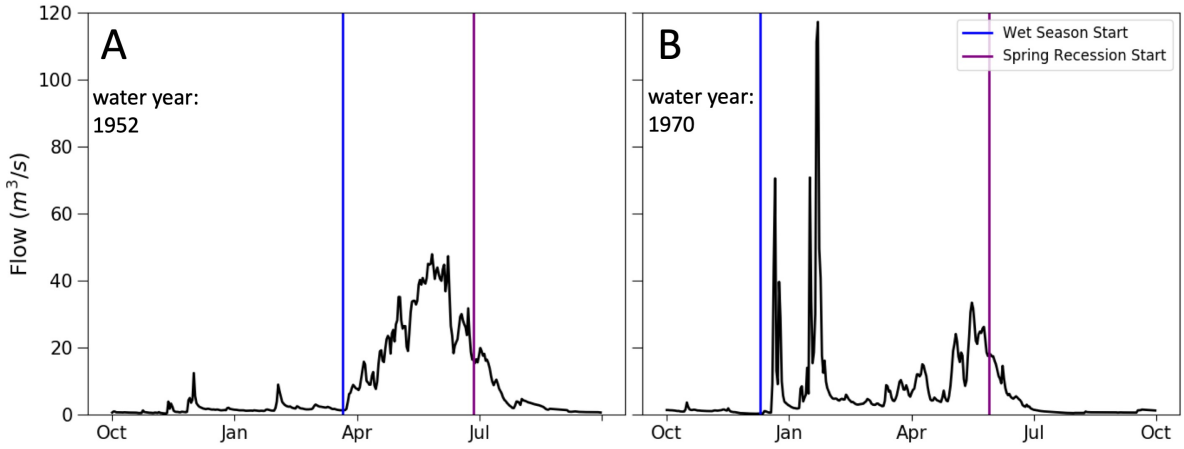

Figure 1-8. Hydrographs of two different water years from a mixed-source stream (USGS gage 11414000) show varying contributions of snowmelt and winter rain storms, resulting in a wide range of results for spring recession start timing and wet season start timing.

1.4.1.3 Spring recession start timing

The spring recession represents the seasonal transition from wet season high flows to dry season low flows. The spring recession start timing is statistically distinct ($p < 0.05$) across the three California stream types, with timing occurring progressively later in the water year from rain-sourced to snowmelt-sourced streams (Figure 1-7.C). This distinction in timing is expected due to climatic influences on hydrology that shift as streams progress from lower to higher elevations and snowpack provides increasing amounts of storage that delay streamflow response to precipitation (Aguado et al. 1992). In California's highest elevations (above 2300 m), the spring recession is cued by a distinct temperature-driven snowmelt pulse. As the snowmelt influence diminishes and warming occurs earlier in lower elevation mixed-source streams (Figure 1-2), the snowmelt pulse may arrive earlier or may not occur at all in dry years with very little snowpack relative to rainfall. In rain-sourced streams the spring recession is expected to occur after the last rain storm of the wet season, which tends to occur several months earlier in the year than the snowmelt pulse on average. The distribution of spring recession start timings in snowmelt-sourced streams is relatively narrow, with the majority of start dates occurring between May 23 and July 6 (average June 6), indicating predictable recession timing in snowmelt streams regardless of water year type (Yarnell et al., 2010).

The most variability in spring recession start timing occurs in mixed-source streams, which due to their occurrence at mid-elevation regions are highly sensitive to changes in temperature and snowpack (Lundquist, Cayan, and Dettinger 2004; Stewart 2008). Figure 1-8 demonstrates how a greater snowmelt pulse is associated with later spring recession timing, occurring 31 days later in water year 1952 than in 1970. This finding aligns with other research on streamflow in the western US, that has indicated both temperature and annual flow volume

are significant drivers of spring snowmelt runoff timing (Aguado et al., 1992, Kormos et al., 2016). Adding to this variability, snowmelt-receiving streams in mid-elevation regions of California have been subject to significant changes in the timing of snowmelt recession peaks due to climate warming (Stewart, 2008). Hamlet et al. (2005) for example estimated peak accumulation of snowmelt runoff in mid-elevation areas of California as occurring 15–45 days earlier throughout the last century, which adds additional variation to the spring recession start timing results in mixed snowmelt and rain regimes. Although rain-sourced streams also exhibit high variability in spring recession timing, the average spring recession start timing across rain-sourced streams (April 7) broadly aligns with the generally accepted end of the rainy season for California (Liu et al., 2018).

1.4.1.4 Dry season baseflow start timing

The start timing of the dry season marks the beginning of the low flow, low variability portion of the water year, in which the rate of recession flows has stabilized and magnitudes reach baseflow level. Similar to spring recession start timing, dry season start timing is statistically distinct among the three stream types ($p < 0.05$) and occurs gradually later on average from rain-sourced (June 6), to mixed-source (July 16), to snowmelt-sourced streams (August 7) (Figure 1-7.D). The timing distribution ranges more than 100 days in rain-sourced streams, which is consistent with the high inter-annual variability of precipitation magnitude and timing (and consequently streamflow) exhibited in California (Dettinger et al., 2011).

Despite high variability across rain-sourced streams, the average dry season start timing in these streams is surprisingly consistent from small to large streams. For instance, the average dry season start timing is June 8 in larger north coast streams (average annual flow 23 cms), and

is similar in flashy ephemeral streams (average annual flow 0.5 cms), with an average start timing of May 27 (from Lane et al. 2017). However, interannual variability in dry season start timing within a single stream can be high, suggesting that central tendencies do not represent dry season timing conditions well in rain-sourced streams.

1.4.2 Performance assessment indices

Assessment indices were created to quantify the accuracy of the SFDA for identifying the timing of functional flow transitions in California reference streamflow. Assessment indices are presented in Table 1-1, and the following section highlights key issues and limitations for each functional flow. The frequency of most identified issues was less than 10%, except for Snow-early-wet and Mixed-early-spring, which are explained in Table 1-1 and below.

Table 1-1. Assessment indices for SFDA timing results.

Index name	Stream type	Issue	Assessment index calculation	Frequency
Fall-day1	All types	Fall pulse flow timing can occur on the very first day of the water year (Oct. 1), when it is difficult to determine from an annual hydrograph if the set date represents an actual peak or if it is capturing a recessing flow carried over from the previous water year.	Percentage of years in which the fall pulse timing is on day one of the water year (Oct. 1).	1%
Wet-season	All types	Occasionally the requirements for wet season start timing are not met so the metrics are not calculated.	Percentage of years in which spring recession or dry season start timing are calculated, but wet season start timing is not calculated.	2%
Spring-dry-gap	All types	A lag between spring recession and dry season start timing of more than five months indicates an anomaly within the water year, such as early spring recession or late dry season start timing, or a year in which the	Percentage of years in which the number of days between spring recession and dry season start timing is	5%

		component timings were based off of a very limited number of storms.	greater than 150 days (five months).	
Snow-late-spring	Snowmelt	Spring recession start timing can be calculated late into the recession period such that it occurs at the end of the snowmelt pulse instead of the beginning. Dry season start timing consequently occurs very soon after the spring recession timing.	Percentage of years in which spring recession start timing and dry season start timing occur within 21 days of each other.	1%
Snow-early-wet	Snowmelt	Wet season start timing in snowmelt streams can be triggered by large rainstorm flows early in the climatic wet season (Nov.-Jan.), and other years it is triggered by the snowmelt pulse (Apr.-May). This results in a wide range of start timing in the snowmelt stream type, triggered by differing hydrologic cues. Identification of timing before February 1 approximates how often wet season start timing is triggered by rainstorms instead of snowmelt.	Percentage of years in which wet season start timing occurs before February 1.	25%
Mixed-spring-wet/Rain-spring-wet	Mixed-source and Rain	In especially dry years, the annual hydrograph can be defined by a single large, brief storm event. This may cause wet season and spring recession start timing to be set based on a single storm such that they occur in close proximity.	Percentage of years in which wet season and spring recession start timing occur within 30 days of each other.	Mixed-spring-wet: 4%/ Rain-spring-wet: 4%
Mixed-early-spring/Rain-early-spring	Mixed-source and Rain	Spring recession start timing can occur before the end of wet season occurrence. This most commonly occurs in hydrographs without a strong snowmelt presence.	Percentage of years in which any high flows (>5th percentile) occur after that year's spring recession start date.	Mixed-early-spring: 21%/Rain-early-spring: 5%
Mixed-late-spring	Mixed-source	Dry season start timing can occur immediately after spring recession start timing, with a small gap of time between. This often occurs when the spring recession is identified too late into the period of receding high flows.	Percentage of years in which spring recession and dry season start timing occur within 21 days of each other.	1%
Rain-late-wet	Rain	Wet season start timing can occur late after the first high flows of the wet season.	Percentage of years in which any high flows (>5th percentile) occur before that year's wet season start date.	8%
Rain-late-dry	Rain	Dry season start timing can occur late into the dry season in rain-sourced streams, well after flows have already receded. This is usually the case when dry season start timing is set in August or later, based on repeated visual inspection.	Percentage of years in which dry season start timing occurs later than August 1.	10%

The methods presented here to identify hydrologic features and determine error differ from previous hydrologic studies, which can often take advantage of validated training sets to

determine accuracy (Cannas et al. 2006; Letcher et al. 2001; Smith and Schwartz 2017). The heuristic methods used in this research are similar to other approaches that require some subjectivity for parameterization of peak detection (Palshikar 2009), and qualitative visual assessment methods are similar to approaches used to validate climate patterns in climate modeling studies that pair qualitative and quantitative model assessment (Gyalistras et al. 1994; Paul and Hsu 2012). Performance assessment based on validation of known hydrologic conditions employed in this study is similar to the approach of Déry et al. (2009), who assessed a new method of spring recession identification across different river types in their study region. The proposed methods, although subjective in the choice of parametrization, present a consistent and repeatable way to identify functional flow components, advancing previous methods of quantifying seasonal streamflow patterns.

1.4.2.1 Issues in SFDA performance

Figure 1-9 presents common issues in the SFDA for each functional flow component, which were often attributed to uncommon hydrologic patterns or effects from smoothing filters that occasionally have the undesired effect of over-dampening storm peaks while detecting broad hydrologic trends. In some water years, the first day of the water year (Oct.1) was identified as the date of the fall pulse flow, which presents ambiguity as to whether the first day of the water year is an actual peak event or is instead part of a continual decline from a peak in the previous water year (Figure 1-9.A). This situation occurs most often in naturalized gage data, with a 3.5% occurrence rate across all naturalized water years and an average occurrence rate of 1% across the entire dataset (Table 1-1, index WSI-day1).

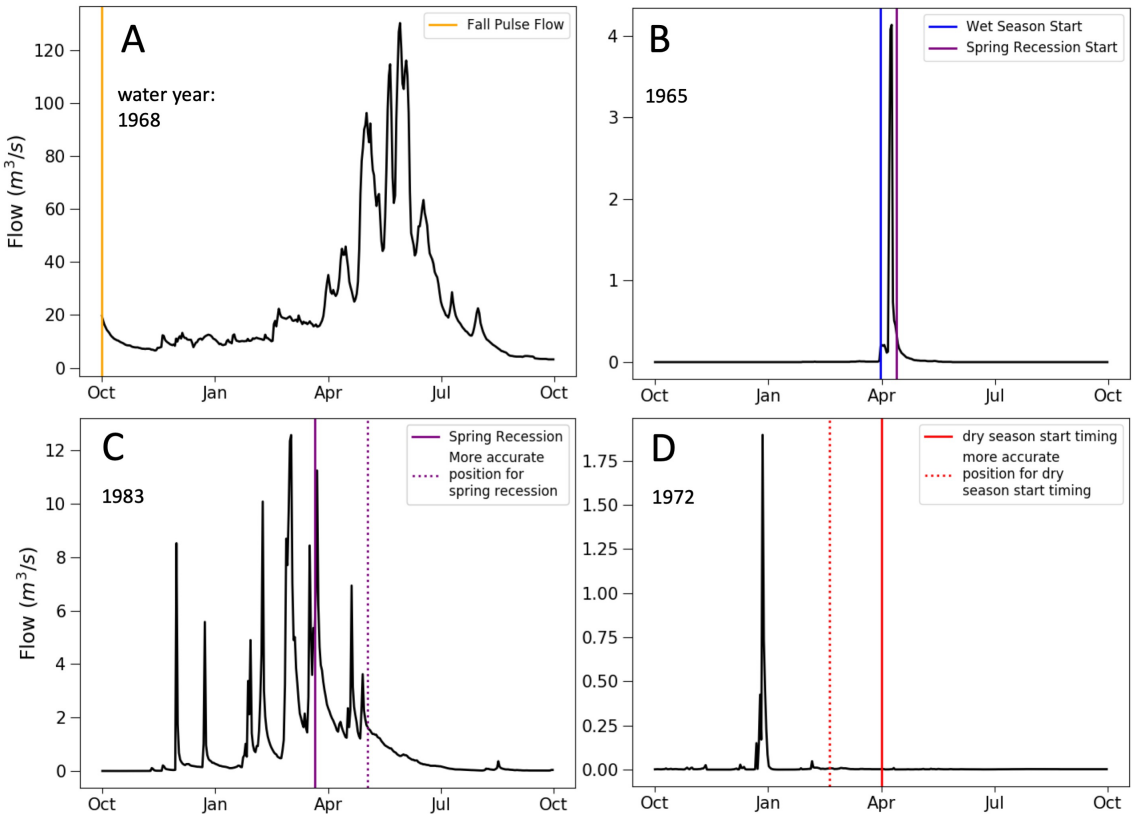

Figure 1-9. Examples in which timing metrics are affected by uncommon hydrologic patterns (A and B) or are identified earlier or later than expected given expert understanding (C and D). Panels C and D illustrate the algorithm results compared to proposed improvements based on the co-authors' understanding of California hydrology. Hydrographs from USGS gages 11213500 (A), 11046300 (B), 11033000 (C), and 11120520 (D).

Both mixed- and rain-sourced streams experienced some water years in which a single large high flow event dominated the annual hydrograph such that start timings of wet season and spring recession were based on the same peak flow (Figure 1-9.B). This occurred in 4% of mixed-source streams and 4% of rain-sourced streams (Table 1, indices Mixed-spring-wet/Rain-spring-wet) and could result in anomalous functional flow metrics based on these rare hydrologic conditions. In mixed-source streams, early identification of spring recession start timing was

found with a frequency of 21% (Table 1-1, index Mixed-early-spring), sometimes due to the effect of over-dampening rainstorm peaks with smoothing filters when attempting to detect broad hydrologic trends (Figure 1-9.C). Conversely, spring recession start timing occurred late in 10% of snowmelt stream water years, when the algorithm was triggered by small peaks along the recession limb instead of the main snowmelt pulse (Table 1-1, index Snow-early-spring). The algorithm for dry season start timing assesses the change in magnitude and slope along the recession limb, so dry water years with very little change in these features are more likely to have issues with component detection. This was often the case when dry season start timing was identified late in the water year (Figure 1-9.D), which occurred in 10% of rain-sourced water years (Table 1-1, index Rain-late-dry). These issues are expected to improve when SFDA parameters are calibrated for smaller regions of streamflow data, instead of applying the same set of parameters across a wide array of input data, as was done in this statewide case study.

1.5 Conclusions

This study developed an objective signal processing algorithm to address the need for a robust method to characterize the timing of seasonal flow transitions from daily streamflow time series. The Seasonal Flow Detection Algorithm (SFDA) improved on existing methods that rely on fixed time steps through the novel application of established signal processing techniques to identify the timing of seasonal flow transitions. The application to California streams demonstrated the ability of this approach to identify the timing of functional flow components from unimpaired daily streamflow time series across a wide range of climatic and geographic settings and extreme seasonal and interannual hydrologic variability. Results highlight

hydrologic distinctions among varying drivers of streamflow, such as progressively later timing of spring recession flow as streams shift from rainfall-sourced to snowmelt-sourced flow regimes. Limitations of the approach were determined through a combination of visual expert-based assessment and quantitative performance assessment. In general, the percentage error in timing calculations did not exceed 10% across relevant water years for any assessment index, with infrequent exceptions. In a parallel effort, functional flow metrics produced by the SFDA for California reference gages are being extrapolated to ungaged streams to inform statewide environmental flow recommendations. Likewise, the SFDA has potential to be applied to other regions or countries sharing highly seasonal climates similar to California, by adjusting algorithm parameters to suit local hydrology. For instance, the SFDA metrics could be applied to assess shifts in streamflow due to climate change, with particular focus on potential changes in timing of seasonal flows. The proposed approach supports improved understanding of high-resolution spatial and temporal trends in hydrologic processes and climate conditions across complex landscapes and can inform environmental water management efforts.

1.6 Acknowledgements

This work was supported by the UC Davis Hydrologic Sciences Graduate Group; the California State Water Resources Control Board [Grant number 16-062-300]; Utah Water Research Laboratory; and funding for G.B. Pasternack was provided by the USDA National Institute of Food and Agriculture [Hatch project number # CA-DLAW- 7034-H]. We thank Jason Hwan and two anonymous reviewers for improving the manuscript with insightful comments.

Chapter 2[2]

Projected effects of temperature and precipitation variability change on streamflow patterns using a functional flows approach

2.1 Abstract

Streamflow patterns are shifting with climate change, and these shifts pose increasing risk to freshwater ecosystems. These emerging changes must be linked with ecological functions of river systems to understand how climate change may affect freshwater biota. In this study we used a functional flows approach to analyze the ecological effects of changing streamflow patterns in snowmelt-dominated watersheds of the Sierra Nevada mountains of California. Our climate change modeling method combined ensemble Global Climate Models (GCMs) and decision scaling methods to incorporate the effects of GCM-projected changes in precipitation variability. Of climate parameters explored, air temperature causes the most change in

[2] This chapter has been published: Patterson, N. K., Lane, B. A., Sandoval-Solis, S., Persad, G. G., & Ortiz-Partida, J. P. (2022). Projected effects of temperature and precipitation variability change on streamflow patterns using a functional flows approach. *Earth's Future*, 10, e2021EF002631. https://doi.org/10.1029/2021EF002631

streamflow, although precipitation variability compounds changes driven by air temperature. The greatest changes in ecologically-relevant streamflow patterns manifest as longer and drier dry season conditions, earlier snowmelt recession, and higher-magnitude peak flows. Although the direction of changes in functional flow metrics are largely consistent across models and watersheds, the magnitude of change depends strongly on human emissions levels. The analytical approach used in this study can serve as a model for integrating multiple approaches in hydroclimatic assessment of ecological change, and the results can help prioritize specific aspects of the flow regime for restoration efforts.

2.2 Introduction

There is international consensus that human emissions have unequivocally caused warming across Earth's atmosphere, oceans, and land, and this warming has caused changes in streamflow patterns on a global scale (IPCC 2015). Intensification of the hydrologic cycle caused by warming has accompanied changes in global weather patterns, leading – among other effects – to heavier and more frequent storms in many parts of the world in the last decade (Mamo 2015). In regions with seasonal snow storage, observed changes in streamflow patterns associated with warming include earlier timing of the spring snowmelt pulse (Déry et al. 2009; Lundquist et al. 2009; Regonda et al. 2005; Siirila-Woodburn et al. 2021), lower dry season baseflows (Godsey, Kirchner, and Tague 2014; Madej 2010; Kormos et al. 2016), and higher peak flows (M. Dettinger 2011; Gershunov et al. 2019). Other shifts in streamflow patterns, particularly a tendency for more frequent, intense droughts, can make water supply more precarious, as witnessed by shortages in major metropolitan areas such as Cape Town, South

Africa and Mexico City, Mexico (Donnenfeld, Crookes, and Hedden 2018; Martinez et al. 2015; Ortiz-Partida et al. 2019). Continued climate change may also shift entire streamflow regimes on a broad scale, as anticipated for a third of US rivers by 2100 (Dhungel et al. 2016). These changes will threaten freshwater ecosystems either through the direct consequence of flow regime shifts on highly adapted biota, or through intensified pressure to divert streamflow for human use. A quantified approach is needed to understand and enable protection of Earth's remaining freshwater ecosystems in light of climate change.

Mountainous regions may be particularly susceptible to climate change since high elevation regions are warming at some of the fastest rates found globally (Pepin et al. 2015). In watersheds with seasonal snowpack accumulation, observed changes in streamflow patterns are often caused by a shift in wintertime precipitation from snow to rain as the climate warms (M. Dettinger, Udall, and Georgakakos 2015; Mao, Nijssen, and Lettenmaier 2015). In the state of California, USA, for example, the snowpack of the Sierra Nevada mountain range has historically provided a gradual release of snowmelt as temperatures warm during the spring, creating a seasonal snowmelt runoff pattern found in many of the state's rivers and streams(Lane et al. 2018). The shift towards less snow and more rain in mountainous regions however has lowered the volume of the spring snowmelt pulse while increasing the prevalence of flashy peak flows from winter storms (Das et al. 2011; T. E. W. Grantham et al. 2018).

Changes to historic streamflow patterns due to climate change will inevitably stress freshwater ecosystems. Aquatic and riparian species adapt their life history to their natural flow regime habitat, so preserving natural flow patterns is a primary element of freshwater ecosystem conservation. For example, the spring recession flow is a characteristic component of the annual hydrograph in mountainous regions of the western U.S. describing the period of gradually

receding flows when warming springtime temperatures melt the accumulated snowpack. This can act as a reproduction cue for both amphibians and riparian vegetation (Mahoney and Rood 1998; Yarnell, Viers, and Mount 2010). Anadromous Pacific salmon of Northern America also rely on aspects of the natural flow regime for reproduction, including peak flows that form clean gravel beds as spawning habitat and spring recession flows that keep fine sediments from accumulating in spawning beds (Escobar-Arias and Pasternack 2010). Freshwater macroinvertebrates are an important component of stream ecosystems, providing food for fish and amphibians. Alterations to natural flow patterns can affect instream conditions required for macroinvertebrate survival such as temperature, and disturbance to stable flow conditions such as rapid fluctuations from dam hydropeaking can cause egg mortality in near-shore habitat (Salmaso et al. 2021). Quantifying the ecological significance of potential shifts in flow regimes due to climate change will be essential for protecting remaining freshwater ecosystems.

Although current and future impacts of climate change on riverine ecosystems are widely acknowledged, such as reductions in snowmelt contributions and increases in precipitation volatility (Aldous et al. 2011; Arthington et al. 2010; Filipe, Lawrence, and Bonada 2013; Kakouei et al. 2018; P. B. Moyle, Katz, and Quiñones 2011), links between changes in streamflow and potential ecological consequences have not been quantified on a large scale. The current understanding of expected streamflow changes in California relies on coarse indicators such as shifts in annual or monthly average flow (T. E. W. Grantham et al. 2018; Zimmerman et al. 2018; He et al. 2019; Z. Liu et al. 2021) or peak flow patterns (Das et al. 2011; M. Dettinger 2011). While these indicators are important for illustrating a general picture of future streamflow patterns, they do not provide the level of detail needed to understand how specific functions of river ecosystems may be affected by particular aspects of streamflow change. Such information

is critical for developing effective conservation and mitigation strategies. To meet the need for an ecologically-based analysis of future streamflow change, the functional flows framework offers a quantitative approach for explicitly linking changes in streamflow to changes in ecological functions of river systems.

The functional flows approach is founded on the premise that specific components of the annual flow regime, or functional flows, support particular ecological functions (Escobar-Arias and Pasternack 2010; Yarnell et al. 2020). For rainfall-snowmelt flow regimes typical of California, functional flow components have been identified for five aspects of the annual flow regime which each provide flows with distinct ecological functions (Figure 2-1) (Yarnell et al. 2020). These flow components can be quantified with functional flow metrics which describe key attributes of streamflow, including magnitude, timing, duration, frequency, and rate of change (N L Poff et al. 1997). Patterson et al. (2020) developed a signal-processing approach to calculate a set of annual metrics describing these functional flows and evaluate natural functional flow patterns over all reference-condition stream gages in California. Signal processing is critical to this methodology because of its ability to capture hydrograph patterns that other conventional methods are unable to detect, while preserving the timing of seasonal flow patterns (Ashraf et al. 2022; Patterson et al. 2020). All functional flow components are represented in this study with the annual functional flow metrics (i.e. all metrics excluding long-term peak flow statistics) and annual peak flow to allow for direct comparison between water years. These include metrics describing the magnitude, timing, duration, and rate of change of functional flow components, such as the start timing of the dry season or the rate of change of the spring recession. Long-term flow statistics from the original suite of metrics would not vary from year to year at a location so they are omitted from this analysis.

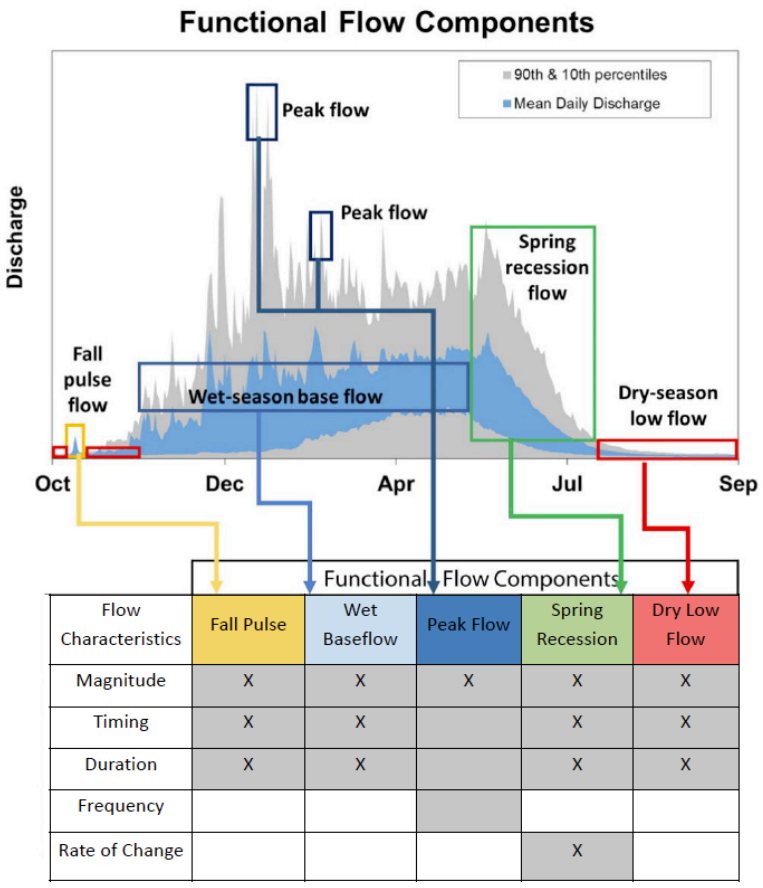

Flow Characteristics	Fall Pulse	Wet Baseflow	Peak Flow	Spring Recession	Dry Low Flow
Magnitude	X	X	X	X	X
Timing	X	X		X	X
Duration	X	X		X	X
Frequency					
Rate of Change				X	

Figure 2-1. Functional flow components (boxes) for a mixed snowmelt-rain runoff regime typical of the mid-elevation Sierra Nevada region capture aspects of the hydrograph most relevant for ecological systems. Functional flow characteristics corresponding to each component are shaded, and metrics used in this study are marked with an X. Figure adapted from (Yarnell et al. 2020).

There are multiple methods available to estimate streamflow alterations due to changes in climate. Most of these use data derived from Global Climate Models (GCMs) in some capacity, as they are the best available tools to simulate climate response to heat-trapping gas emissions. Decision scaling, on the other hand, is a tool for water resources decision making which is informed by GCMs but uses a bottom-up risk assessment approach, testing the sensitivity of user-defined metrics to a range of hydroclimatic conditions representing potential future climatic

scenarios (L. R. Brown and Bauer 2010; C. Brown et al. 2012). Decision scaling has been applied to climate change planning in California's Central Valley by measuring the effects of shifted average temperature and precipitation scenarios on a set of performance metrics (Schwarz, Ray, and Arnold 2019). While decision scaling demonstrates the sensitivity of a system to various shifts in climate, it does not quantify the likelihood of these shifts to occur across different timescales as GCMs do for various emissions trajectories. We therefore combine the two approaches by focusing decision scaling analysis on GCM-projected future climate conditions, in order to understand future climate changes that are considered likely to occur. The decision scaling approaches that have been taken so far, even when overlaid with probabilities of occurrence from GCM projections, generally only consider coarse climate metrics like average precipitation or temperature (Schwarz, Ray, and Arnold 2019). These shifts alone may not represent how future changes will stress riverine ecosystems. In this GCM-based analysis we develop a new set of climate statistics describing precipitation variability at event-, seasonal-, and interannual scales, and apply them alongside temperature and precipitation volume shifts to investigate the separate and combined effects of these climate parameters on functional flows.

With high aquatic biodiversity (P. Moyle et al. 2015), a legacy of intensive water management (Hanak 2011), and ample hydrologic data and models compared to most regions worldwide (Escriva-bou et al. 2016), California and specifically the Sierra Nevada mountain range serves as an ideal study system for ecohydrologic research. In California, down-scaling and bias-correction of GCMs has already been performed through Local Constructed Analogs (LOCA) (Pierce, Cayan, and Thrasher 2014), a statistical scheme that downscales and bias-corrects daily minimum and maximum temperature and precipitation outputs from GCMs (Pierce, Cayan, and Thrasher 2014; Pierce, Cayan, and DeHann 2016). California LOCA

datasets have been used to simulate long-term daily streamflow time series under alternative climate change scenarios (RCP4.5 and 8.5) (Pierce, Kalansky, and Cayan 2018) and to predict possible impacts on water resources, including changes in hydroclimatic metrics relevant for water resources management (Persad et al. 2020).

The objective of this study is to assess climate-driven changes in seasonal streamflow patterns in a snowmelt dominated region, using functional flows to link streamflow change to key ecological functions. We calculate functional flow change with the novel Seasonal Flows Detection Algorithm, using this tool for the first time to assess potential ecological effects of climate change. To better inform aquatic ecosystem protection in light of ongoing climate changes, we address the following research questions: (1) Which aspects of ecologically-relevant streamflow are most vulnerable to change in future scenarios, as measured by functional flow metric change? (2) How do streams across the western Sierra Nevada differ in their response to climate change, and how consistent is streamflow response across locations and models? (3) Which drivers of climate change (air temperature, precipitation volume, or precipitation variability) cause the most change in functional flow metrics? We use a hybrid approach to climate change modeling, drawing on both decision scaling methods and ensemble GCMs. Our study consists of two complementary analyses, at both regional and single watershed spatial scales, that allow us to gain a thorough understanding of both how and why streamflow in the Sierra Nevada area may shift due to climate change. Notably, we build on previous decision scaling modeling efforts that used temperature and cumulative precipitation changes alone by also incorporating the effects of potential changes in precipitation variability.

2.3 Methods

This study consists of two parts: (1) An analysis of climate change driven trends in functional flows in streamflow derived from ensemble GCMs for 18 catchments in the western Sierra Nevada mountains, and (2) A case study of a single catchment from Part 1 using decision scaling to determine the contribution of different climate drivers to observed changes in functional flow metrics (Figure 2-2). The two parts of the study give complementary insights into interrelated facets of climate change, including differences in streamflow change across watersheds, the relative influence of climatic drivers, and the similarity of results between the GCM and decision-scaling approaches. In both parts of the study, changes in ecologically-relevant streamflow were quantified using changes in functional flow metrics.

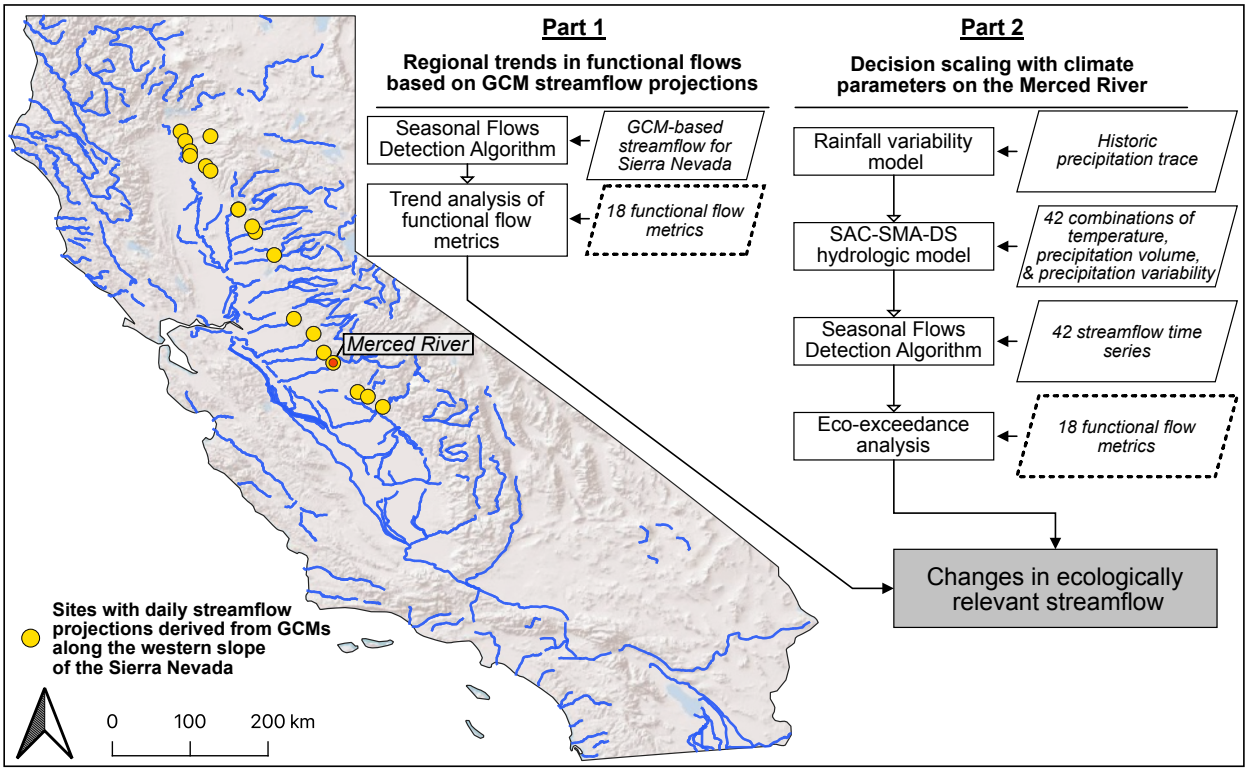

Figure 2-2. The study approach consists of two parts. Part 1 is a GCM analysis of daily streamflow projections for 18 sites along the western slope of the Sierra Nevada mountains in California. In Part 2, the Merced River is used as a case study for a decision scaling analysis with multiple climate parameters.

2.3.1 Study Area

The western slope of the Sierra Nevada mountains in California was selected for this analysis to showcase watersheds of the Sierra Nevada with significant contribution to state water supply that are at a transitional elevation, where future shifts from snow to rainfall may have severe consequences for both riverine ecology and statewide water management. We chose 18 sites in the mid-elevation band of the western slope of the Sierra Nevada mountains, within the elevation range of 150-1000m, the approximate elevation boundary of the Sierra Nevada foothill ecoregion (Cleland et al. 2007) (Figure 2-2). These selected sites all have a highly seasonal Mediterranean climate typical of California, and vary from primarily snowmelt-dominated flow

regimes to mixed snowmelt and rain regimes (Lane et al. 2018). Data at each site consisted of modeled daily streamflow timeseries for 150 years, from 1950-2099.

The watershed-level case study is focused on the Merced River watershed, one of the sub-basins included in the Part 1 regional study. This watershed is 2686 km sq in size, with an elevation of 274 m at its outlet at Lake McClure and a high point of 4000 m at Mt. Lyell in Yosemite National Park. From Lake McClure, the lower segment of the Merced River continues west to join the San Joaquin River, eventually feeding the Sacramento-San Joaquin Delta. The Merced River watershed has a highly seasonal climate, with the majority of precipitation falling between November and March. Wintertime precipitation falls as snow in areas above about 800 meters, and streamflow in the Merced River experiences a distinct snowmelt pulse in the spring as warming temperatures melt the accumulated winter snowpack. The Merced River is important for California water resources as a contributor to the Sacramento-San Joaquin Delta, the hub of California's water supply system (Koczot et al. 2021).

2.3.2 Data Inputs

Modeled daily streamflow data for sites in California were obtained from the 4th California Climate Change Assessment Group (Mallakpour, Sadegh, and Aghakouchak 2018; Pierce, Cayan, and Thrasher 2014; Pierce, Cayan, and DeHann 2016). Streamflow data were generated using the Variable Infiltration Capacity (VIC) land surface model with climate forcings from a suite of GCM simulations. Ten GCMs were selected from the Fifth Coupled Model Intercomparison Project (CMIP5), based on the DWR Climate Change Technical Advisory Group's assessment of climate models most appropriate for California-specific analysis

(CCTAG 2015). Each GCM was run with two Representative Concentration Pathways (RCPs) representing medium (RCP4.5) or high (RCP8.5) future emissions scenarios, providing 20 total climate scenarios for analysis. Data inputs to the VIC model were obtained from GCMs using downscaled and bias-corrected data generated using the LOCA method (Pierce, Cayan, and Thrasher 2014; Pierce, Cayan, and DeHann 2016). A detailed description of the LOCA method and its application to this dataset is available from (Mallakpour, Sadegh, and Aghakouchak 2018).

For the decision scaling case study on the Merced River we used unimpaired daily streamflow modeled from 1950-2013 using the SAC-SMA-DS model at Lake McClure, the site of New Exchequer Dam (Schwarz et al. 2018). SAC-SMA-DS couples the Sacramento Soil Moisture Accounting lumped conceptual hydrologic model (SAC-SMA, (Bumash, Ferral, and McGuire 1973)) with a streamflow routing model (Lohmann et al. 1998). Model performance was tested by (Schwarz et al. 2018) for the Merced River basin and other subbasins draining the west slope of the Sierra Nevada using Nash-Sutcliffe efficiency, reporting very good performance for both calibration (1951–1980) and validation periods (1981–2002). The model operates at a daily timestep and includes process models for soil moisture accounting, potential evapotranspiration, snow processes, and flow routing. Input air temperature and precipitation data used in the model was generated by (Livneh et al. 2015) by detrending historic data from 1950-2013 and spatially distributing the data over 1/16th grids. This data represents historic climate conditions and was used to generate the control streamflow dataset for comparison with subsequent climate scenarios.

Schwarz et al. (2018) applied a decision scaling approach for streamflow in the Merced River watershed by incrementally shifting temperature and precipitation volume inputs to perturb

the SAC-SMA-DS model. In this study, we applied a similar decision scaling approach and additionally considered potential changes in precipitation variability. Precipitation variability shifts are based on metrics developed by (Persad et al. 2020) and are split into three categories: Event Intensity, Seasonal Variability, and Interannual Variability (Table 2-1).

Table 2-1. Precipitation variability parameters used in the Merced River decision scaling framework. Precipitation traces adjusted according to the precipitation variability metrics were then routed to streamflow with the SAC-SMA-DS model in the Merced River Basin.

Metric	Description	Implementation
Event Intensity	Proportion of annual precipitation occurring in the three wettest days of the year.	The three wettest days of the year are scaled with a multiplier, and dry season precipitation is adjusted with a multiplier to achieve net zero difference in annual precipitation.
Seasonal Variability	Proportion of annual precipitation occurring in the wet (November-March) and dry (April-October) season months.	Precipitation in all days of the wet season months is scaled with a multiplier. Precipitation in the dry season is then adjusted with a multiplier to account for the change in the wet season, to achieve net zero difference in annual precipitation.
Interannual Variability	This metric incorporates two measures of interannual intensity: (1) The number of years in the period of record that occur under the 20th percentile or above the 80th percentile of annual precipitation, and (2) The percentile of total annual precipitation of the wettest and driest years on records.	Two adjustments take place: (1) Years under (over) the 80th (20th) percentile of annual precipitation are scaled with a multiplier enough to reach the level of the 80th (20th) percentile of annual precipitation, pre-adjustment. (2) The wettest (driest) year on record is scaled with a multiplier.

2.3.3 Data Analysis

2.3.3.1 Part 1: Sierra Nevada regional analysis

The Seasonal Flows Detection Algorithm (SFDA) (Patterson et al. 2020) was used to calculate 18 annual functional flow metrics across the Sierra Nevada daily streamflow

timeseries. These metrics describe the magnitude, timing, duration, frequency, and rate of change of five functional flow components identified for Mediterranean climate regions: 1) fall pulse, 2) wet season baseflow, 3) peak flows, 4) spring recession, and 5) dry season baseflow that each serve ecological purposes as described in (Yarnell et al. 2020).

The dataset generated by the SFDA consists of a 150-year timeseries for each functional flow metric, at each site, for each GCM, and for each future emission scenario. Flow metric timeseries were tested for change over time to explore how climate change signals from GCMs are expressed through changes in functional flows. The Mann-Kendall statistical test was used to test for monotonic (single direction) change in flow metric timeseries with a 0.05 significance threshold (95% confidence interval). To prepare data for Mann-Kendall trend analysis, each timeseries was tested for autocorrelation using the Ljung-Box statistical test and autocorrelation was corrected using iterative differencing. Annual hydrographs of three sites across the study region using the RCP8.5 emissions scenario were plotted to visualize the changes to functional flow metrics between historic (1950-2015) and future (2035-2100) time periods (RCP4.5 figures in Supplementary Materials (SM)). The three sites, selected to visualize results in the north, central, and southern parts of the study region, span a range of latitude and stream sizes.

Mann-Kendall trend results for the functional flow metric timeseries were then tested for agreement across models and sites using the Gini index. The Gini index is used in numerous applications such as economics, ecology, and classification problems, and can be described as a measure of purity or homogeneity (Cutler et al. 2007). In the context of this study, the Gini index was calculated on Mann Kendall trend outcomes for each site, with the Gini purity index interpreted as a measurement of model agreement. Each site has 10 trend outcomes for each functional flow metric, representing the 10 GCMs with RCP8.5 emissions (RCP4.5 GCM

outcomes were calculated separately). Agreement among the 10 model outcomes was measured using the Gini index for each emissions scenario. Further description of the Gini index and its application to the study is available in the SM.

2.3.3.2 Part 2: Merced River case study

In the watershed-level case study, we applied a decision-scaling approach to investigate climate change impacts on functional flows in the upper Merced River watershed. While a region-wide analysis is useful for illustrating broadly how western Sierra Nevada streams may respond to climate change, it is important to also evaluate these effects at the watershed level. The Merced River analysis offers a deeper investigation of temperature and various aspects of precipitation, explored separately and in congruence, and how they may affect ecologically-relevant streamflow in a full range of future climate scenarios. Across temperature, precipitation volume, and the three precipitation variability parameters, five total climate parameters were used to create an ensemble of climate scenarios to test on the Merced River. Climate modeling scenarios were created according to three strategies: (1) One-at-a-time (OAT) scenarios in which each parameter is shifted individually in stepwise increments, (2) Extreme end scenarios in which combinations of parameters are set at their highest values, and (3) Mid-range scenarios, in which combinations of parameters are shifted together to either $\frac{1}{3}$ or $\frac{2}{3}$ of their full range. The range of values for precipitation variability parameters were calculated for the Merced River Basin from gridded GCM outputs for ten GCMs at two emissions scenarios (the same models used in the regional California analysis) (Persad et al. 2020). The modeled temperature range is based on temperature change in Merced County from end-of-century (2070-2099) GCM

projections under the RCP8.5 emissions scenario and was accessed on the CalAdapt website (Pierce, Kalansky, and Cayan 2018). Due to the highly variable nature of annual precipitation projections and the lack of uniform change in direction, we deemed the range from -30% to 30% change appropriate for creating a broad yet suitable range of future precipitation conditions. This closely matches the range of annual precipitation changes for Merced County in end-of-century GCM projections under the RCP8.5 emissions scenario, at -28% to 43% (Pierce, Kalansky, and Cayan 2018). Further details of the decision scaling methodology are available in the SM.

Each of the 42 total climate scenarios (including the control) was used in turn to force the SAC-SMA-DS model to produce a 64-year daily streamflow timeseries. These scenarios do not reflect change through time like the suite of timeseries used for the regional analysis in Part 1, but instead reflect 64 years of the specified climate conditions, which were then compared to the control to assess change. Each daily streamflow timeseries was input to the SFDA to produce a series of annual functional flow metrics. SFDA parameters were set to match the Low Volume Snowmelt and Rain natural streamflow class for California (Lane et al. 2018), with slight parameter adaptations made to optimally capture seasonal streamflow patterns. Annual hydrographs are plotted for the control as well as OAT scenarios with maximum change in each climate parameter, for representative dry, normal, and wet years. Magnitude and timing of the spring recession and dry season are overlaid on the hydrographs for each scenario to showcase the changes to flow metrics caused by each climate parameter.

Finally, an ecological exceedance analysis was performed to determine the frequency that climate scenarios exceeded historic ranges of functional flow metrics, i.e. the relative frequency, in percentage, that a given scenario exceeded historic metric ranges. “Eco-exceedance” was calculated for each functional flow metric as the percentage years (out of 64 annual values) that

the metric exceeded the (a) full range and (b) 10th to 90th percentile range of values in the control scenario. The resulting distributions of timing and magnitude metric values for all climate scenarios are plotted. Included in these plots are the boundaries of the (a) full range and (b) 10th to 90th percentile range of control values, plotted as boxes to provide context for the climate scenarios and to give a visual separation of historically rare events (occurring outside the 10-90% range). Reported values of eco-exceedance are based on exceedance of the full range of metric values under the control scenario.

2.4 Results

2.4.1 Part 1: Sierra Nevada Regional Analysis

Annual hydrographs of three sites across the western Sierras study region at the RCP8.5 emissions scenario (Figure 2-3) visualize the changes to functional flow metrics described in more detail through the trend analysis (RCP4.5 figure in SM). Across the selected sites, regional differences appear although the direction of change in the hydrograph due to climate change is consistent. Across all three rivers, a shift towards earlier dry season and spring recession timing is prominent, although the degree of change differs between sites. For example, the average shift in earlier dry season timing is 22 days for the Merced River at Lake McClure, versus 44 days for the Yuba River at Englebright Dam. This shift to earlier timing of the spring recession and dry season is likely due to an earlier melt-off of winter snowpack in the headwaters of these watersheds, brought on by higher temperatures. All three sites show evidence of increased rainfall in the winter season through the elevation of flashy winter month flows, which is due to the apparent shift in precipitation phase from snowfall to rain as temperatures warm in climate

simulations. However, wet season timing shifts are comparatively slight, on average between 5 and 15 days earlier at the selected sites. Median flow magnitude of the wet season increased for all three rivers, although this is balanced by a shorter duration of the wet season. Average annual flow generally does not change across sites or models. Changes in the fall pulse flow were slight and not uniform in direction, which is likely due to the random nature of the first fall-season rainfall.

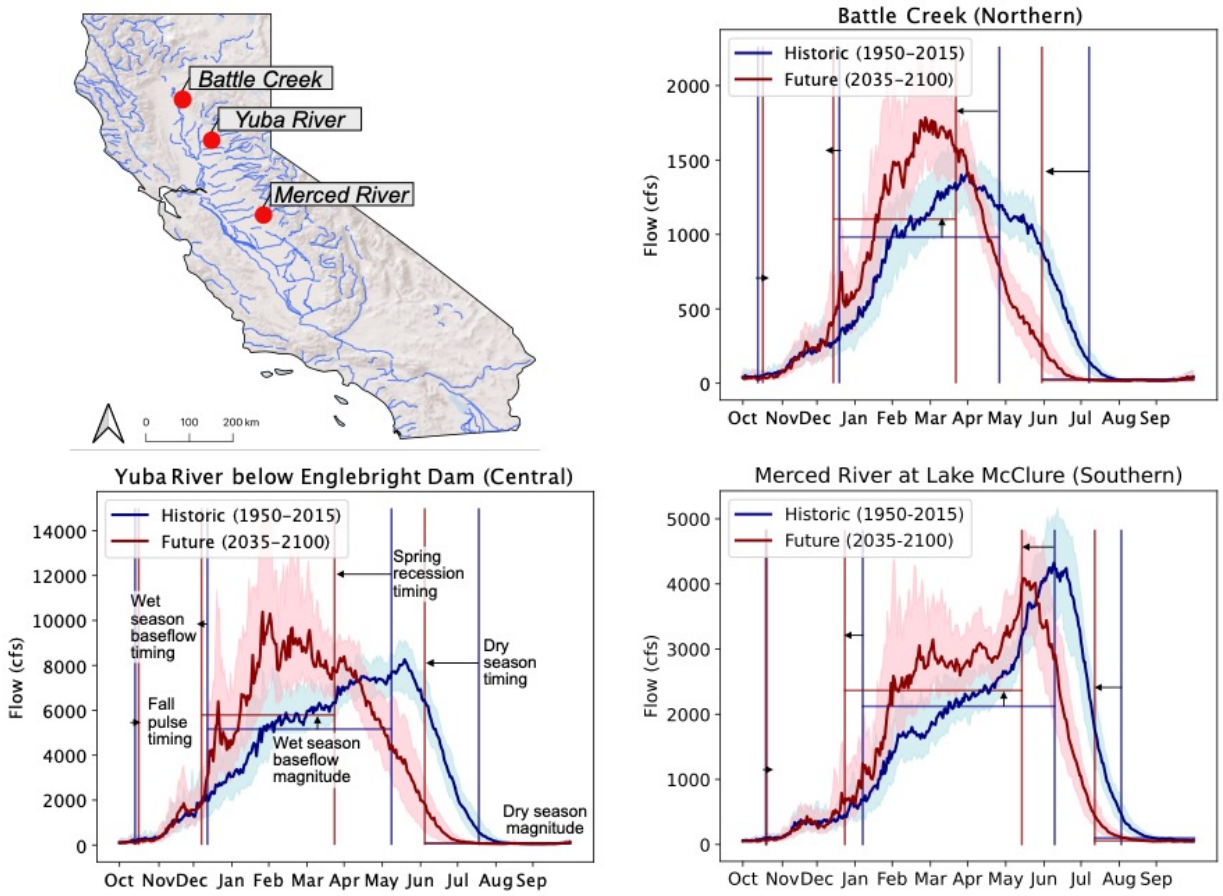

Figure 2-3. Historic (1950-2015) and future (2035-2100) simulated daily streamflow for three sites, aggregated over ten RCP8.5 GCMs (RCP4.5 in SM). Shifts in functional flow metrics for the historic and future time periods are

marked with arrows. Several metrics such as dry season and spring recession timing show consistent direction of change, although the magnitude of change varies across sites and models.

Across the 18 study catchments, the range in shifts to earlier dry season and spring recession start timing shows variation from days to several weeks in RCP8.5 emissions scenarios models (Figure 2-4) (RCP 4.5 figure in SM). Six of the 18 catchments exhibit more than a month of shift towards earlier timing in both dry season and spring recession. Notably, shifts across all catchments occur towards earlier timing instead of later timing, although some shifts are slight. No clear pattern emerges in the magnitude of shifts across latitudes.

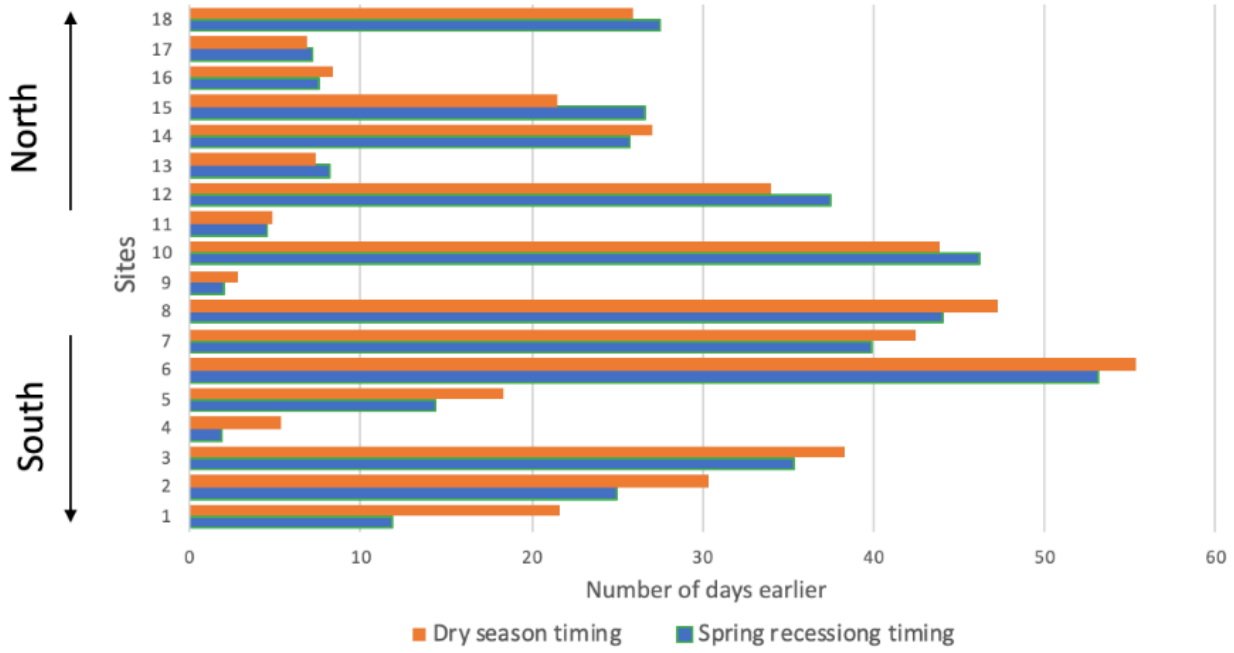

Figure 2-4. Timing shifts in dry season and spring recession functional flow metrics across all study catchments illustrate the variability of shifts across the Sierra Nevada study region. All sites exhibit a shift towards earlier timing to varying amounts.

Figure 2-5 depicts the consistency of functional flow metric trends across sites and models for RCP8.5 emissions scenarios (RCP4.5 figure in SM). The bar for each functional flow metric represents the number of models experiencing statistically significant change (out of 10 total), averaged across the 18 total sites, and the direction of the bar indicates positive or negative change. The star rating indicates the degree of agreement in the model outcomes for that particular trend according to the Gini index, where an index between 0-25% is given one star, 25-50% is two stars, and above 50% is three stars (further description of the Gini index provided in the SM). In the RCP8.5 scenario, 7 out of 18 metrics exhibit a significant trend across the period of record in at least half of the sites (3 out of 18 metrics for RCP4.5). Across most metrics that experience change, this change is in the same direction across sites and models. This consistency generally holds true for models in both RCP8.5 and RCP4.5 emissions scenarios, although models under the RCP4.5 scenario produce less change across some sites. Several metrics experiencing no change, such as fall pulse metrics, show high agreement in the no-change outcome. Coefficient of variation (CV) and annual peak flow stand out with relatively high agreement in future increases. The average increase in CV is 37% across all sites at RCP8.5 levels (24% for RCP4.5), indicating substantially more variable flows in the annual hydrograph. Annual peak flow volumes increased an average of 39% across all sites at RCP8.5 emissions levels (25% for RCP4.5).

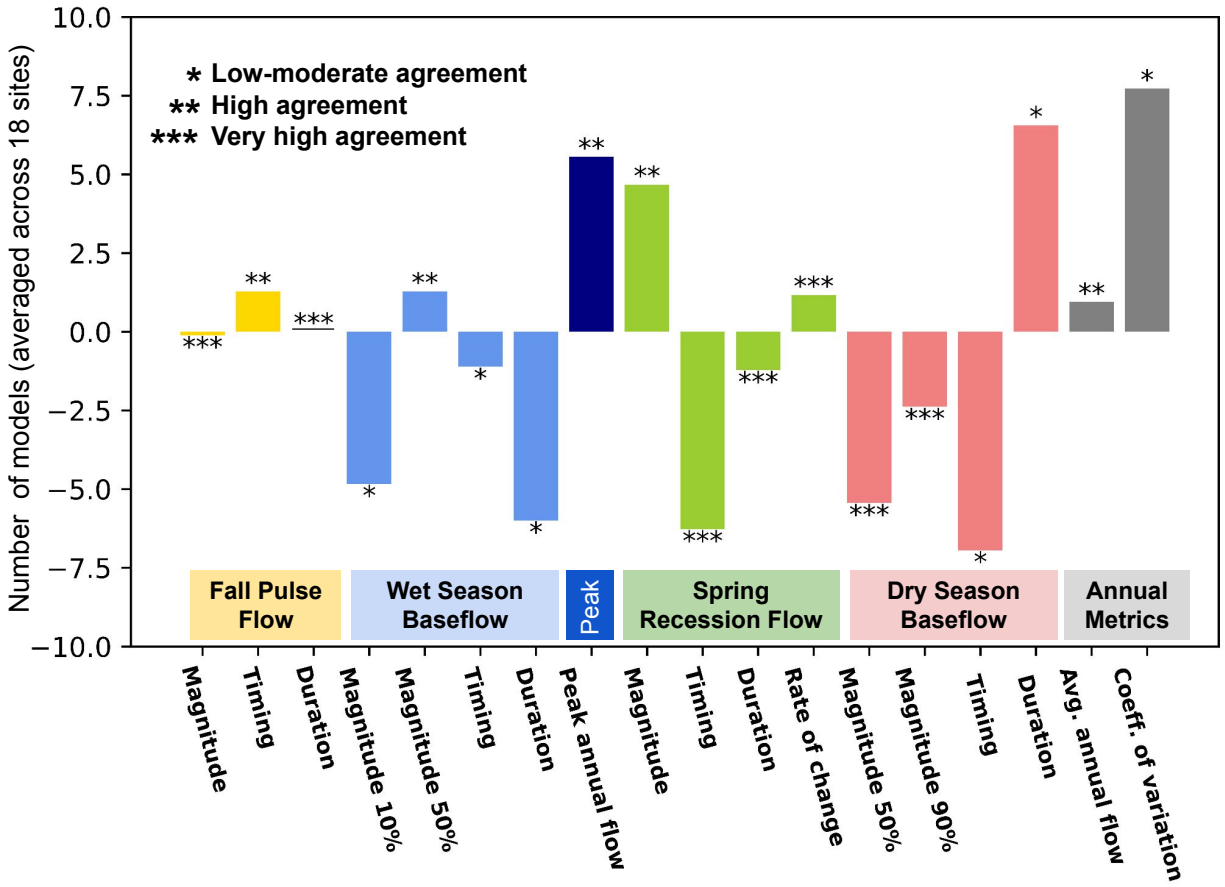

Figure 2-5. Results for functional flow metric trend analysis for models under the RCP8.5 emissions scenario (RCP4.5 in SM), where metrics are grouped according to seasonal flow components (colored boxes). Bars represent the number of models experiencing significant change (out of 10 total), averaged across the 18 total sites, where the direction of each bar indicates positive or negative change. Stars above the bars indicate model agreement according to the Gini index, where index values of 0-25% get one star, 25-50% get two stars, and 50-100% get three stars.

Under the RCP8.5 scenario, a trend in earlier timing of the dry season and spring recession appears among more than half of models across sites, although agreement is only moderate across models. The average change in spring recession timing across all sites and models is 23 days earlier, with the highest change in one site being 53 days earlier at Mill Creek, in the northern end of the study area (average 16 days earlier and maximum change 39 days earlier, under the RCP4.5 scenario). Similarly, in dry season start timing, average change is 25

days earlier with an at-a-site maximum of 55 days earlier (average 17 days earlier and maximum change 35 days earlier, under the RCP4.5 scenario). Coupled with these changes are a weak agreement in lower median and 90th percentile flow magnitude of the dry season, and higher magnitude of spring recession flows.

Table 2-2. Differences in functional flow metric value between historic (1950-2015) and future (2035-2100) periods for all models and sites. Under each emissions scenario, difference values are averaged across all models at a site,

and the minimum, average, and maximum difference values are reported from across the 18 sites. Magnitude differences are reported in percent change.

Functional flow component	Metric	RCP8.5			RCP4.5		
		minimum difference	average difference	maximum difference	minimum difference	average difference	maximum difference
Fall Pulse	Magnitude (%)	-16.6	-0.6	12	-17.7	0.6	13.1
	Timing (days)	-2.4	2.7	4.3	-2.1	1.1	3
	Duration (days)	-0.2	0.1	0.5	-0.2	0.1	0.4
Wet Season Baseflow	Magnitude 10th percentile (%)	-35.7	-16	12	-26.2	-5.2	10.8
	Magnitude 50th percentile (%)	10.7	15	21.4	5.3	10.7	18
	Timing (days)	-22.5	-3.9	6.6	-13	-1	8
	Duration (days)	-42	-19.4	-4.2	-32.9	-15.2	-4.4
Peak Flow	Annual peak magnitude (%)	18.3	38.8	58.3	13	24.6	35.4
Spring recession	Magnitude (%)	8.7	51.8	112.1	3.8	35.6	80.2
	Timing (days)	-53.1	-23.2	-1.9	-38.7	-15.8	-0.2
	Duration (days)	-9.6	-1.6	3.4	-5.8	-1	3
	Recession rate of change (%)	-0.98	0.03	1.02	-1.22	-0.04	0.47
Dry Season	Magnitude 50th percentile (%)	-49.8	-21	-1.5	-45.2	-16.4	-1
	Magnitude 90th percentile (%)	-48.2	-9.9	55	-39.4	-1.8	36.7
	Timing (days)	-55.4	-24.5	-2.8	-35.2	-16.7	-2.9
	Duration (days)	3.2	20.8	43	1.9	15.8	32
Annual Metrics	Average annual flow (%)	-0.9	5.9	10.3	-0.2	5.3	8.8
	Coefficient of variation (%)	21.3	36.9	61	14.9	24	38.6

Changes in duration of certain functional flow seasons are linked with changes in seasonal timing. Since dry season start timing generally shifts earlier while wet season start timing remains about the same, duration of the dry season is longer among more than half of sites, with an average increase of 21 days among sites under the RCP8.5 scenario (16 days under the RCP4.5 scenario). Wet season baseflow experiences a decrease in duration among more than half of models across sites, with moderate agreement. The average decrease is 19 days among sites under the RCP8.5 scenario (15 days under the RCP4.5 scenario). Both fall pulse duration and spring recession duration have little to no trend towards change, with a high to very high agreement in this outcome among models and sites.

2.4.1.1 Part 2: Merced River case study

In this analysis, shifts in temperature, precipitation volume, and precipitation variability were applied separately and in combination as a suite of 42 climate scenarios (scenarios described in SM), which were then routed to streamflow on the Merced River using the SAC-SMA-DS hydrologic model. Given the consistency in direction of hydrologic change seen across the western Sierra Nevada in the regional analysis (Part 1), the results for the Merced River are expected to be representative of the direction of change anticipated for neighboring catchments in the western Sierras.

Annual hydrographs for representative dry, average and wet years demonstrate how daily flow is altered by each climate parameter at its maximum level (Figure 2-6). The spring snowmelt pulse is the most strongly affected component of the annual flow regime across climate change scenarios. The temperature change scenario with 5°C increase affects the snowmelt pulse most prominently, both lowering the magnitude of the snowmelt pulse by more

than half and shifting the onset of the spring snowmelt recession earlier by several weeks. Lowered precipitation volume (30% decrease) also lowers the magnitude of the pulse to a similar extent, but does not significantly alter the timing of the spring recession. The temperature increase scenario also causes higher wet season peak flows by several thousand cfs in average and wet years. Similar increases in peak flow magnitude are caused by the scenarios that maximize precipitation volume (30% increase), precipitation event intensity, and interannual precipitation variability. Dry season timing is also influenced by the early onset of the snowmelt pulse flow, and occurs nearly a month earlier in the 5°C temperature increase scenario in average and wet years (Figure 2-6).

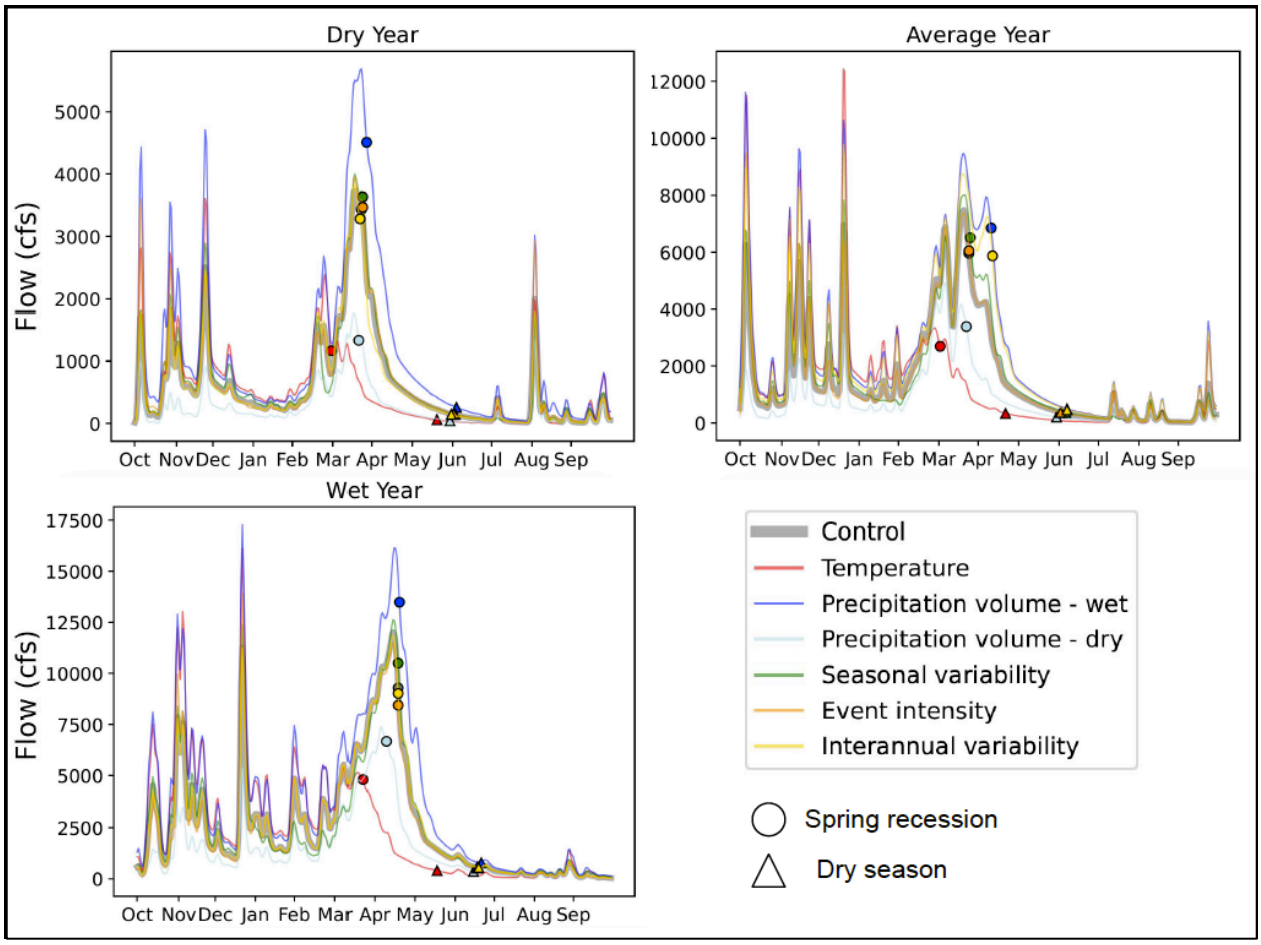

Figure 2-6. Annual hydrographs for dry, average, and wet years, modeled under climate perturbation scenarios where individual climate parameters are shifted to the maximum level. Magnitude and timing of the start of the spring recession and dry season are plotted, demonstrating shifts including a large decrease of spring recession magnitude in some scenarios.

The eco-exceedance analysis provides further evidence that temperature was the most influential climate parameter, leading to the greatest exceedance of historical functional flow metric levels (Figure 2-7). Temperature-driven changes are by far the most pronounced in spring recession and dry season functional flows, with eco-exceedance reaching 20-30% in these components for the OAT scenario with highest temperature perturbation. Eco-exceedances due to temperature do not increase linearly, but begin to accelerate for spring recession and dry

season metrics after 3°C increase (Table SM5). Of the extreme end scenarios tested, those with maximum temperature experience the greatest eco-exceedances across nearly all functional flow metrics. Changes in precipitation volume or variability can also compound the effects of increased temperature. When adding maximum values of all three precipitation variability metrics (event intensity, seasonal variability, and interannual variability) to the warmest and driest future scenario, eco-exceedance of spring recession metrics increases by 10% and dry season eco-exceedance increases by 6% (to 39% total exceedance in both situations). In the mid-range scenarios tested, combinations of temperature and all three precipitation variability metrics cause the greatest eco-exceedance. See Table SM5 for eco-exceedance values across all scenarios.

Changes in precipitation volume primarily drive changes in peak flow (if volume is increased) or in dry season metrics (if volume is decreased). Eco-exceedances caused by precipitation volume are also not linear, but accelerate when the magnitude of precipitation volume change exceeds 20% increase or decrease (Table SM5). The degree of eco-exceedance from maximum precipitation volume change is roughly similar to the change caused at the maximum level of all variability shifts (event intensity, seasonal variability, and interannual variability), and eco-exceedance caused by combining precipitation volume decrease and variability increase is approximately additive.

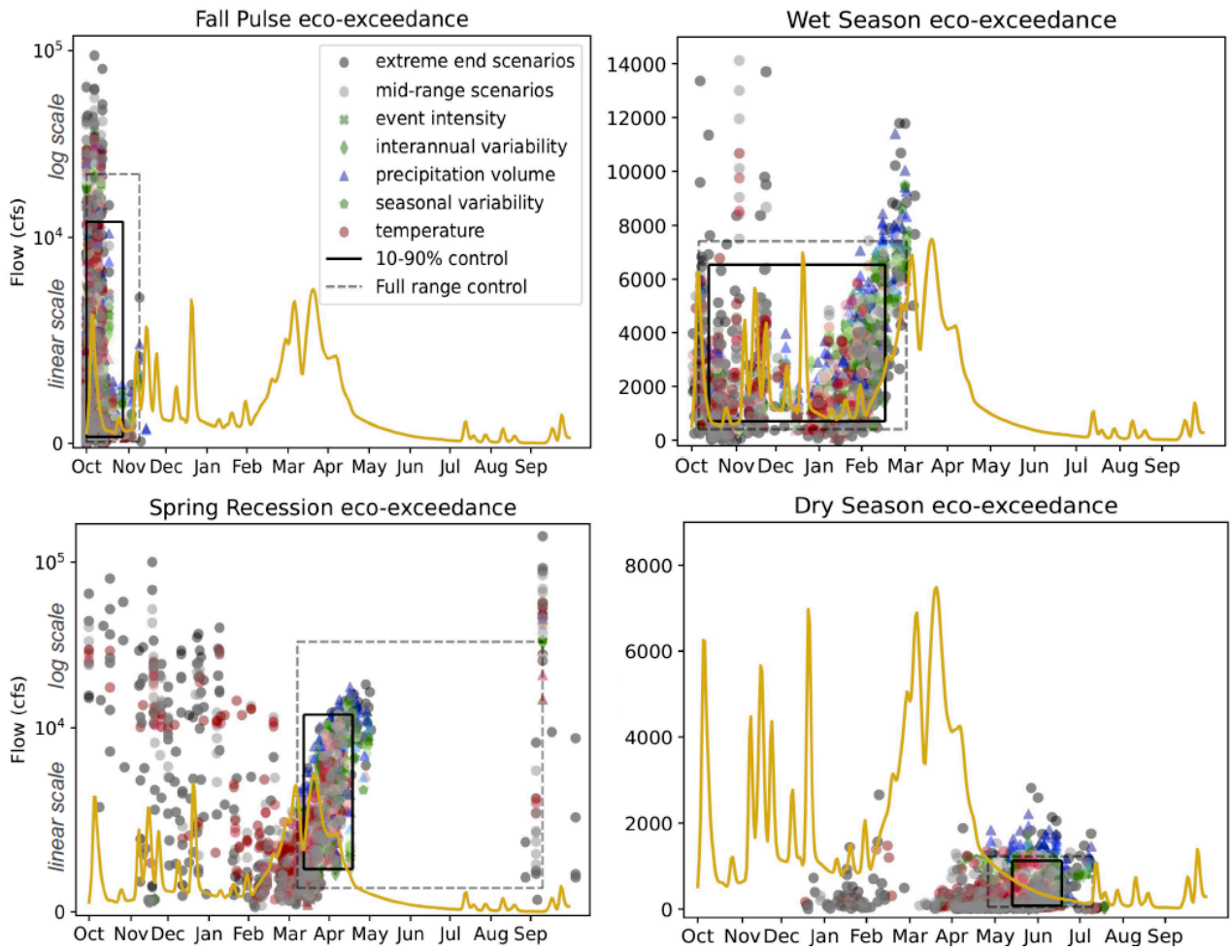

Figure 2-7. Timing and magnitude functional flow metrics for four annual flow components. Metrics calculated from models with maximum perturbations of individual climate parameters and combinations of climate parameters. Control conditions are graphed as boxes representing full range and 10-90th percentile values of metrics.

The mid-range climate scenarios explore outcomes when climate parameters are shifted to a lesser degree than the extreme end scenarios. These included temperature increases of 1.7-3.4°C, precipitation volume changes of -10% to 10%, and precipitation variability changes $\frac{1}{3}$ to $\frac{2}{3}$ of maximum calculated values. Dry season and spring recession metrics are again the most prone to eco-exceedance (up to 17%), with temperature as the most influential parameter. Peak flows also experience high eco-exceedance (up to 14%) in mid-range scenarios with increased

precipitation volume and variability. Individual precipitation variability parameters (event intensity, seasonal variability, or interannual variability) rarely cause eco-exceedance over 3% in any functional flow metric category, but the variability parameters combined with precipitation volume changes cause higher degrees of eco-exceedance than either of these climate parameters applied alone. Of the three precipitation variability parameters, interannual variability causes the greatest eco-exceedance when applied individually at the highest level, with 7.5% eco-exceedance in dry season functional flow metrics and 4% eco-exceedance overall.

2.5 Discussion

This study quantifies expected changes in ecologically-relevant aspects of the annual flow regime across a wide range of possible temperature and precipitation changes in mountainous watersheds of California. The direction of changes in functional flow metrics is largely consistent across the Sierra Nevada study catchments, though the magnitude of change differs across models and sites and generally increases in the higher emissions scenario. The greatest changes in functional flow metrics across both study parts included longer dry season duration and lower dry season magnitude, earlier spring recession timing, and higher peak flow magnitude. In the Merced River case study, precipitation variability is found to compound streamflow changes caused by changes in temperature or precipitation volume, and the effects are often synergistic.

2.5.1 Dominant climate drivers of streamflow change

Results from the Merced River case study indicate that temperature change is the most influential driver of change in functional flow metrics. Given the high confidence in projected

increases in air temperature relative to precipitation changes both in the western US and globally (IPCC 2015), this finding suggests river ecosystems may be more at-risk due to streamflow changes than previously understood. Although many studies have connected air temperature increases with observed or anticipated changes in streamflow (Aldous et al. 2011; Mittal et al. 2016; Musselman et al. 2021; Null et al. 2013), our analyses build on this relationship by assessing the interactions of temperature increase with other aspects of climate change. Changes in streamflow caused by changes in either temperature or precipitation volume are exacerbated by increases in precipitation variability and the effects are often synergistic. For example, the hydrologic dry season, one of the most impacted flow components across climate change scenarios, exhibits even longer and drier conditions when precipitation variability increases are combined with temperature increases. Other studies focused on drought in California also confirm that temperature is at least as influential on drought conditions as precipitation volume (Luo et al. 2017). The relative influence of temperature was found to decrease at lower elevations however, demonstrating the importance of temperature for high elevation watersheds and confirming the need to study the complex interactions of temperature and precipitation.

The use of three unique climate parameters describing precipitation variability at event-, seasonal-, and interannual-scales allowed for further assessment of the aspects of precipitation change that may most influence future flow conditions. Interannual precipitation variability, the climate parameter representing greater extremes between wet and dry years, causes the most functional flow metric change compared to the other precipitation variability metrics. Greater extremes between wet and dry years is anticipated with climate change in California, and has already been experienced in the last decade with the abrupt shift from the drought of 2012-2016 to the record-breaking winter of 2017 (Mallakpour, Sadegh, and Aghakouchak 2018; Persad et

al. 2020; Swain et al. 2018). The extreme variability scenario, which combines all precipitation variability metrics (event intensity, seasonal variability, and interannual variability) to their highest values while keeping average precipitation relatively constant, causes similar levels of eco-exceedance to changes in precipitation volume of either -30% or 30%. For example, the extreme variability scenario produced similar levels of dry season eco-exceedance as a 30% precipitation reduction, as well as similar levels of peak flow eco-exceedance to a 30% precipitation increase. Although GCM forecasts for California are highly uncertain about change in annual total precipitation (Persad et al. 2020), expected changes in variability alone may have similar ecological effects to a drastic increase or decrease in total precipitation.

While the focus of this study was on the potential changes to functional flow metrics caused by model perturbations representing climate changes and not the internal hydrologic model storages and fluxes, below we discuss expected hydrologic drivers of our results. Hydrologic processes related to snowpack accumulation and melt, soil moisture, and runoff are all likely to have influenced the simulated streamflow changes (Schwarz et al. 2018). Rising temperatures influence snowpack by both increasing the proportion of precipitation falling as rain versus snow, and hastening the melting off of snowpack in the spring (Stewart 2008), as our results show with higher temperature alone advancing the onset of the spring recession by several weeks in the Merced River Basin. However, wetter conditions (i.e. higher precipitation volume scenario) tend to delay the onset of the spring recession and dry season baseflow (Figure 2-6), so it is possible that increased precipitation in the future could occasionally mask changes in snowmelt rate caused by warming. By contrast, drier conditions (i.e., lower precipitation volume scenario) accelerate the onset of spring recession and dry season baseflow timing independently of temperature increases (Figure 2-6). Snowpack persistence and melt time is also

important in sustaining river flow during the summer dry season (Godsey, Kirchner, and Tague 2014), and our regional analysis results suggest that reduced snowpack will contribute to dry season baseflows with lower magnitude by 16-21% and longer duration by 2-3 weeks, beginning earlier in the summer. Temperature is again an important driver in changes to dry season hydrology, likely due to both snowpack effects in the spring and higher evapotranspiration rates during warm periods, which can reduce soil moisture and dry season baseflow magnitude. In our Merced River case study, a temperature increase of 5°C causes more change to dry season conditions than a 30% reduction in precipitation volume. Precipitation variability, especially in the form of longer dry spells during warmer months, may compound dry season conditions by further increasing soil moisture deficits. Mounting soil moisture deficits are expected to accompany and follow prolonged dry periods in the western U.S. independent of annual precipitation changes, due to an increased proportion of evapotranspiration in the water budget compared to historical conditions (Cayan et al. 2010). In the Merced River case study, changes to precipitation event intensity (one of three precipitation variability scenarios) altered dry season baseflow metrics to the same extent as a 10% precipitation volume reduction, and caused similar increases in peak flows to a 30% increase in precipitation volume. These results are partly due to the concentration of precipitation into the wet season caused by the increase in event intensity. Intense storms also tend to exceed soil infiltration capacity to greater extents than low-intensity rainfall events, causing more runoff in a single event and less soil moisture replenishment (R. E. Horton 1941). In the high event intensity scenario, this increase in runoff is paired with less rainfall and soil infiltration outside of the wet season, reducing dry season baseflows by as much as 47%. Our findings related to precipitation variability interactions expand on studies by (T. E.

W. Grantham et al. 2018) and (Schwarz, Ray, and Arnold 2019) focused on temperature and precipitation volume impacts alone.

Although the maximum projected changes in climate parameters would result in serious ecological consequences, it is important to balance these potential outcomes with the possibility of less extreme climate outcomes. Functional flow metrics exhibit generally the same direction of change in RCP4.5 and RCP8.5 emissions scenarios, but the magnitude of these changes is often less severe in RCP4.5 scenarios. This clearly aligns with the importance of temperature increase on streamflow patterns found in our study system. Differences in emissions scenarios appear in metrics indicating stream flashiness; annual peak flow increases an average 25% in RCP4.5 scenarios, whereas models under the RCP8.5 emissions scenario see an average increase of 40%. Likewise, change in CV is markedly lower under the RCP4.5 scenario, at an average of 25% versus 37% under the RCP8.5 scenario. The wide range of potential outcomes produced by the different models under each emissions scenario also demonstrates that, if the least sensitive projections play out, shifts in certain functional flow metrics could be slight. The timing of the spring recession and dry season, which are greatly affected in some model outcomes, would experience change of only 2-3 days on average in the models producing the least change. This full range of outcomes reveals the uncertainty of aquatic ecological consequences from climate change, although the high end of potential change can help guide proactive mitigation of the most extreme effects. Although our results are supported by the use of two modeling approaches, it is possible that different hydrologic modeling strategies (e.g., Budyko models or stochastic models) could produce different outcomes or magnitudes of change in functional flows. With the high variability in projected changes to California climate, especially regarding precipitation

variability, it will be important to confirm our initial findings with further research on the potential outcomes of climate change on California's streamflow.

2.5.2 Predicted changes in functional flows and potential ecological consequences

Across both the GCM-based regional analysis and the decision scaling analysis on the Merced River, the dry season and spring recession functional flow components stand out as substantially impacted by future climate scenarios. Peak flows and variability in the annual flow regime (measured by CV) are also highly susceptible to increases in future climate scenarios, although to a lesser degree. The dry season and spring recession are highly influenced by annual snowmelt, which is widely understood to be declining and occurring earlier across the mountainous western North America due to decreased winter snow accumulation and a shift in precipitation phase from snow to rain (Lundquist et al. 2009; Mote et al. 2018; Stewart, Cayan, and Dettinger 2005). Storms and subsequent peak flows, often caused by atmospheric river events on North America's west coast, are already increasing in severity across western North America (Das et al. 2011; Gershunov et al. 2019). These functional flow components and the species most dependent on them are considered particularly vulnerable as expected changes in snowmelt runoff and storm severity continue.

Flow metrics related to the spring recession and dry season flow components exhibit the most substantial changes across both RCP4.5 and RCP8.5 emissions scenarios in the Sierra Nevada analysis, and particularly in temperature increase scenarios in the Merced River case study. Timing of both flow components shift significantly earlier across models in both

emissions scenarios; the average timing of spring recession and dry season start dates shifts 3-4 weeks earlier in the RCP8.5 future period of 2035-2100 (2-3 weeks earlier in RCP4.5). These changes in seasonality could affect entire ecosystems, and may be evident through impacts to species such as amphibians that breed during snowmelt recession flows (Yarnell, Viers, and Mount 2010), migratory salmonids (Keefer, Peery, and Caudill 2008), and riparian vegetation that requires both gradual snowmelt flow declines and sustained dry season baseflows to establish (Mahoney and Rood 1998). Several changes anticipated for the dry season in California streams may compound to create severe conditions for riverine species during dry years. Results from the Sierra Nevada watersheds indicate that dry season flow magnitude will decline while the duration could increase anywhere between a few days and several weeks. These conditions could threaten coldwater species such as anadromous salmonids, which have evolved a migratory life history to avoid exposure to warm stream temperatures during summer months (P. B. Moyle et al. 2013). Annual peak flows and stream flashiness, as measured by CV, were also found to increase across most models and catchments. A periodic disturbance regime of high flows may be beneficial for creating new habitat and inundating floodplains in California streams (Junk, Bayley, and Sparks 1989; Lytle and Poff 2004). However, if frequency or magnitude of flood flows exceeds historic occurrence, excessive scouring could cause channel degradation and incision (Simon and Rinaldi 2006). Increases in scouring flows could also harm stream macroinvertebrates, which are vulnerable to effects of shear stress (Puijalon and Bornette 2013).

While a growing body of research anticipates the effects of climate change on river ecosystems, these effects must be contextualized in the existing state of alteration of most populated watersheds (Guitron 2020). In present conditions, human impacts on aquatic ecosystems such as dams and diversions often create much greater hydrologic alterations than

the gradually changing flow patterns accompanying climate change (Dyer et al. 2014; Liang et al. 2015; Mittal et al. 2016). In some systems, the primary effects of climate change may be human responses in water management, such as an increase in dry-season diversions to offset increasing frequency of droughts. Changing stream conditions may also compound alterations already caused by dams, impoundments, and urbanization (Dey and Mishra 2017). In addition to severe worldwide threats from freshwater habitat alteration (Vorosmarty et al. 2010), river biota may be especially vulnerable to climate change because of their limited mobility to migrate as environmental conditions shift (O'Briain 2019).

2.5.3 The functional flows approach

Applying a functional flows approach (Escobar-Arias and Pasternack 2010; Yarnell, Viers, and Mount 2010) enabled us to explicitly link a suite of potential climatic changes to potential ecological effects. This study identified for the mid-elevation Sierra Nevada that the functional flows most vulnerable to climate change are the dry season, the spring recession, and peak flows. Within these functional flows, specific metrics were particularly vulnerable to change. For example, the magnitude and start timing of the spring recession shifted considerably, while the duration and rate of change were less affected. Conversely, most dry season metrics including median magnitude, start timing, and duration, were highly sensitive to climate changes. The approach also identified functional flow components relatively unaffected by changing climate conditions, which included the fall pulse flow and certain aspects of the wet season. Each of the functional flow characteristics identified as vulnerable to climate change in this study can be linked to ecological functions for the western Sierra Nevada study region to serve as a guide

for mitigation strategies. This prioritization of management needs according to functional flows could help focus conservation efforts on at-risk ecological functions. This would allow water managers to anticipate the effects of climate changes on river ecosystems and more efficiently allocate resources to mitigate consequences.

2.5.4 Management Implications

While dams have profoundly altered streamflow regimes and disrupted native fish assemblages in California and globally (L. R. Brown and Bauer 2010; Vorosmarty et al. 2010), flow regulation may also provide an opportunity to recreate natural flow patterns and buffer stream biota from impending climate changes (Kondolf, Podolak, and Grantham 2013). In historically snowmelt-driven systems, dam outflows can be adjusted to provide spring recession flows with the timing, magnitude, and rate needed to protect native biota based on the functional flows. On the Truckee River, a snowmelt-fed system in the eastern Sierra Nevada, dam regulation to preserve spring recession flows has proven successful for enhancing native trout and riparian cottonwood populations (S. B. Rood et al. 2003). In streams with low dry season baseflows, further decreases in dry season flow due to climate change, as found in this study, could strand fish or create no-flow periods. Allocating reservoir releases to support instream flows during dry periods is a potential adaptation strategy, although this could create conflict with agricultural water needs, which are also greatest during dry periods (Aldous et al. 2011). Reservoir releases of cold water to support instream flow conditions during dry periods may provide the added benefit of buffering coldwater species such as salmon from climate change-induced warming (Null et al. 2013). As climate change continues to threaten vulnerable

freshwater ecosystems, dam regulation (potentially up to and including dam removal) may become an increasingly necessary strategy to preserve freshwater biodiversity.

2.6 Conclusions

The results of this study demonstrate how ecologically relevant aspects of the annual flow regime are expected to shift in mid-elevation seasonally snowmelt-dominated catchments in California. This study represents the first utilization of the SFDA to analyze climate change with a functional flows approach. The combination of two very different approaches in climate change research - GCM analysis and decision scaling - allowed for a robust investigation into both physically-based future climate scenarios, and the individual climate parameters that most strongly influence streamflow. The precipitation variability component of our decision scaling gave new insight into event-, seasonal-, and interannual-scales of precipitation variability, and demonstrated how it may compound climate change effects caused by temperature increase or precipitation volume change. The direction of future changes in streamflow are found to be relatively consistent across the western Sierra Nevada although the magnitude of changes will depend on rates of human emissions in the future, as shown by the differences in functional flow metric outcomes between RCP4.5 and RCP8.5 scenarios. We found temperature to be the most influential aspect of climate change affecting ecologically-relevant streamflow, although precipitation variability magnified changes caused by temperature increase. The greatest changes in ecologically-relevant streamflow manifested as longer and drier dry season conditions, earlier snowmelt pulse, and higher magnitude peak flows. Findings from this research are informative for water managers considering methods to buffer freshwater biota from the potentially harmful

effects of climate change, and this approach demonstrates how to combine multiple analytical methods for an improved understanding of various aspects of climate change on freshwater ecosystems. The analytical approach used in this study can serve as a model for combining different approaches in hydroclimatic studies to better understand both the drivers and outcomes of streamflow change in a warming climate.

2.7 Data Availability

All software created by the authors for this publication, including processed data and figures, is available as an archived Github repository at https://zenodo.org/badge/latestdoi/444150938, via DOI: 10.5281/zenodo.5815719 \cite{patterson_2022}. The software is copyrighted under the MIT license. We thank Iman Mallakpour for providing daily streamflow projections for sites across northern California, which were developed by Scripps Institute of Oceanography (http://loca.ucsd.edu/). We also thank Ben Livneh and colleagues for making their gridded hydrometeorological dataset publicly available, which we used for decision scale modeling in the Merced River Basin (Livneh et al. 2015). We are also grateful to Wyatt Arnold for providing access and guidance for using the SAC-SMA-DS model (Schwarz et al. 2018), archived publicly at https://gitlab.com/cadwr-climate-change/sac-sma-decision-scaling. Each dataset used for this study is publicly available.

Chapter 3

Dendrochronology reveals the response of a riparian forest to water management policies in an arid basin

3.1 Abstract

Riparian corridors in arid climates sustain life in otherwise inhospitable environments, creating zones of ecological and cultural importance. However, rivers in arid climates are often managed to provide water for human populations at the expense of a river's freshwater biodiversity. Environmental flows are an increasingly common tool for supporting ecosystems on regulated rivers, though their usefulness is best understood by linking streamflow to measured ecological response. In this study, ecosystem response to environmental flows is assessed using

mature cottonwood tree-ring growth and carbon isotope concentrations as bio-indicator proxies for river ecosystem health. We examine the ecological impacts of environmental flows on the Lower Truckee River, in Nevada, USA, an arid climate river that has been subject to decades of heavy diversion and management. Tree-ring width and carbon isotope concentrations in tree-ring tissue provide two separate proxies for tree response to water availability. Annual flow records upstream and downstream from the river's primary diversion point are assessed with a recently developed tool providing functional flow metrics to quantify changing in streamflow patterns. Most long-lived trees downstream of diversions responded strongly to changes in flow management, with significant increases in health proxies and growth increases of 157%. Dry season flow magnitude had the strongest influence on cottonwood growth out of the tested functional flow metrics, although modeling indicated a strong influence of factors outside of streamflow. Not all trees within a floodplain respond similarly to changes in flow metrics, suggesting that trees may draw from different water sources. Results offer promising evidence that environmental flows can lead to measurable improvement in riparian forest productivity, although site-specific considerations including channel form and location on the floodplain are important in determining response to changes in flow patterns.

3.2 Introduction

Rivers worldwide and particularly in arid environments have experienced profound levels of human alterations that affect flow patterns, channel form, and species composition (Grill et al. 2019; Kondolf, Podolak, and Grantham 2013; Vorosmarty et al. 2010). River alterations commonly resulting from dams, such as disruption of natural flow, sediment, and chemical

regimes, threaten freshwater biodiversity on continental and global scales (Maavara et al. 2020; Magilligan and Nislow 2005; N Leroy Poff et al. 2007). River ecosystem health depends on numerous interacting physical and biogeochemical processes involving flow, sediment and temperature regimes, water quality, channel form and floodplain connection, and vegetation composition (N. LeRoy Poff and Ward 1989; Wohl et al. 2015). Native species with sensitive habitat requirements, known as bio-indicators, are therefore often used to gauge the health of altered river ecosystems, because these species respond to a wide range of environmental influences that determine their abundance (Huang et al. 2013; Norris and Thoms 1999). Pairing bio-indicator abundance with physical habitat indicators such as streamflow metrics creates a more robust measurement of river ecosystem health and effects of alteration.

Trees are a particularly useful bio-indicator; through annual growth rings trees record their response to environmental conditions across their lifetime, which can range from decades to centuries. In arid environments where water availability is a limiting growth factor, tree-ring widths tend to correlate with water availability, recording a tree's response to drought conditions (Meko et al. 2015). Cottonwood trees (*Populus spp.*) dominate floodplain habitats in many arid regions of the Northern Hemisphere (Friedman et al. 2005), and their extent covers most of the United States and Canada (Cooke and Rood 2008). Cottonwoods can be an excellent bio-indicator species for ecohydrological analysis, because their life history and growth are closely tied to flow regime patterns, providing an ecological record of past hydrologic conditions on the floodplain (S. Rood et al. 2013). Cottonwood trees are also a keystone species of floodplains across North America, providing habitat, food sources, and temperature regulation of riparian and instream ecosystems (Cooke and Rood 2008; Hillman et al. 2016; Beechie et al. 2010).

Cottonwood trees in arid regions tend to be facultative phreatophytes, meaning they are deep-rooted and rely on groundwater for survival, such as river-supported groundwater (Rood, Bigelow, and Hall 2011). Cottonwoods cannot survive long without continuous access to root water, and mortality has been documented on numerous occasions where cottonwoods lost access to a stable water supply (Foster, Mahoney, and Rood 2018b; Rood, Braatne, and Hughes 2003; Schook et al. 2020; Scott, Shafroth, and Auble 1999; Stella et al. 2013). In addition to river-supported groundwater, cottonwoods have been found to source water from shallow soil water delivered through precipitation or overbank flooding (Phelan, Pearce, and Rood 2022). Plasticity of rooting structures within species indicates an ability to adapt to local water availability (Rood, Bigelow, and Hall 2011).

In arid regions, cottonwood growth rings often correlate with streamflow availability (Schook et al. 2016; Foster, Mahoney, and Rood 2018b), although this relationship is not conclusive in all studies (Scott et al. 1999, St. George 2014). Other cottonwood bio-indicator metrics such as the ratio of ^{13}C to ^{12}C in tree-ring cellulose are related to water stress in arid environments, and can be used alongside ring widths to improve understanding of biological response to water availability (Schook et al. 2020). Studying cottonwood-flow interactions gives insight into what river conditions are favorable for riparian ecosystems, which is especially instructional in human-managed river systems.

Streamflow metrics can be paired with bio-indicators to better understand how particular aspects of streamflow affect river ecosystems. Selecting appropriate streamflow metrics to assess river ecological status and set restoration targets has been the focus of many studies (Poff et al. 1997; Carlisle et al. 2017; Olden and Poff 2003; Yarnell et al. 2020). Functional flows theory has emerged in recent years as an approach to understanding river flow and alterations by linking

specific components of annual flow regimes to ecology-supporting functions (Escobar-Arias and Pasternack 2010; Yarnell et al. 2020). Functional flows refer to the magnitude, timing, duration, frequency, or rate of change of specific seasonal flows, and support processes such as habitat formation and sediment movement, maintenance of chemical and temperature regimes, and life history cues such as migration and spawning (Yarnell et al. 2020). In California, functional flows have been applied to distinguish natural flow regimes (Patterson et al. 2020), to predict functional flow requirements for ungaged streams (Grantham et al. 2022), and have been paired with macroinvertebrate abundance metrics to assess hydrologic alteration (Steel et al. 2018).

An important application of river health assessment is designing or evaluating environmental flow programs. Environmental flows are prescribed streamflow patterns on regulated rivers meant to sustain river ecosystems while balancing human water needs (Arthington et al. 1992; Glenn et al. 2017). Restoration of riparian corridors and fisheries have been attempted on dammed rivers using environmental flow programs, though results are often mixed (Glenn et al. 2017; Konrad et al. 2011; Olden et al. 2014). In some cases, insufficient monitoring of river health takes place following environmental flow implementation, which limits the ability to adapt and learn from these experimental flows (Glenn et al. 2017).

The objective of this study is to assess ecosystem response to environmental flows using mature cottonwood tree-ring growth and carbon isotope concentrations as bio-indicator proxies for river ecosystem health. We examine the ecological impacts of river diversions through various periods of flow regulation, including the return of streamflow after decades of heavy diversion. We ask three research questions, outlined in Table 3-1.

Table 3-1. Research questions and testing.

Research question	Analytical method	Quantitative test to answer research question
Q1. Among 16 total functional flow metrics, which were most affected by river diversions and subsequent environmental flows?	Regime shift analysis on each functional flow metric time series to determine the year of greatest shift and degree of change, in percent and absolute value.	Functional flow metrics are ranked by the percent magnitude of their regime shift and interpreted by this ranking.
Q2. How strong was the response of mature cottonwood trees to environmental flows, comparing between trees upstream and downstream of primary river diversions?	Tukey's Honestly Significant Difference test applied to determine significant changes in growth or carbon isotope discrimination before and after 1973 (for DS trees) or 1982 (for US trees).	A significant increase or decrease response from a majority of trees is interpreted as a strong response. A significant increase or decrease among 25-50% of trees is considered some response. Less significant response than this is interpreted as no clear response from trees.
Q3. What aspects of streamflow and climate are the most influential on mature cottonwood growth?	Bayesian hierarchical model developed to relate cottonwood growth with potential environmental influences.	For output parameter distributions, record the percentage of parameters whose 95% credibility range does not overlap with zero across the 82 tested trees. Significance above 10% is considered relatively high influence, from 5-10% is considered moderate influence, and below 5% is considered low influence.
Q4. How do different periods of flow regulation affect the influence of streamflow and climate on mature cottonwood growth?	Bayesian hierarchical model parameters are categorized by regulation period before and after 1973 (for DS trees) or 1982 (for US trees) so that differences in parameter values can be compared.	Compare the percent significant response calculated in Q3 between tree growth in periods before and after 1973/1982. When the difference in percent significance for a given parameter is double or higher, this is considered a large difference in influence between regulation periods. A difference between 25-50% is considered some difference in influence between regulation periods, and less than this is interpreted as no clear difference between regulation periods.

We hypothesize that increases in streamflow following decades of heavy diversions caused sustained shifts in functional flow metrics, leading to measurable improvements in mature cottonwood growth and health. We expect that metrics describing the spring recession and dry season will have a significant influence on cottonwood growth, since these flows may affect growing season conditions.

Our functional flow approach to assessing streamflow, paired with annual tree-ring width, will allow for a seasonal-scale analysis of flow and ecological effect in a level of detail not before possible. The additional measure of carbon isotope concentrations in tree-ring wood adds strength to the analysis and may reveal tree responses not apparent from tree-ring width alone. While many systems have been studied for the ecological effects of stream dewatering, this study system offers the unique opportunity to investigate the effects of both dewatering and the reintroduction of streamflow through environmental flow policies.

3.3 Methods

3.3.1 Study Area

The Truckee River is an interstate river crossing through California and Nevada, USA, acting as a link between its source in the northern Sierra Nevada mountains and its terminus at Pyramid Lake in the Great Basin Desert (Figure 3-2). The river supports riparian ecosystems along its entire 195-km length, but the environment shifts dramatically as the river passes east of Truckee Meadows into the rain shadow of the Sierra Nevada. Mean temperature in this area ranges from 0°C in January to 23°C in July, though temperature increases are apparent over the

last thirty years (Figure 3-1). Mean annual precipitation varies from 50 in/year in the basin's Sierra Nevada headwaters to 7 in/year in the desert east of Reno, NV.

On the 95-km river segment downstream of Reno, known as the Lower Truckee River, the river is low-angle, alluvial, and meandering, although portions of the channel have been straightened and entrenched for flood control (US Army Corps of Engineers 1995). Average annual river flow at the Reno, NV USGS gage (#10348000) is about 20 cms, and peak flows (in the top 5th percentile) reach above 70 cms. These highest magnitude floods are primarily caused by heavy rainfall or rain-on-snow events (Adams 2012). In the vegetated reaches of the Lower Truckee River, Fremont cottonwoods and willows populate the riparian corridor. Cottonwoods serve as the only native tree and the foundational species of the lower river's floodplain habitat.

The Truckee River has been subject to more than a century of heavy flow modifications (US Army Corps of Engineers 1995; Gourley 1998; Kramer 1988). Several dams regulate flow on major tributaries of the Truckee River and together have a significant effect on mainstem flow. The largest flow alteration on the lower river is the Newlands Irrigation Project, constructed in 1905, which diverts flow at Derby Dam to agricultural areas in the Carson Valley to the south. Diversions for agriculture continued uncontested for several decades, causing the Lower Truckee River to run dry annually (Kramer 1988).

By the 1970's, the Lower Truckee riparian corridor had experienced considerable ecological decline. The previously expansive riparian cottonwood forests had diminished to leave only discontinuous relict stands, without new cohorts to replace aging trees (Rood et al. 2003). Prolonged river diversions also caused Pyramid Lake levels at the river's outlet to drop severely, bringing native cui-ui fish and Lahontan Cutthroat Trout nearly to extinction (Gourley 1998).

At this time, increased attention to the river system's ecological damage began leading to policy changes to promote restoration. In 1973, a lawsuit by the Pyramid Lake Paiute Tribe resulted in the Gesell Opinion (U.S. District Court in Washington, D.C.), which required all river flows beyond allocations for the Newlands Project to remain instream to support Pyramid Lake and its fisheries (Horton 1997; Kramer 1988). This achievement resulted in significant increases in flow along the final 60 km of the river, and mostly ended the seasonal dewatering of the river in this corridor (Figure 3-1). In 1982, an additional landmark lawsuit filed by the Pyramid Lake Paiute Tribe led to the implementation of an environmental flow regime operated from Stampede Reservoir, a major tributary dam, to support Pyramid Lake fisheries with enhanced spring snowmelt flows (Kramer 1988). In the 1990's, these spring recession flows were refined with a deliberate ramping rate to achieve a water stage decline of approximately 1 cm per day (Rood et al. 2003). This rate was designed to support cottonwood seedling survival according to the cottonwood recruitment box model (Rood et al. 2003). Both 1973 and 1982 marked historic changes in the Lower Truckee River's regulated flow regime. These dates are therefore used as a focus in streamflow and dendrochronological analysis in this study.

Since establishment of the environmental flow regime, aerial imagery has recorded remarkable recovery of riparian cottonwood populations through new seedling recruitment, especially where paired with physical channel restoration (Rood et al. 2003). For example, The Nature Conservancy implemented restoration projects in the study area between 2003-2006 (Peternel-staggs, Saito, and Fritsen 2008). These restoration efforts focused on channel grading to raise the streambed, re-establishment of meandering, creation of side pools, and native revegetation, with a goal of laterally reconnecting the channel and floodplain (Peternel-staggs, Saito, and Fritsen 2008).

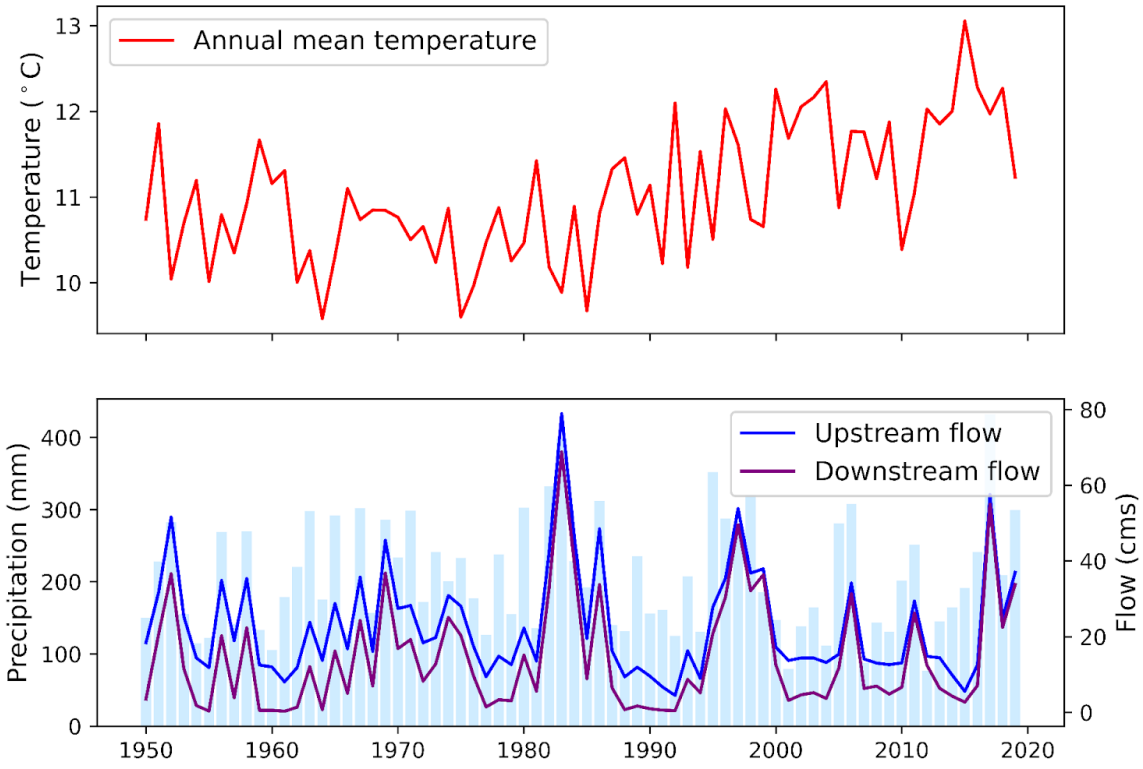

Figure 3-1. Annual temperature, streamflow, and precipitation patterns for the Lower Truckee River since 1950. Streamflow is plotted for gages above and below Derby Dam, the river's primary diversion point.

3.3.2 Experimental Design

The four study questions (Table 3-1) are addressed by analyses on either functional flow metrics or tree-ring derived data. Along with these primary analyses, some supporting data analysis and visualization is also described below in more detail.

3.3.3 Site Selection

Study sites were selected at five separate cottonwood groves along the Lower Truckee River to compare ecological response across varying hydrologic influences (Figure 3-2). Three sites are above Derby Dam, the river's primary diversion point, and two sites are below. All five sites are downstream of Stampede Reservoir. Of the three upstream sites, sites US-1 and US-2 are at The Nature Conservancy's channel restoration sites, while site US-3 is near the Ranch 102 restoration area but has not undergone any physical channel restoration.

The two downstream sites, DS-1 and DS-2, are both on Pyramid Lake Paiute Tribe land. The two sites are 30-km apart. They have distinct channel form and substrate compositions although their flow patterns are similar. Site DS-1 is along a single-strand, somewhat narrow portion of river channel, with cobbles present on the point bar. DS-2 is along a slightly wider portion of river with a sandbar present, with finer sand substrate on the floodplain based on observation.

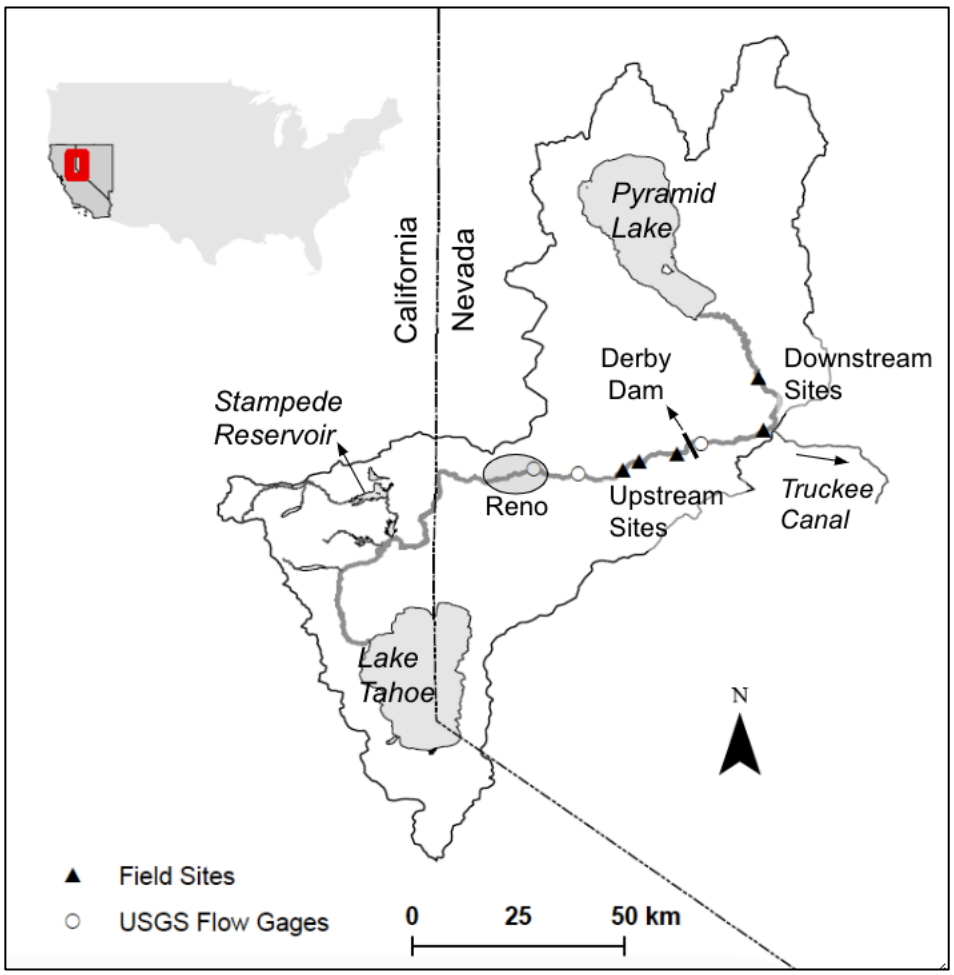

Figure 3-2. Map of the Truckee River Basin, with cottonwood field sites marked. The Truckee River flows from Lake Tahoe northeast to Pyramid Lake, and the Lower Truckee River begins downstream of the Reno metropolitan area. The upstream sites are labeled US-1-3, in order from upstream to downstream, and the downstream sites are labeled DS-1 and DS-2, also from upstream to downstream.

3.3.4 Hydrology and Climate Data

Daily streamflow data for the Lower Truckee River was available from long-term USGS streamflow gages above and below the Derby Dam diversion point (Figure 3-2). Above Derby Dam, gages representing flow at the upstream sites is primarily drawn from the Truckee River at

Vista (#10350000), with some gaps in the record filled with the nearby Reno gage (#10348000) using a linear regression ($r^2 = 0.975$). Flow representing the downstream sites comes from the Truckee River gage below Derby Dam (#10351600). After filling gaps, both gages had periods of record beginning in 1918 that were analyzed until 2019 to align with collected tree-ring data.

Daily flow data was processed using the Seasonal Flows Detection Algorithm using parameters adjusted for the Low Volume Snowmelt and Rain natural flow class to calculate 18 annual functional flow metrics (Patterson et al. 2020). These metrics describe the magnitude, timing, duration, frequency, and rate of change of five functional flow components identified for Mediterranean climate regions: 1) fall pulse, 2) wet season baseflow, 3) peak flows, 4) spring recession, and 5) dry season baseflow that each serve ecological purposes as described in (Yarnell et al. 2020). The functional flow components and associated functional flow metrics used in this study are visualized in Figure 3-3.

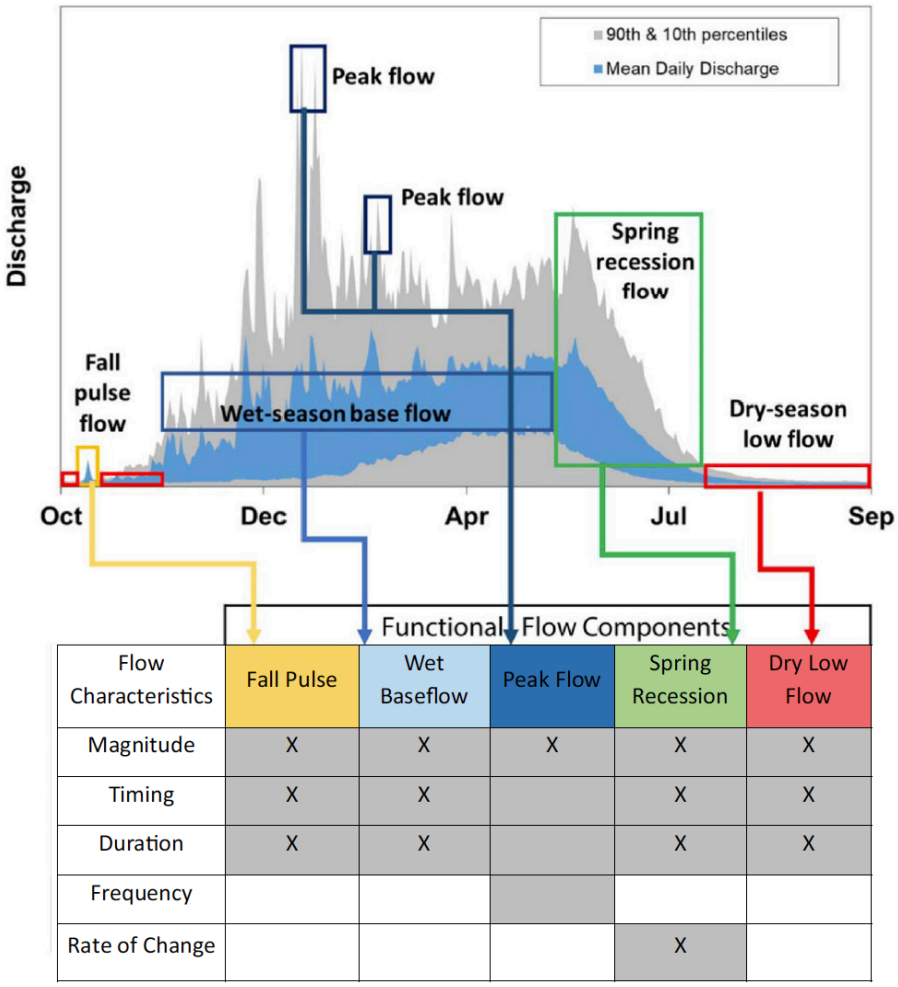

Flow Characteristics	Fall Pulse	Wet Baseflow	Peak Flow	Spring Recession	Dry Low Flow
Magnitude	X	X	X	X	X
Timing	X	X		X	X
Duration	X	X		X	X
Frequency					
Rate of Change				X	

Figure 3-3. Five functional flows (boxes) for a mixed snowmelt-rain runoff regime typical of the mid-elevation Sierra Nevada region capture aspects of the hydrograph most relevant for ecological systems. Functional flow characteristics corresponding to each component are shaded, and metrics used in this study are marked with an X. Figure adapted from Yarnell et al. (2020).

In addition to daily streamflow data from gages, this study measured water surface elevations at each site approximately monthly in 2020 to develop a stage-stage rating curve. These curves were created by pairing gage height at the nearest USGS gage station with water

level measurements at each field site (Figure 3-4). The stage-stage curves were used to ensure that water level measured at long-term gaging stations would be a reasonable representation of conditions at each study site. Plots of the stage-stage curve for each study site are in the Supplemental Materials.

Two shallow groundwater wells were installed on the floodplain near the river's edge, one above Derby Dam at US-2 and one below at DS-1. The wells were instrumented with unvented data loggers (Level Troll 400, In-Situ, Inc.) to measure water level at 15-minute intervals. An In-Situ BaroTroll was installed at one of the sites to adjust water level measurements for atmospheric pressure. Data from the shallow wells allow a direct connection to actual tree-available water and how it fluctuates along with river water level. These findings are included in the interpretation of our modeling to link tree growth to river flow.

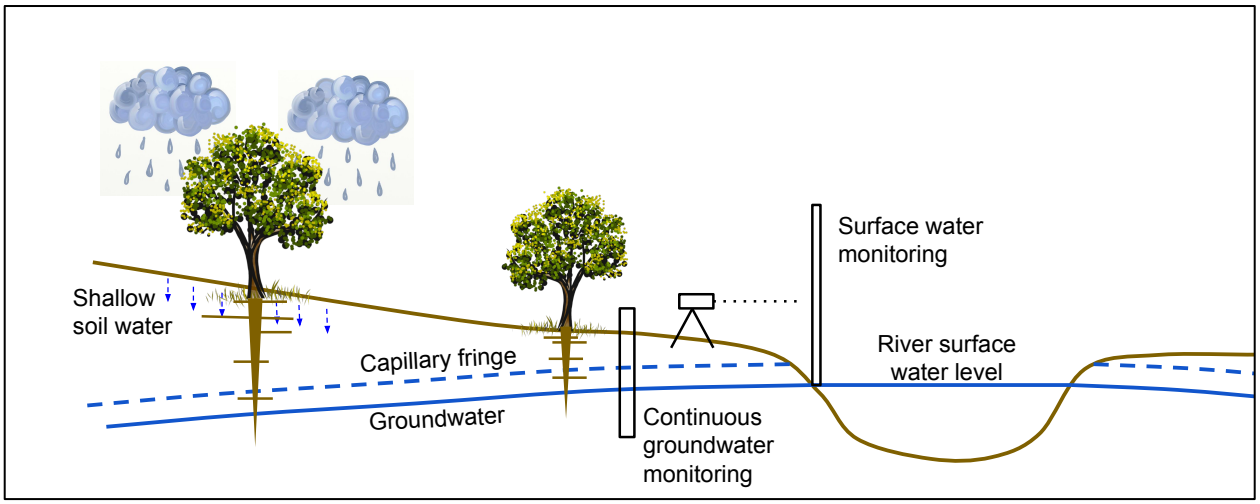

Figure 3-4. Schematic of the study field sites and the potential water sources available to floodplain cottonwoods. Shallow roots may have access to soil water recharged from precipitation, and deep roots access river-supported groundwater or the capillary fringe. Continuous groundwater monitoring at shallow wells was performed at two sites, and periodic measurements of river surface water level were taken at all sites.

3.3.5 Dendrochronology

Tree cores were collected from the five sites along the Lower Truckee River during the summer of 2020. Cores were collected from about 20 trees at each site, for 100 total individuals. Subsequent inspection of tree-rings and quality control required removing 18 cores, lowering the final total to 82. Trees were selected for coring from those present across the width of the floodplain while walking from the channel to the outer edge of the cottonwood forest, so that selected individuals included a full range of distances from the channel. An effort was made to include the largest trees at each site, although measured trees included a variety of sizes. We prioritized selection of healthy, straight trees without apparent signs of damage, but selection was otherwise random. Information collected for each tree included GPS coordinates, recorded to 5 decimal places with GAIA GPS software on a smartphone (v2022.7, GAIAGPS.com), diameter at breast height, and a categorical assessment of crown fullness. Trees were revisited in the spring of 2021 when flowers were visible to also identify sex of each tree, although many of the trees did not have visible flowers and could not be sexed.

We cored trees with a 5.15mm-diameter Haglof increment borer at the lowest level on the trunk permitting borer handle rotation. Duplicate cores were taken at roughly 25% of trees at each site. Collected cores were mounted on wooden mounts and sanded with progressively finer grits down to 30 microns. Prepared cores were then cross-dated using skeleton plots (Stokes and Smiley 1968), followed by ring width measurement using a dissecting microscope and Velmex sliding scale with MeasureJ2X software. Ring width results were quality controlled using COFECHA, achieving series intercorrelation values of 0.3-0.6 for each site (Holmes 1983).

We then converted the resulting radial increment measurements to basal area increment (BAI), as BAI tends to remain constant over time, while radial increments decrease over time as tree diameter increases. BAI was calculated using measured trunk diameter and radial increments in the dplyr package in R (A. G. Bunn 2010). Bark width was removed from dbh measurements using a regression of bark width and dbh created from a sample of trees measured across the study area.

Because cottonwoods' trunks become buried over time by floodplain deposits, the earliest rings on record from ground-level increment boring can be considered a lower limit on tree age, with a high likelihood that full excavation methods would reveal additional rings and an earlier establishment age. Since the goal of this study was to examine growth and stress over time, and not to assess establishment conditions, we use growth records as measured without extra efforts to determine establishment date.

3.3.5.1 Stable carbon isotope discrimination

A subset of tree cores were tested for stable carbon isotope discrimination ($\Delta^{13}C$) in individual growth rings (n=402). Trees from US-1, US-3, and DS-5 were used for testing because these sites had the best series intercorrelation. The four best-correlated, longest-lived trees at each of the three sites were selected for a pooled site measurement of $\Delta^{13}C$ across the trees' shared growth period (54-90 years each). Between four and six trees is considered a reliable sample size for $\Delta^{13}C$ measurements (Leavitt 2010).

In addition to the pooled sampling strategy, two trees from the US-3 pool were measured individually. The individuals were located in two different areas of the floodplain, one close to the channel and one further out on the floodplain by about 25 meters. These two trees were

measured individually so that potential differences in $\Delta^{13}C$ could be examined based on floodplain location.

To prepare samples for testing, purified cellulose was extracted from ring wood samples to remove potential age effects that can occur when testing raw wood samples (Friedman et al. 2019). α-cellulose extraction was performed using an adaptation of methods from Leavitt and Danzer (1993) and Rinne et al. (2005). Samples were packaged in 4×6mm tin capsules and analyzed at the University of California, Davis Stable Isotope Facility using continuous flow ratio mass spectrometry with a PDZ Europa ANCA-GSL elemental analyzer interfaced to a PDZ Europa 20-20 mass spectrometer. Final delta values were reported relative to the Vienna Pee Dee Belemnite international isotope reference according to the equation:

$$\delta^{13}C = \left({R_{sample}}/{R_{standard}}\right) - 1 * 1000 \quad (1)$$

where $\delta^{13}C$ is the reported stable carbon isotope output, R_{sample} is the $^{13}C/^{12}C$ ratio in the tree-ring samples, and $R_{standard}$ is the Vienna Pee Dee Belemnite $^{3}C/^{12}C$ ratio. $\delta^{13}C$ values were then converted to carbon isotope discrimination values ($\Delta^{13}C$) according to Farquhar et al. (1982):

$$\Delta^{13}C = \delta^{13}C_{air} - {\delta^{13}C_{plant}}/{1} + {\delta^{13}C_{plant}}/{1000} \quad (2)$$

In the equation for carbon isotope discrimination, annual values of $\delta^{13}C_{air}$ account for changes in atmospheric carbon dioxide due to global fossil fuel emissions over time, called the Suess effect. We used annual values of atmospheric ^{13}C from Dombrosky (2020) for the conversion.

3.3.6 Analyses

3.3.6.1 Q1: Flow regulation effects on hydrology

To quantify changes to streamflow following flow management policies on the Truckee River, we performed a regime shift analysis on each functional flow metric from upstream (Vista gage) and downstream (Below Derby Dam gage) records from 1918-2019. Each metric's record (102 years total) was inspected along a 60-year sliding window (split into two intervals of 30 years each), and the window containing the greatest difference in paired interval conditions was identified as the record's regime shift point. Percentage change across the metric record from before and after the regime shift was quantified, to compare the relative strength of each metric's shift.

3.3.6.2 Q2: Flow regulation effects on tree growth

We tested BAI from each tree and $\Delta^{13}C$ from select trees for significant changes in growth caused by river regulation using Tukey's honestly significant difference (HSD) statistical test. Tukey's HSD tests for a statistically significant difference in means between two populations, and significance was set as a threshold of $p<0.05$. For each tree, the two comparison populations were grouped by separating annual BAI before and after 1973 for sites below Derby Dam, and before and after 1982 for upper sites. We required a minimum of 15 years for each testing pool to eliminate potential age-related growth effects as well as trends associated with short-term climate fluctuations. This limited the analysis to trees with BAI records beginning at

or before 1967 or 1958, for upstream or downstream trees respectively. In total, 16 trees from the upstream sites and 14 trees from the downstream sites were suitable for the analysis. Trees at site US-2 all had records beginning after 1967 and were therefore not included.

3.3.6.3 Bayesian hierarchical model

To model cottonwood annual BAI based on hydrologic and climatic influences, we assumed a normal distribution of growth such that:

$$BAI_{i,t,r} \sim Normal\left(\mu_{i,s(t),r}, \sigma\right) \quad 3$$

in which growth is indexed based on individual trees (t), which are nested into categories of site (s, out of five total sites) and regulation period (r) in a hierarchical framework. Regulation periods are defined differently for sites upstream and downstream of Derby Dam, based on important policy dates which are confirmed by detectable changes in annual hydrologic metrics. For upstream sites, regulation periods are split before and after 1982, and for downstream sites, regulation periods are defined before and after 1973. We defined the mean (μ) as a linear mixed-effects model with varying coefficients (β terms) and a random effect (α term):

$$\mu_{i,s(t),r} = \alpha_{s(t(i)),r(i)} + \beta_{1s(t(i)),r(i)}P_i + \beta_{2s(t(i)),r(i)}T_i + \beta_{3s(t(i)),r(i)}VPD_i + \beta_{5-18s(t(i)),r(i)}Q_{5-18} \quad 4$$

where T= temperature, P=precipitation, VPD=vapor pressure deficit, and Q5-18 represent the suite of functional flow metrics calculated from annual flow hydrographs and described in Figure 3-3.

With a large set of input flow variables, it is likely that the statistical significance quantified for each variable represents partial influence on growth in cases where correlated variables share a path of influence on tree growth. Therefore, a sensitivity analysis was performed in which alternate versions of the Bayesian model were run with different combinations of variables, to account for potential masking of variables significance by removing correlated variables. Alternate model versions were designed to highlight metrics from a particular functional flow component, removing the metrics from other components. Two additional models were also designed to highlight temperature and vapor pressure deficit variables by removing most other variables. Results from the primary model described in Equation 1 are presented in the main text, and further description and outputs for the alternate models are in the Supplemental Materials.

The model was implemented as a linear mixed-effects model in a Bayesian framework. We specified standard, vague priors with normal distributions centered around either -1, 0, or 1 based on the direction of influence each variable was expected to have on tree growth. Models were implemented in RJAGS, an open-access software package designed for Bayesian data analysis in the R statistical programming language (Plummer 2003). JAGS uses Markov chain Monte Carlo (MCMC) methods to sample model parameter values from their joint posterior distribution. For each model, four parallel MCMC chains were run until chains were well-mixed, as determined visually from output traceplots. Models were specified with 5000 adaptive iterations and 3000 burn-in iterations (to increase sampling efficiency), a thinning interval of 20

(to reduce autocorrelation), and a total sampling number of 1000. We calculated the mean of the posterior distribution for each model parameter and the 95% credible interval defined between the 2.5th-97.5th percentiles.

Precipitation, temperature, and VPD were all considered as variables in the Bayesian model. Modeled monthly values of precipitation, temperature (both average and maximum) and VPD (both average and maximum) were obtained from PRISM (Daly et al. 2008) across a set of 14 4km grids, averaged to cover a continuous reach of the Lower Truckee River including all study sites. Precipitation was considered as both a cumulative annual value over the water year and a cumulative value over the growing season months (April-July). All model variables were standardized (by subtracting the mean and dividing by the standard deviation) to allow for direct comparisons between parameters in the posterior samples. BAI, the outcome variable, was first log-transformed and then standardized.

The Widely Acceptable Information Criterion (WAIC) measures model predictive accuracy while accounting for model complexity and was used to score model performance (McElreath 2020). A lower WAIC score indicates better predictive accuracy, although values are best used as relative comparisons between models of similar structure. WAIC scores for the primary model and the alternates are presented in the Supplemental Materials (Table A3-3).

3.3.6.3.1 Q3: Streamflow and climate influence on cottonwood growth

We determined significance for each model parameter as whether the 95% credible interval overlapped with zero, where a credible interval containing zero was deemed not significant. To determine the total significance of a given parameter, parameter significance was calculated at the tree level and total significance was reported as a percent (out of 82 individual

trees). These total parameter significance values are reported separately for tree growth in the historic and modern regulation periods, because of differences in parameter values that emerge with this distinction. The importance of each streamflow and climate variable was interpreted by its relative ranking among the other tested variables. The analysis of streamflow and climate influence primarily focuses on model parameters for the modern regulation period, because the majority of model parameter values for the historic regulation period ranged from very low (<5%) to 0% significance.

3.3.6.3.2 Q4: Effects of regulation period on tree growth influences

Splitting tree growth analyses by historic and modern regulation periods (before and after 1973 for DS trees, 1982 for US trees) allowed us to gain insight into the differences these flow management periods potentially have on cottonwood growth response to environmental conditions. To accomplish this, the total percent significance in parameters for each tree was separated by regulation period, and significance results were compared according to the rubric described in Table 3-1. To further examine differences in flow regulation period, density plots were created for the posterior distribution of certain parameters exhibiting notable difference between historic and modern periods.

3.4 Results

3.4.1 Q1: Flow regulation effects on hydrology

Distinct differences in streamflow patterns above and below the Derby Dam diversion point were apparent through flow daily records. Annual flow patterns varied between historic

and modern periods of flow management, and between wet and dry years (Figure 3-5). Wet water years experienced less flow abstraction overall, and very little during high flow periods. Even in a wet water year such as 1943, however, flows between July-November were nearly eliminated below Derby Dam. In dry years diversions become more apparent as a larger fraction of annual flow, in both historic and modern management. Modern management practices however avoid full dewatering of the lower river, unlike historic practices.

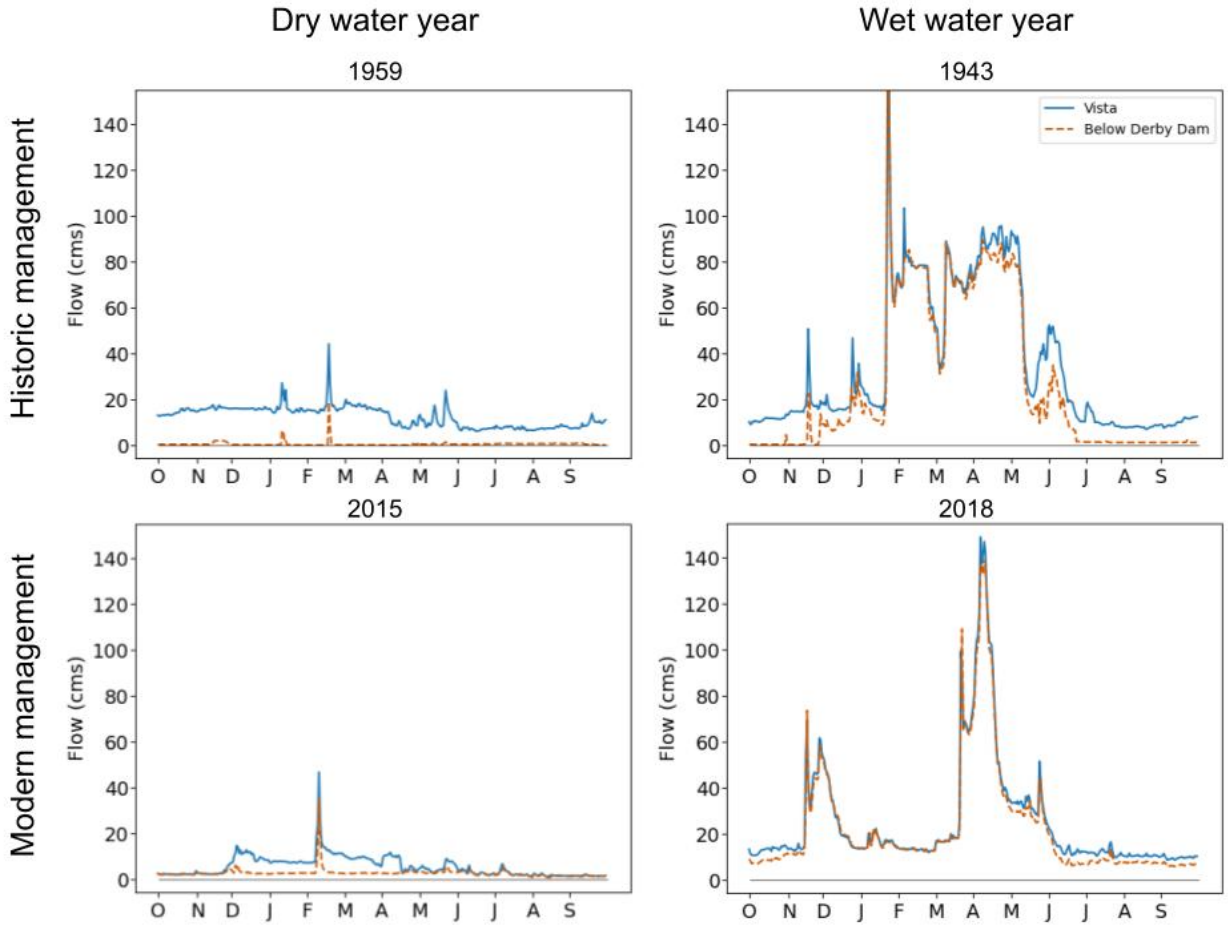

Figure 3-5. Comparisons of streamflow from gages above and below Derby Dam across modern and historic management periods, in select wet and dry water years. Differences in flow between the two gages are predominantly from diversions at Derby Dam.

The regime shift analysis revealed large shifts in dry season magnitude metrics below Derby Dam. 1972 and 1974 emerged as regime shift years for 50th and 90th percentile dry season flow magnitude. Both metrics more than quadrupled in the later regime, increasing by 727% and 318% respectively. These results align strongly with the environmental flows introduced in 1973. Other large metric changes around this shift period included an increase in average annual flow of 77%, a lowering of coefficient of variation (a measurement of stream flashiness) by 45%, an increase in wet season magnitude by 31%, and an increase in wet season duration of 30% (Figure 3-6).

Upstream functional flow metrics did not experience changes as large as downstream, but several metrics changed by more than 10%, with most regime shifts occurring between 1985-1989. The spring recession rate of change lowered by 24% with a regime shift in 1961, though inspection of the plotted records show that a gradual lowering of the spring recession rate of change continued until the mid 1990's. This aligns with flow policies enacted in the mid-1990's to match spring flow recession with the cottonwood recruitment box model described by Rood et al. (2003) (Figure 3-6). Regime shift results for the rest of the functional flow metrics at both streamflow gauges are tabulated in the Supplemental Materials (Table A3-1).

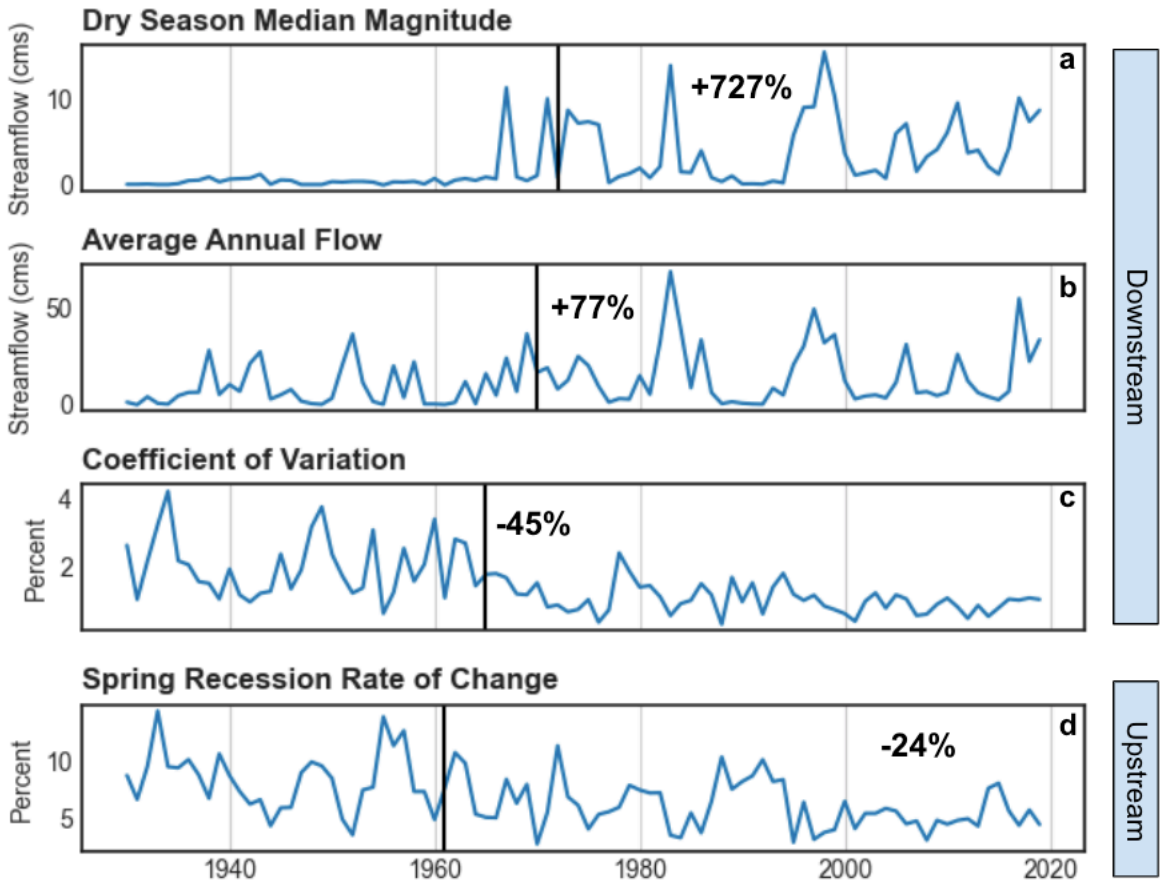

Figure 3-6. Select streamflow metrics show change through time at flow gages above and below Derby Dam. Regime shifts are marked to illustrate where a transition in average flow metric values occurred, and the percent shift in metric value is specified for each flow metric.

Water level measurements taken at each field site were plotted against water level change at the nearest USGS gage site (for upstream and downstream sites) (SM Fig. A3-1 - A3-6). Across the three upstream sites, slopes of water level change varied somewhat, suggesting differences in channel geometry at each site affecting variations in water level with streamflow. Site US-2 had the steepest slope in water level changes, followed by US-1, then US-3. The site-specific slopes of water level rise were all less than the gage slopes, such that an increment of

change in water level at the gage would be 56-80% less at the field sites. The cottonwood sites are generally on open floodplains in wider channels than the constricted channel sites used for USGS gages, so the differences in water level slopes are expected. The two downstream sites differed from each other much more than the upstream sites. DS-2 has a nearly 1:1 ratio of water level change with the nearest USGS gage, while the water level at DS-1 changes at roughly half the rate of the USGS gage. This apparent difference in channel geometry may contribute to differences in tree growth examined in the following sections.

Groundwater measurements from the shallow wells were compared to water level from the nearest gage, with plots available in the Supplemental Materials (A3-7 – A3-8). Groundwater tracked tightly with river surface water levels, revealing matched patterns down to daily resolution. Both river level and groundwater responded similarly to hydrologic events such as winter rainstorms, spring recession, and diurnal fluctuations from snowmelt in the spring or riparian vegetation transpiration in the summer.

3.4.2 Q2: Flow regulation effects on tree health

3.4.2.1 Tree response through basal area increment

Although some years show correlated flow patterns between upstream and downstream trees, over time the two groups exhibited independent growth patterns (Figure 3-7). Growth distinctly rose between 1930 and 1970 at the downstream sites, followed by fairly stable growth at a higher level than the first three decades on record. Growth at the upstream sites has fluctuated over time, occasionally aligning with rises and drops in growth also experienced at the downstream sites. Certain years with notable weather patterns stand out across both groups, such

as a drop in growth in the exceptionally dry year of 1977, and a sharp increase in growth in the record-breaking wet year of 2017.

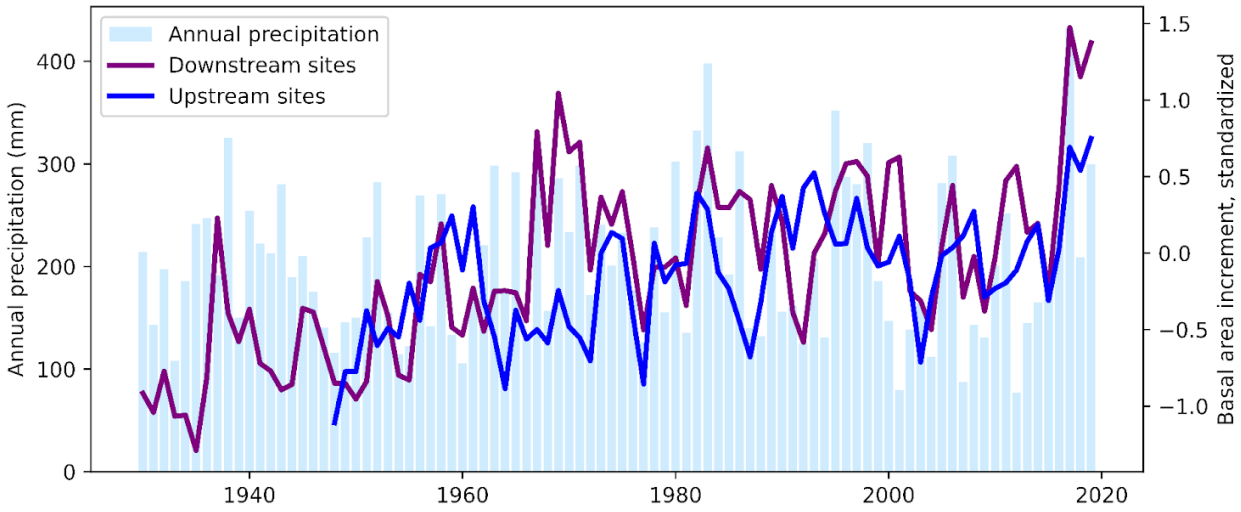

Figure 3-7. Annual basal growth across trees upstream and downstream of Derby Dam, revealing an increased growth trend in downstream trees from 1950-1970.

Outcomes from Tukey's HSD test indicate a clear increase in tree growth at downstream sites after 1973, across the 14 trees tested (Figure 3-8). Ten out of 14 trees (71%) exhibited a significant increase in growth ($p<0.05$), and only one tree experienced a significant decrease. The average growth increase among these trees was 157%, or a nearly three-fold increase in annual growth. Upstream trees were more mixed, with 8 out of 16 trees experiencing significant increase in growth after 1982, and two trees significantly declined in growth. Although $\Delta^{13}C$ measurements available for Tukey's HSD test were limited, their outcomes align with the BAI results. The downstream $\Delta^{13}C$ record showed increase over time, indicating increased health, while the upstream records revealed both increase and decrease in $\Delta^{13}C$ at the two tested sites.

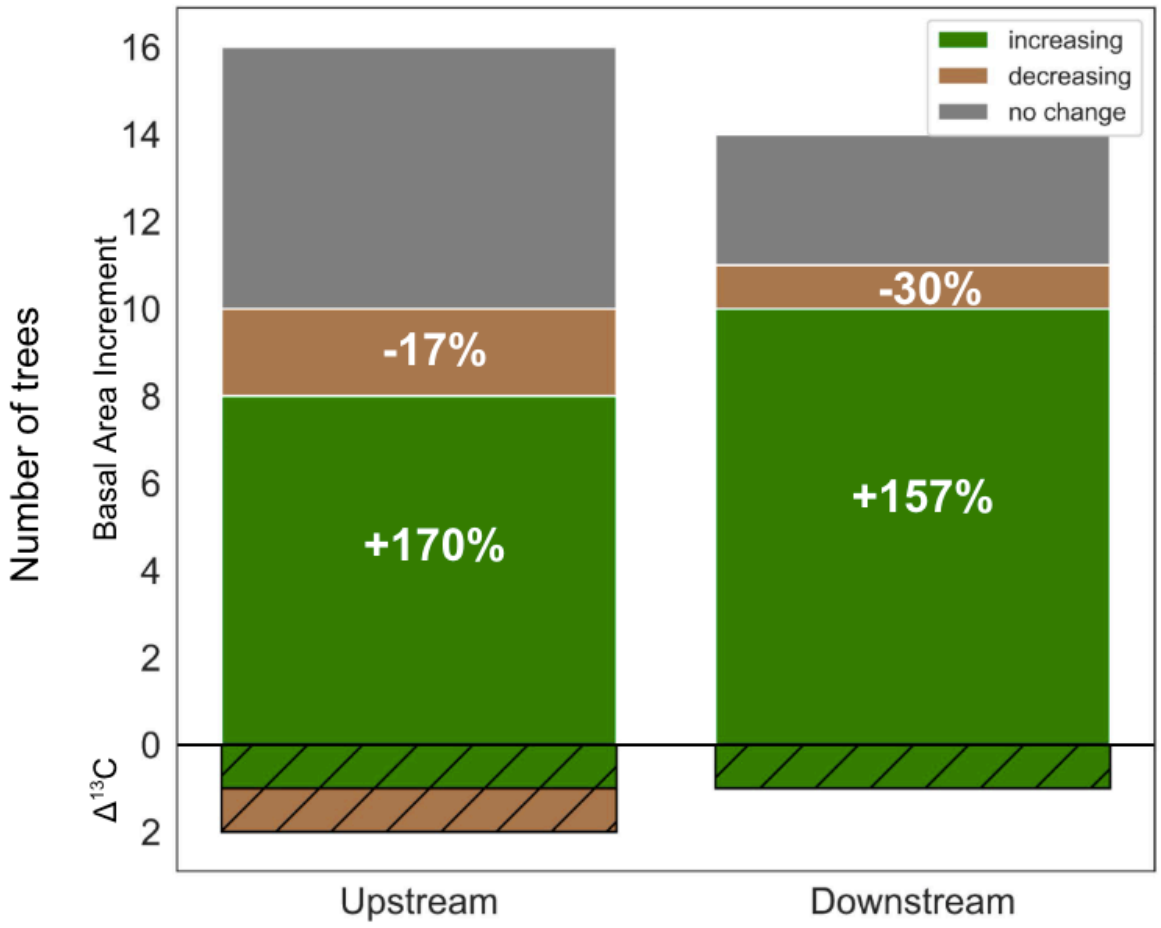

Figure 3-8. Significant changes in growth and $\Delta^{13}C$ (Tukey HSD, $p<0.05$) before and after major environmental flow policy changes across trees in sites upstream and downstream of Derby Dam. The average percent increase or decrease in BAI is noted.

3.4.2.2 Tree response through stable carbon isotope ($\Delta^{13}C$) concentrations

Although $\Delta^{13}C$ measurements were performed on a small subset of annual rings, patterns of $\Delta^{13}C$ concentration revealed responses to streamflow conditions that are less apparent from aggregate BAI analysis. Figure 3-9 illustrates growth and carbon isotope concentrations of four long-lived trees at site DS-2, which exhibit distinct patterns aligning with the 1973 turning point

in flow management. Increases in $\Delta^{13}C$ after 1973 were statistically significant, as confirmed in the Tukey's HSD test. From the beginning of the shared record in 1930, $\Delta^{13}C$ reveals a gradual onset of water stress that began to reverse in the 1970's. Most years in the modern management era show less water stress than the historic era. BAI patterns demonstrate a similar response; very low levels of growth occurred before the 1970's, followed by much higher growth in the modern management period after 1973. Although trees respond to very dry years such as 2008, growth rebounds afterwards, showing a resiliency to drought conditions.

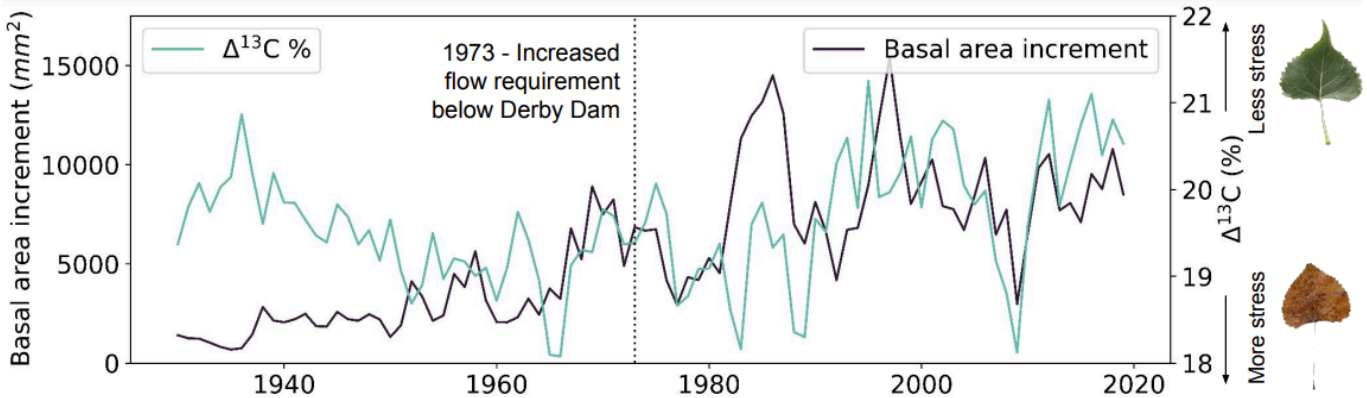

Figure 3-9. Both growth and $\Delta^{13}C$ in select trees below Derby Dam exhibit a clear improvement in health around the time of flow management shifts in 1973.

At US-3, the tree-rings from two individuals were kept separate for $\Delta^{13}C$ measurements (instead of pooling samples as done for other sites) so that differences in $\Delta^{13}C$ dynamics could be compared across individuals of about the same age and size (Figure 3-10). Two broad patterns emerge over time, beginning with a period of distinctly lower absolute value $\Delta^{13}C$ in the tree further from the channel (indicating more water stress), followed by a rise in $\Delta^{13}C$ so that the two trees are well-correlated for the rest of the measured period. The shift in $\Delta^{13}C$ patterns in the tree

further from the channel aligns with a court decision to reoperate flows out of Stampede Reservoir, which controls flow from a major tributary in the upper watershed, to recreate spring snowmelt flows for native fish spawning. Since US-3 is above Derby Dam, the 1973 change in flow patterns did not affect trees at that site. It is possible however that the 1982 shift in flow regulations at Stampede Reservoir may have contributed to this tree's reduction in water stress.

These results also indicate that trees show different levels of stress response to fluctuations in water availability. Since the two trees investigated here are subject to the same streamflow and climate, other tree-specific factors may be affecting individual water availability over time. These factors may include differing groundwater access controlled by rooting depth or location on the floodplain, or stress caused by resource availability or predation. In this example, the tree further from the floodplain appears more responsive to changes in water availability, potentially initiated by a response to changing streamflow patterns.

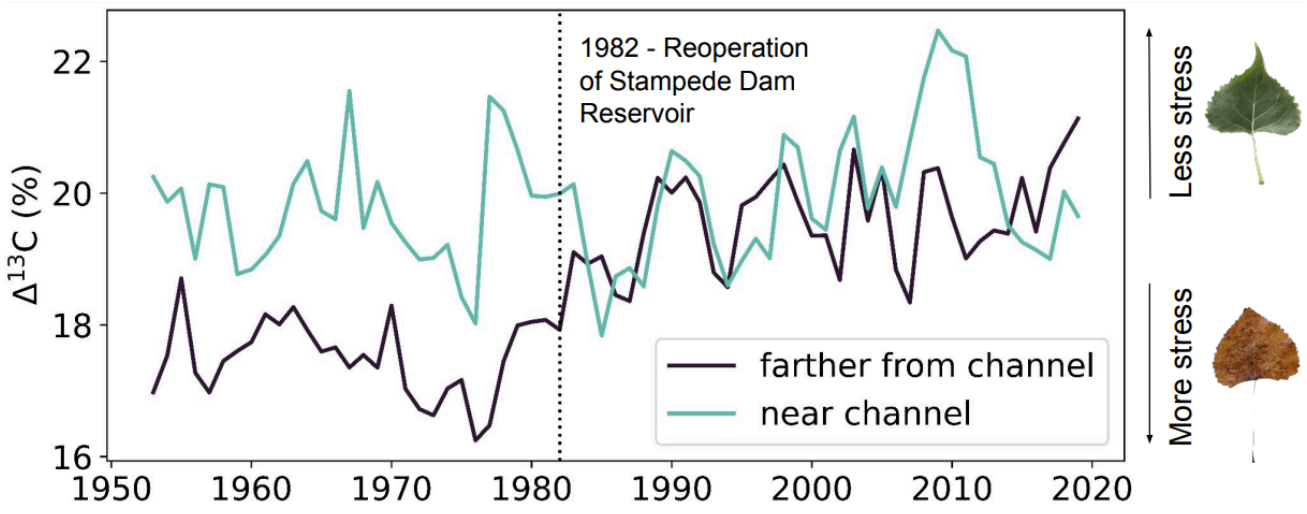

Figure 3-10. $\Delta^{13}C$ for two individual trees upstream of Derby Dam illustrates a period of differing water stress followed by a reduction in water stress for one of the trees, aligning with the reoperation of an upstream dam to provide environmental flows.

3.4.2.3 Q3: Streamflow and climate influences on tree growth

Model performance was first broadly assessed by comparing observed and model-predicted values of log-transformed BAI (Figure 3-11). Values tended to center around a 1:1 line with R^2 of 0.88, indicating fairly accurate model prediction. The root mean squared error percent (RMSPE) of the model was 20.8%. There was no discernible difference in prediction accuracy between BAI values from historic and modern management periods, although modern era BAI values were generally higher. Higher growth in the modern management era may be due to a combination of higher water availability and higher growth in younger trees. This potential juvenile effect was controlled for in modeling by removing the first five years of growth records from each tree.

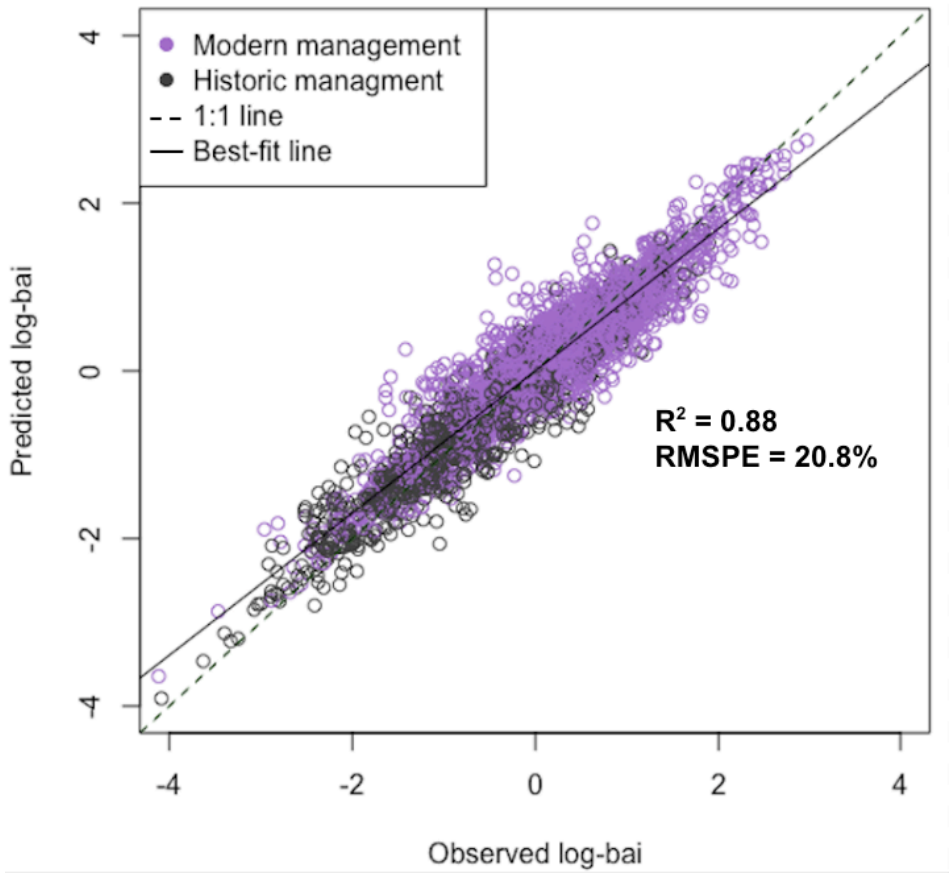

Figure 3-11. Predicted versus observed log-transformed BAI from Bayesian modeling suggests that the model performs well, based on the relatively close adherence to a 1:1 line with $R^2 = 0.88$ and RMSPE of 20.8%.

Across the functional flow metrics and climate variables, significance was low overall. Metrics with the highest parameter significance in the modern regulation era included spring recession rate of change (13%), wet season start timing (12%), wet season magnitude and duration (both 9%), and dry season median magnitude (9%) (Figure 3-12). In the historic regulation era, the metric with the highest parameter significance was average annual flow with a moderate influence at 8%, and all other parameters were at or below 5% significance. Functional flows with the lowest levels of significance across either regulation period included peak flows

(2%) and the fall pulse (0-2%), suggesting these metrics have low influence on mature cottonwood growth. Variables describing climate also had low significance overall (<5%). Interestingly, metrics describing spring recession magnitude, timing, or duration had no influence on tree growth, although rate of change was the most significant parameter in the modern regulatory period.

Differences in tree growth that were not explained by the streamflow or climate variables defined in the models were quantified through random effect coefficients for each tree. Random effects were highly significant across models, with tree-level significance occurring in 46% or 23% of trees in the modern or historic era, respectively (Figure 3-12). Random effects may capture effects unique to each tree such as competition, predation, physical damage, and factors affecting access to water such as rooting depth or localized floodplain conditions. Attempts to discern a correspondence of random effects with distance to the active channel or tree age did not produce apparently significant relationships.

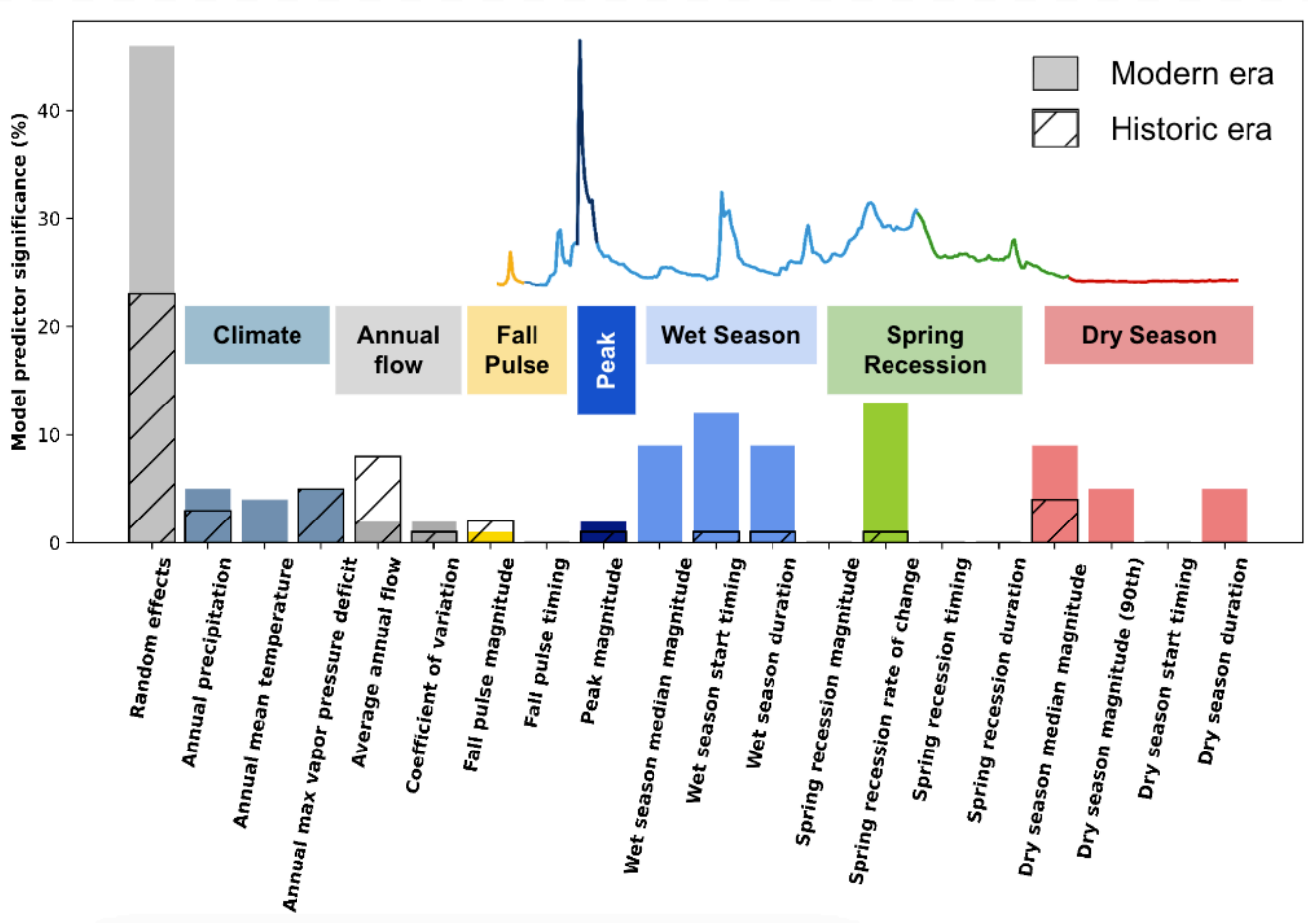

Figure 3-12. Coefficient significance across all model variables, distinguished by parameters for either historic or modern regulation periods. Values are reported as the percent of individual trees with a significant coefficient for the given variables. A model hydrograph is overlaid to visualize the functional flow components represented by streamflow metrics.

3.4.2.4 Q4: Effects of regulation period on tree growth influences

Both site and regulation era were structured as hierarchies in the models, so that differences in streamflow and climate influence could be examined across these categories. Across all sites, parameters were significant 2.6 times more often in the modern regulatory period, versus historic conditions. Parameters for the modern regulation era were more than

double the significance of the historic period for most variables describing the wet season, spring recession, and dry season. However, exceptions to this generality emerge across sites and some variables. In the DS sites, dry season median magnitude and precipitation had higher coefficient values in the historic regulation period, although parameter significance was higher at US sites in the modern period (**Error! Reference source not found.**). The influence of precipitation on g rowth also differs when examining annual or growing season precipitation. In both management eras, annual precipitation has notably more influence on DS-1 growth than growing season precipitation.

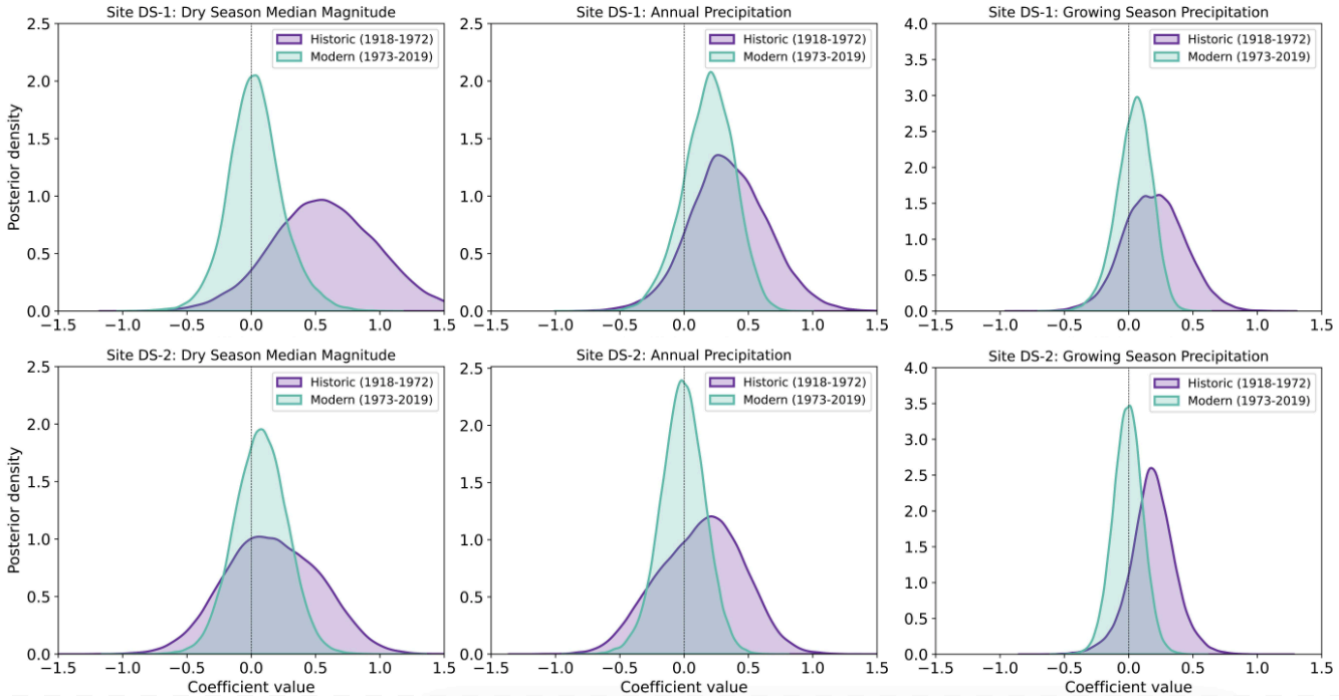

Figure 3-13. Probability densities of model coefficients for median dry season magnitude, annual precipitation, and growing season precipitation at downstream sites, split by flow regulation period, reveal how the importance of these coefficients depends on the regulation period.

3.5 Discussion

In this study we assessed the response of mature cottonwood trees to environmental flow regulations in an arid climate. Analysis of streamflow and dendrochronological records along the Lower Truckee River confirmed our hypothesis that ongoing environmental flows significantly shifted certain streamflow metrics, including dry season flow magnitude, aligning with increases in annual growth and decreases in water stress. However, the importance of certain flow metrics to growth such as wet season metrics did not match our expectations. The close association found between river surface level and shallow groundwater suggests that river flows are the primary control on cottonwood water availability, and supported our approach of linking cottonwood health to streamflow.

For the past three decades, growth across both the upstream and downstream sites has remained fairly stable, with fluctuations that may represent response to water availability and other environmental conditions (Figure 3-7). This contrasts with the historic regulation period before 1973, when growth at the downstream sites was 157% lower in most trees (Figure 3-8) and carbon isotope measurements indicated a sustained increase in water stress at site DS-2 from the start of measurements in 1930 until 1970. None of the study sites exhibited sustained trends of declining growth or increased water stress in response to recent severe droughts such as the 2012-2016 drought, suggesting that mature floodplain trees are resilient to these conditions when provided sufficient environmental flows.

The increase in flow below Derby Dam secured by the Pyramid Lake Paiute Tribe in 1973 was very likely the major driver of improvements in tree growth and health witnessed in the following decades. Our findings build directly on those of Rood et al. (2003), who found that environmental flows set in the 1970's and 1980's improved conditions for recruitment of new cottonwoods. We extend this conclusion with evidence that environmental flows also improved growing conditions for mature cottonwoods downstream of Derby Dam, some of which were declining in health up until the 1970's. Effects on upstream trees are less conclusive, but carbon isotope measurements suggest that some trees may have benefitted from increases in water availability possibly driven by environmental flows established in the upper watershed in 1982.

Functional flow analysis of flow records confirmed large changes in some flow metrics following establishment of environmental flow regulations, especially increases in dry season magnitude downstream of Derby Dam. Cottonwoods require access to water year-round and the relationship of cottonwood growth to groundwater access during dry periods is well-established (Foster, Mahoney, and Rood 2018a; Schook et al. 2022; Stromberg and Patten 1990). Other flow metric changes such as increases in average annual flow and wet season duration were likely also beneficial to cottonwoods, indicated by their moderate to high significance on cottonwood growth in the Bayesian model.

Spring recession rate of change declined significantly over the past several decades to become more gradual, aligning with strategies implemented by agencies operating dams and diversions along the river to provide suitable conditions for cottonwood seedling recruitment (Rood et al. 2003). Gradual spring recession rates have demonstrated importance for many other species aside from cottonwoods seedlings, such as macroinvertebrates (Paetzold, Yoshimura, and Tockner 2008; Steel et al. 2018) and amphibians (Yarnell, Viers, and Mount 2010). The high

influence of spring recession rate of change on mature cottonwood growth in the Bayesian models was unexpected, since the importance of this flow component has usually been associated with cottonwood seedling root growth in the shallow capillary fringe (Foster, Mahoney, and Rood 2018a; Amlin and Rood 2002; Willms, Pearce, and Rood 2006). Mature cottonwoods have been found to access shallow soil water however, especially where groundwater is deep, so it is possible that trees on the Lower Truckee River strategically source from shallow soil water when river flows are high (Williams and Cooper 2005; Snyder and Williams 2000).

Modeling results for the modern regulatory period indicate moderate to high significance of wet season metrics (magnitude, timing, and duration) on tree growth. The relatively high rate of significance across these metrics compared to other functional flows was not expected, especially in comparison to spring recession flows, which occur during annual tree growth. It is possible that aspects of the wet season create favorable growing conditions for cottonwoods that persist beyond the wet season. For example, high correspondence has been found between wet season streamflow and soil moisture, potentially promoting groundwater flow on hillslopes (McNamara et al. 2005, Moore et al. 2011). When winter precipitation and streamflow are not sufficiently high, dry soil regions can prevent this lateral flow (McNamara et al. 2005). It is possible that more sustained wet season conditions at the study sites, indicated by longer and higher magnitude wet seasons, promote hydraulic connection of the stream and floodplain that benefit cottonwood growth during the subsequent growing season.

Dry season flow magnitude had a moderate influence on cottonwood growth, occurring primarily during the modern regulatory period. However, at DS sites most of this influence occurs during the historic management era, when dry season flow magnitudes were severely

limited. Shallow groundwater tables may have dropped below the cottonwood rooting zone for prolonged times during this period, creating the observed growth response. A drop in groundwater levels below the rooting zone has been found in other dewatered streams in arid environments, leading to reduced tree growth (Foster, Mahoney, and Rood 2018a; Schook et al. 2022). When dry season flows were significantly increased in 1973 it is possible that mature cottonwood roots regained perennial connection with the groundwater table, leading to the weakened correspondence with dry season flow magnitude. Rood et al. (2013) similarly found that cottonwoods only responded to streamflow fluctuations in years when water was limited.

Changes in streamflow caused by changes in river regulation in the 1970's and 1980's have clearly contributed to improvements in growth and health in mature cottonwoods based on significant increases in growth and decreases in stress confirmed by Tukey's test. However, modeling points to other environmental factors influencing tree health. Annual precipitation is somewhat significant to tree growth, and the modeling sensitivity analysis suggests that its influence is through paths outside of its direct effect on annual streamflow. The importance of precipitation on cottonwoods is notable given the extremely arid conditions on the Lower Truckee River (about 200mm annually), and suggests that trees may uptake shallow soil water occurring from this low level of precipitation. This aligns with other studies finding an importance in summertime precipitation (Cooper et al. 1999) or shallow soil water for cottonwood water use during dry periods. Cottonwood tree rooting systems include a collar of shallow roots adapted for uptaking shallow soil water originating from precipitation or overbank flows, which provide a different pathway for water availability besides groundwater supported by river flows (Hultine, Bush, and Ehleringer 2010; Phelan, Pearce, and Rood 2022; Williams and Cooper 2005).

Although some consensus exists, trees within a site did not all respond similarly to streamflow and climate influences. Water demand of individual trees may vary due to factors affecting evaporative demand such as light exposure, or stress-inducing factors such as competition or predation (Rood et al. 2013). Groundwater dynamics on the floodplain likely have an important influence on individual tree growth, and the dynamics of this relationship at each site may depend on more complex factors than distance to the channel. Factors affecting tree groundwater availability may include substrate composition, topography of the channel and floodplain, and vegetation composition (Stella et al. 2013). The texture of sediments can influence tree water availability, as fine-textured sediments are more capable of storing plant-available water than sands (Cooper et al. 1999). The differences in stage-discharge relationships at each site may also indicate unique shallow groundwater dynamics that affect tree response to water availability at each site. Groundwater dynamics were not the primary focus of this study and measurement was therefore limited, but further study is an important path for future research. Although there was no clear signal of tree stress at the outer margins of the floodplains, the outer edges of riparian forests in arid environments can be especially vulnerable to water limitation, which in severe cases can lead to riparian corridor narrowing (Rood et al. 2013). An important avenue for further research could also include measurement of water table levels at the floodplain margins.

Although the low significance of functional flow and climate variables suggests importance of other factors influencing growth, it may also indicate limitations in the model structure. An ensemble of variable combinations were tested in different models, but variable significance did not greatly improve across any of these model alternatives. Introducing a lag effect into the model could reveal increased variable significance if water availability has a

multi-year effect on growth (Rood et al. 2013). However, Pearson correlations of model variables on growth for current-year and one-year lags produced weaker correlations for lagged variables than current-year variables, and justified our decision to prioritize regulation period as a primary focus in the hierarchical model. Next steps in future research could include exploring the effects of lagging flow and climate variables in growth models, as well as considering biological growth effects that may strongly influence individual trees.

$\Delta^{13}C$ revealed significant increase in DS tree health after 1973, which further supports the improvement in DS tree health after 1973 indicated by increased growth. However, $\Delta^{13}C$ did not produce a more immediate response to increased flows than growth, as other researchers have witnessed (Schook et al. 2016). It is possible that trees on the Lower Truckee River floodplain have a more stable floodplain water table than the smaller system studied in Schook et al. (2020), and changes in $\Delta^{13}C$ would not appear as abruptly. The individuals measured for $\Delta^{13}C$ at site US-3 gave an indication that variations in tree physiology or groundwater dynamics within the floodplain may play an important role in tree water availability and stress, based on the relative complacency of $\Delta^{13}C$ in the individual closest to the active channel (Figure 3-10). Other studies have found an influence of hydrogeomorphic heterogeneity on cottonwood water availability (Schook et al. 2016; Stella et al. 2013; Willms, Pearce, and Rood 2006). No clear patterns emerged when comparing the growth sensitivity of all trees and their floodplain locations. It is possible that $\Delta^{13}C$ could reveal a trend in water sensitivity based on location not apparent from growth alone, but the cost of $\Delta^{13}C$ measurements limited its application in this study.

The environmental flows established on the Truckee River have been considered a success, based on recoveries of several native riparian and aquatic species (Rood et al. 2003). Environmental flows have been implemented in other arid watersheds of the western U.S. to

restore riparian vegetation, with mixed success (Glen et al. 2017, Williams and Cooper 2005). On the Colorado River, the experimental "Minute 319 Pulse Flow" negotiated in 2014 had less success than expected in its goal of recruiting new cottonwood and willow seedlings, with most of the satellite-measured revegetation diminishing a year after the pulse flow event (Glen et al. 2017). In Alberta, Canada, an environmental flow strategy similar to that on the Truckee River reported more success for cottonwood establishment and growth (Foster et al. 2018). Minimum flows were raised during summer dry conditions, paired with gradual ramping of spring recession flows. Mature cottonwood growth rose following the establishment of environmental flows, which was considered a likely response to the increase in minimum flows (Foster et al. 2018). In these examples, a permanent environmental flows program providing sufficient instream flows during dry periods has benefitted mature cottonwoods, versus experimental flood pulses negotiated on an individual basis. The permanence of environmental flows on the Truckee River has likely contributed to the river's ecological improvement, which has benefitted fish and riparian birds along with riparian vegetation (Rood et al. 2003).

Our study provides strong evidence that degraded riparian corridors can respond positively to environmental management programs that balance ecosystem needs with human needs. Mature cottonwood trees are important to preserve because of their cultural and ecological value, provision as both habitat and food source to riparian and riverine communities (Sabo et al. 2008), and as the source of seed for future cottonwood regeneration. In regions where cottonwood riparian forests have been depleted, manual replanting requires a substantial effort with many seedling mortality risks (Rood et al. 2016). Preserving existing cottonwood forests is therefore a more effective strategy for preserving riparian and riverine ecosystems. Differences in growth and $\Delta^{13}C$ patterns across and within sites, along with high model significance in random effects

suggests that factors affecting individual tree health play an important role in determining cottonwood growth. Site-specific considerations including channel form and individual tree physiology are important in determining response to changes in flow patterns, along with the proven effectiveness of environmental flow implementation.

3.6 Acknowledgements

Funding for this project was provided by the UC Davis College of Agricultural and Environmental Sciences. We thank The Nature Conservancy and the Pyramid Lake Paiute Tribe for permission to conduct research on their land and for their local expertise. Laboratory space, equipment, and guidance for cottonwood sample processing was provided by Dr. Adam Csank at the University of Nevada, Reno. We gratefully acknowledge Dr. Stewart Rood, Charles Gourley, and Lisa Heki for project consultation and shared expertise.

Concluding Remarks

The goal of this dissertation was to quantify and understand hydrologic alteration of rivers and its ecologic effects by characterizing streamflow, using a functional flows approach. Across three chapters of research and five years of effort, tools were developed, tested, and applied to achieve this goal. This work validated functional flows as an effective strategy for ecological streamflow analysis with evidence that they can be used to differentiate California's natural flow regimes, quantify streamflow response to climate change, and reveal the links

between flow management and riparian forest health. Across this dissertation, the importance of seasonal streamflow timing was uniquely recognized for its role in governing life history patterns in aquatic ecosystems. The explicit quantification of functional flow timing achieved with the Seasonal Flows Detection Algorithm (SFDA) allowed for direct assessments of timing alterations in ecologically-relevant flows, which were explored in the subsequent studies.

Chapter 1 details the development of a tool called the Seasonal Flows Detection Algorithm (SFDA), which identifies and quantifies functional flow metrics from daily streamflow time series for flow patterns typical of Mediterranean climates such as California. Although not perfect, the SFDA achieved 90% accuracy in its identification of functional flow components across variable streams and water year types. Through this project, the importance of timing of seasonal flows became apparent. The timing of predictable wet and dry periods in a stream guide life cycle events of aquatic and riparian species such as spawning, seed release, and migration (Gasith and Reth 1999; Lytle and Poff 2004). Proper timing of flow seasons maintain the temperature, nutrient, and biological cycles that freshwater species are adapted to (Yarnell et al. 2015). It became evident through this project that accurately identifying the timing of these seasonal flow transitions is much more challenging than conventional methods of streamflow analysis such as calculating monthly flow averages or annual percentiles of magnitude. To meet this challenge, a signal processing method was developed incorporating iterative signal smoothing, windowing, and feature detection, techniques less commonly applied in hydrologic science. The resulting SFDA tool is flexible yet robust, and was used to successfully differentiate natural streamflow classes in California according to their functional flow metrics. Building on this work, Grantham et al. (2022) leveraged functional flow metrics calculated with the SFDA at reference reaches in California to model functional flow ranges for all ungaged stream reaches

across the state. Chapters 2 and 3 of this dissertation featured applications of the SFDA to characterize streamflow and quantify alterations through the lens of functional flows.

In Chapter 2, expected changes to ecologically relevant streamflow due to climate change were quantified for western drainages of the Sierra Nevada mountains, California. This research combined two different techniques for hydrologic climate change analysis, using streamflow routed with climate forcings from 1) a suite of Global Climate Models, and 2) a set of scaled perturbations of temperature, precipitation volume, and precipitation variability (i.e., decision scaling). Perturbations of three different components of precipitation variability allowed a thorough investigation into how expected increases in climate volatility may affect functional flows. The greatest changes in ecologically-relevant streamflow patterns manifest as longer and drier dry season conditions, earlier snowmelt recession, and higher-magnitude peak flows. Of climate parameters explored, air temperature causes the most change in functional flows, although precipitation variability, especially interannual variability, compounds changes driven by air temperature. Notably, the severity of future streamflow change depends heavily on the projected level of human emissions. This research explicitly links climate change to potential aquatic ecosystem risk, and adds to the body of knowledge justifying urgent action to address climate change.

In Chapter 3, dendrochronology was paired with seasonal flow analysis to infer how mature cottonwood trees along the Lower Truckee River, Nevada, respond to climate and water management influences. The Truckee River has a legacy of heavy management including both decades of intensive streamflow diversions and subsequent environmental flows. Cottonwoods clearly responded to environmental flows first established in the 1970's, with both increased growth and decreased water stress. Of the functional flow metrics tested, dry season flow

magnitude was the most altered and subsequently restored with environmental flows, and was moderately linked to cottonwood growth. However, the influence of dry season flow magnitude on cottonwood growth was only present before the onset of environmental flows in trees downstream of flow diversions, suggesting that stable connection of cottonwood roots with the alluvial water table may have been restored with environmental flows. Precipitation also had some influence on cottonwood growth, especially outside of periods of high river flow, which may indicate a preferential use of shallow soil water recharged by precipitation during low flow periods. A surprising connection between spring recession rate of change and mature cottonwood growth was also found, although this flow metric is more commonly associated with establishment of cottonwood seedlings. Functional flow metric analysis allowed for a detailed investigation into streamflow conditions affecting cottonwood growth, and suggested a higher association of growth with metrics in the wet season, spring recession, and dry season functional flow components, which changed over time along with river management periods. This research offers promising evidence that environmental flows can lead to measurable improvement in riparian forest productivity, and showcases this study site as a model for river restoration in other arid watersheds.

Twenty years ago, Postel and Richter (2003) urged that "the time is ripe for a global river restoration movement." This message still resounds today, and the need is greater than ever to preserve and restore river ecosystems. This dissertation advances river science and management using functional flows theory to effectively characterize streamflow patterns with established links to ecological functioning. This theory was tested in the field in a watershed-scale study of streamflow-ecosystem interactions, revealing the ecological effects of an environmental flows program. Functional flows were also applied to determine how ecologically-relevant flows may

shift in a warming climate. The challenges ahead for river management may be great, but with ecologically-founded river science and an openness to truly balance ecosystem needs with human needs, there is certainly hope for a global movement towards river restoration.

References

Aadland, Luther. 1993. “Stream Habitat Types: Their Fish Assemblages and Relationship to Flow.” *North American Journal of Fisheries Management* 13 (4): 790–806. https://doi.org/10.1577/1548-8675(1993)013<0790:shttfa>2.3.co;2.

Abatzoglou, J T, K T Redmond, and L M Edwards. 2009. “Classification of Regional Climate Variability in the State of California.” *Journal of Applied Meteorology and Climatology* 48: 1527–41. https://doi.org/10.1175/2009JAMC2062.1.

Abdi, Hervé, and Lynne J Williams. 2010. “Tukey’s Honestly Significant Difference (HSD) Test.” *Encyclopedia of Research Design*. Thousand Oaks, CA: Sage.

Adamowski, Jan, and Karen Sun. 2010. “Development of a Coupled Wavelet Transform and Neural Network Method for Flow Forecasting of Non-Perennial Rivers in Semi-Arid Watersheds.” *Journal of Hydrology* 390 (1–2): 85–91. https://doi.org/10.1016/j.jhydrol.2010.06.033.

Aguado, E, D Cayan, L Riddle, and M Roos. 1992. “Climatic Fluctuations and the Timing of West Coast Streamflow.” *Journal of Climate* 5: 1468–83.

Ahearn, Dylan S., Richard W. Sheibley, Randy A. Dahlgren, and Kaylene E. Keller. 2004. “Temporal Dynamics of Stream Water Chemistry in the Last Free-Flowing River Draining the Western Sierra Nevada, California.” *Journal of Hydrology* 295 (1–4): 47–63. https://doi.org/10.1016/j.jhydrol.2004.02.016.

Aldous, Allison, James Fitzsimons, Brian Richter, and Leslie Bach. 2011. “Droughts, Floods and Freshwater Ecosystems: Evaluating Climate Change Impacts and Developing Adaptation Strategies.” *Marine and Freshwater Research* 62: 223–31.

Amlin, Nadine M, and Stewart B Rood. 2002. “Comparative Tolerances of Riparian Willows and Cottonwoods to Water-Table Decline.” *Wetlands* 22 (2): 338–46.

Arthington, Angela H., Robert J. Naiman, Michael E. McClain, and Christer Nilsson. 2010. “Preserving the Biodiversity and Ecological Services of Rivers: New Challenges and Research Opportunities.” *Fresh* 55: 1–16. https://doi.org/10.1111/j.1365-2427.2009.02340.x.

Arthington, Angela H, J M King, J H O'Keefe, S E Bunn, A Day, B J Pusey, D R Bluhdorn, and R Tharme. 1992. "Development of an Holistic Approach for Assessing Environmental Flow Requirements for Riverine Ecosytems." In *Proceedings of an International Seminar and Workshop on Water Allocation for the Environment*, 69–76. Centre for Water Policy Research, UNE, Armidale.

Ashraf, F B, Ali Torabi Haghighi, Joakim Riml, Mathias G Kondolf, Bjørn Kløve, and Hannu Marttila. 2022. "A Method for Assessment of Sub-Daily Flow Alterations Using Wavelet Analysis for Regulated Rivers." *Water Resources Research* 58. https://doi.org/10.1029/2021WR030421.

Bart, Ryan, and Allen Hope. 2014. "Inter-Seasonal Variability in Baseflow Recession Rates: The Role of Aquifer Antecedent Storage in Central California Watersheds." *Journal of Hydrology* 519: 205–13. https://doi.org/10.1016/j.jhydrol.2014.07.020.

Booker, D J, and M C Acreman. 2007. "Generalisation of Physical Habitat-Discharge Relationships." *Hydrology and Earth System Sciences* 11 (1): 141–57.

Brown, Casey, Yonas Ghile, Mikaela Laverty, and Ke Li. 2012. "Decision Scaling: Linking Bottom-up Vulnerability Analysis with Climate Projections in the Water Sector." *Water Resources Research* 48: 1–12. https://doi.org/10.1029/2011WR011212.

Brown, Larry R, and Marissa L Bauer. 2010. "Effects of Hydrologic Infrastructure on Flow Regimes of California's Central Valley Rivers: Implications for Fish Populations." *River Research and Applications* 26: 751–65. https://doi.org/10.1002/rra.

Bumash, R. J.C., R. L. Ferral, and R. A. McGuire. 1973. "A General Stream Flow Simulation System-Conceptual Modeling for Digital Computers." Report by the Joint Federal State River Forecasts Center, Sacramento, California.

Bunn, A G. 2010. "A Dendrochronology Program Library in R (DplR)." *Dendrochronologia* 28 (4): 251–58.

Bunn, Stuart E., and Angela H. Arthington. 2002. "Basic Principles and Ecological Consequences of Altered Flow Regimes for Aquatic Biodiversity." *Environmental Management* 30 (4): 492–507. https://doi.org/10.1007/s00267-002-2737-0.

Burnett, N J, S G Hinch, N N Bett, D C Braun, M T Casselman, S J Cooke, A Gelchu, S Lingard, C T Middleton, and C F H White. 2017. "Reducing Carryover Effects on the Migration and

Spawning Success of Sockeye Salmon through a Management Experiment of Dam Flows." *River Research and Applications* 33: 3–15. https://doi.org/10.1002/rra.3051.

Buttle, J M. 2011. "Streamflow Response to Headwater Reforestation in the Ganaraska River Basin, Southern Ontario, Canada." *Hydrological Processes* 25: 3030–41. https://doi.org/10.1002/hyp.8061.

"California Central Valley Unimpaired Flow Data." 2007. Bay-Delta Office; California Department of Water Resources. Sacramento; California. http://www.waterboards.ca.gov/waterrights/water_issues/programs/bay_delta/bay_delta_plan/water_quality_control_plan.

Cambray, J.A. 1991. "The Effects on Fish Spawning and Management Implications of Impoundment Water Releases in an Intermittent South African River." *Regulated Rivers: Research & Management* 6 (1): 39–52. https://doi.org/10.1016/j.otc.2010.04.018.

Cannas, Barbara, Alessandra Fanni, Linda See, and Giuliana Sias. 2006. "Data Preprocessing for River Flow Forecasting Using Neural Networks: Wavelet Transforms and Data Partitioning." *Physics and Chemistry of the Earth* 31 (18): 1164–71. https://doi.org/10.1016/j.pce.2006.03.020.

Carlisle, Daren M., Theodore E. Grantham, Ken Eng, and David M. Wolock. 2017. "Biological Relevance of Streamflow Metrics: Regional and National Perspectives." *Freshwater Science* 36 (4): 927–40. https://doi.org/10.1086/694913.

Carter, David B, and Curtis S Signorino. 2010. "Back to the Future: Modeling Time Dependence in Binary Data." *Political Analysis* 18: 271–92. https://doi.org/10.1093/pan/mpq013.

Cayan, Daniel R, Tapash Das, David W Pierce, Tim P Barnett, Mary Tyree, and Alexander Gershunov. 2010. "Future Dryness in the Southwest US and the Hydrology of the Early 21st Century Drought." *PNAS* 107 (50): 21271–76. https://doi.org/10.1073/pnas.0912391107.

Cayan, Daniel R, and David H Peterson. 1989. "The Influence of North Pacific Atmospheric Circulation on Streamflow in the West." *Geophysical Monograph* 55: 375–97.

"[CCTAG] Climate Change Technical Advisory Group. Perspectives and Guidance for Climate Change Analysis." 2015. Sacramento (CA): California Department of Water Resources, Statewide Integrated Regional Management Division.

Cleaveland, W S, and Clive Loader. 1996. “Smoothing by Local Regression: Principles and Methods.” In *Statistical Theory and Computational Aspects of Smoothing*, 10–49. Physica-Verlag HD. https://doi.org/10.2307/1271204.

Cleland, D.T., J.A. Freeouf, J.E. Keys, G.J. Nowacki, C.A. Carpenter, and W.H. McNab. 2007. “Ecological Subregions: Sections and Subsections for the Conterminous United States.” Washington, DC.

Cooke, Janice E.K., and Stewart B. Rood. 2008. “Trees of the People: The Growing Science of Poplars in Canada and Worldwide.” *Canadian Journal of Botany* 85 (12): 1103–10. https://doi.org/10.1139/b07-125.

Cooper, David J., David M. Merritt, Douglas C. Andersen, and Rodney A. Chimner. 1999. “Factors Controlling the Establishment of Fremont Cottonwood Seedlings on the Upper Green River, USA.” *Regulated Rivers: Research & Management* 15 (5): 419–40. https://doi.org/10.1002/(sici)1099-1646(199909/10)15:5<419::aid-rrr555>3.3.co;2-p.

Craven, Peter, and Grace Wahba. 1979. “Smoothing Noisy Data with Spline Functions - Estimating the Correct Degree of Smoothing by the Method of Generalized Cross-Validation.” *Numerische Mathematik* 31 (4): 377–403. https://doi.org/10.1007/BF01404567.

Cutler, David Richard, Thomas C Edwards, Karen H Beard, Adele Cutler, Kyle T Hess, Jacob Gibson, and Joshua J Lawler. 2007. “Random Forests for Classification in Ecology.” *Ecology* 11: 2783–92. https://doi.org/10.1890/07-0539.1.

Daly, Christopher, Michael Halbleib, Joseph I Smith, Wayne P Gibson, Matthew K Doggett, George H Taylor, Jan Curtis, and Phillip P Pasteris. 2008. “Physiographically Sensitive Mapping of Climatological Temperature and Precipitation across the Conterminous United States.” *International Journal of Climatology*. https://doi.org/10.1002/joc.

Das, Tapash, Michael D Dettinger, Daniel R. Cayan, and Hugo Hidalgo. 2011. “Potential Increase in Floods in California’s Sierra Nevada Under Future Climate Projections.” *Climate Change* 109: S71–94. https://doi.org/10.1007/s10584-011-0298-z.

Déry, Stephen J, Kerstin Stahl, R D Moore, Paul H Whitfield, Brian Menounos, and Jason E Burford. 2009. “Detection of Runoff Timing Changes in Pluvial, Nival and Glacial Rivers of Western Canada,” no. June. https://doi.org/10.1029/2008WR006975.

Dettinger, Michael. 2011. “Climate Change, Atmospheric Rivers, and Floods in California - a Multimodel Analysis of Storm Frequency and Magnitude Changes.” *Journal of the American Water Resources Association* 47 (3): 514–23. https://doi.org/10.1111/j.1752-1688.2011.00546.x.

Dettinger, Michael D., Fred Martin Ralph, Tapash Das, Paul J. Neiman, and Daniel R. Cayan. 2011. “Atmospheric Rivers, Floods and the Water Resources of California.” *Water* 3 (4): 445–78. https://doi.org/10.3390/w3020445.

Dettinger, Michael D. 2016. “Historical and Future Relations Between Large Storms and Droughts in California.” *San Francisco Estuary and Watershed Science* 14 (2): 1–21. https://doi.org/10.15447/sfews.2016v14iss2art1.

Dettinger, Michael, Bradley Udall, and Aris Georgakakos. 2015. “Western Water and Climate Change.” *Ecological Applications* 25 (8): 2069–93.

Dey, Pankaj, and Ashok Mishra. 2017. “Separating the Impacts of Climate Change and Human Activities on Streamflow: A Review of Methodologies and Critical Assumptions.” *Journal of Hydrology* 548: 278–90. https://doi.org/10.1016/j.jhydrol.2017.03.014.

Dhungel, S, D G Tarboton, J Jin, and C P Hawkins. 2016. “Potential Effects of Climate Change on Ecologically Relevant Streamflow Regimes.” *River Research and Applications* 32 (9): 1827–40. https://doi.org/10.1002/rra.

Dombrosky, Jonathan. 2020. “A ~ 1000-Year 13C Suess Correction Model for the Study of Past Ecosystems.” *The Holocene* 30 (3): 474–78. https://doi.org/10.1177/0959683619887416.

Donnenfeld, Zachary, Courtney Crookes, and Steve Hedden. 2018. “A Delicate Balance Water Scarcity in South Africa.”

Dyer, Fiona, Sondoss Elsawah, Barry Croke, Rachael Griffiths, Evan Harrison, Paloma Lucena-Moya, and Anthony Jakeman. 2014. “The Effects of Climate Change on Ecologically-Relevant Flow Regime and Water Quality Attributes.” *Stochastic Environmental Research and Risk Assessment* 28: 67–82. https://doi.org/10.1007/s00477-013-0744-8.

Escobar-Arias, M I, and Gregory B Pasternack. 2010. “A Hydrogeomorphic Dynamics Approach to Assess In-Stream Ecological Functionality Using the Functional Flows Model, Part 1—Model Characteristics.” *River Research and Applications* 26: 1103–28. https://doi.org/10.1002/rra.

Escriva-bou, Alvar, Henry McCann, Ellen Hanak, Jay Lund, and Brian Gray. 2016. “Accounting for California’s Water.” *The California Journal of Politics and Policy* 8 (3): 1–26. https://doi.org/10.5070/P2cjpp8331935.

Falcone, J A, Daren M Carlisle, D M Wolock, and M R Meador. 2010. “GAGES: A Stream Gage Database for Evaluating Natural and Altered Flow Conditions in the Conterminous United States.” *Ecology* 91 (2): 621.

Farquhar, G D, J R Ehleringer, and K T Hubick. 1989. “Carbon Isotope Discrimination and Photosynthesis.” *Annual Review of Plant Physiology and Plant Molecular Biology* 40: 503–37.

Filipe, Ana Filipa, Justin E Lawrence, and Nuria Bonada. 2013. “Vulnerability of Stream Biota to Climate Change in Mediterranean Climate Regions: A Synthesis of Ecological Responses and Conservation Challenges.” *Hydrobiologia* 719: 331–51. https://doi.org/10.1007/s10750-012-1244-4.

Foster, Stephen G., John M. Mahoney, and Stewart B. Rood. 2018a. “Functional Flows: An Environmental Flow Regime Benefits Riparian Cottonwoods along the Waterton River, Alberta.” *Restoration Ecology* 26 (5): 921–32. https://doi.org/10.1111/rec.12654.

Foster, Stephen G, John M Mahoney, and Stewart B Rood. 2018b. “Functional Flows: An Environmental Flow Regime Benefits Riparian Cottonwoods along the Waterton River, Alberta.” *Restoration Ecology* 26 (5): 921–32. https://doi.org/10.1111/rec.12654.

Friedman, Jonathan M, Craig A Stricker, Adam Z Csank, and Honghua Zhou. 2019. “Effects of Age and Environment on Stable Carbon Isotope Ratios in Tree Rings of Riparian Populus.” *Palaeogeography, Palaeoclimatology, Palaeoecology* 524: 25–32. https://doi.org/10.1016/j.palaeo.2019.03.022.

Gasith, Avital, and V H Resh. 1999. “Streams in Mediterranian Climate Regions: Abiotic Influences and Biotic Responses to Predictable Seasonal Events.” *Annual Review of Ecology and Systematics* 30: 51–81.

Gershunov, Alexander, Tamara Shulgina, Rachel E S Clemesha, Kristen Guirguis, David W Pierce, Michael D Dettinger, David A Lavers, et al. 2019. “Precipitation Regime Change in Western North America: The Role of Atmospheric Rivers.” *Scientific Reports (Nature Publisher Group)* 9 (9944): 1–11. https://doi.org/10.1038/s41598-019-46169-w.

Glenn, Edward P., Pamela L. Nagler, Patrick B. Shafroth, and Christopher J. Jarchow. 2017. "Effectiveness of Environmental Flows for Riparian Restoration in Arid Regions: A Tale of Four Rivers." *Ecological Engineering* 106: 695–703. https://doi.org/10.1016/j.ecoleng.2017.01.009.

Godsey, S E, J W Kirchner, and C L Tague. 2014. "Effects of Changes in Winter Snowpacks on Summer Low Flows: Case Studies in the Sierra Nevada, California, USA." *Hydrological Processes* 28: 5048–64. https://doi.org/10.1002/hyp.9943.

Gourley, Chad R. 1998. "Restoration of the Lower Truckee River Ecosystem: Challenges and Opportunities." *Journal of Land, Resources, and Environmental Law* 18 (1): 113–22.

Grantham, Theodore E, Daren M Carlisle, Jeanette Howard, Robert Lusardi, Alyssa Obester, Samuel Sandoval-solis, Bronwen Stanford, et al. 2022. "Modeling Functional Flows in California's Rivers." *Frontiers in Environmental Science* 10 (787473): 1–11. https://doi.org/10.3389/fenvs.2022.787473.

Grantham, Theodore E W, Daren M Carlisle, Gregory J Mccabe, and Jeanette K Howard. 2018. "Sensitivity of Streamflow to Climate Change in California." *Climatic Change* 149: 427–41.

Greet, Joe, J Angus Webb, and Roger D Cousens. 2011. "The Importance of Seasonal Flow Timing for Riparian Vegetation Dynamics: A Systematic Review Using Causal Criteria Analysis." *Freshwater Biology* 56: 1231–47. https://doi.org/10.1111/j.1365-2427.2011.02564.x.

Grill, G, B Lehner, M Thieme, B Geenen, F Tickner, S Antonelli, S Babu, P Borreli, and C Zarfl. 2019. "Mapping the World's Free-Flowing Rivers." *Nature* 569 (215–221). https://doi.org/10.1038/s41586-019-1111-9.

Guitron, Daisy. 2020. "Hydrologic Classification of Altered Rivers in California." Master's Thesis. University of California, Davis.

Gyalistras, Dimitrios, Hans Von Storch, Andreas Fischlin, and Martin Beniston. 1994. "Linking GCM-Simulated Climatic Changes to Ecosystem Models: Case Studies of Statistical Downscaling in the Alps." *Climate Research* 4: 167–89.

Hall, Francis R. 1968. "Base-Flow Recessions—A Review." *Water Resources Research* 4 (5): 973–83. https://doi.org/10.1029/WR004i005p00973.

Hamlet, Alan F., Philip W. Mote, Martyn P. Clark, and Dennis P. Lettenmaier. 2005. "Effects of Temperature and Precipitation Variability on Snowpack Trends in the Western United States." *Journal of Climate* 18 (21): 4545–61. https://doi.org/10.1175/JCLI3538.1.

Hanak, Ellen. 2011. *Managing California's Water: From Conflict to Reconciliation*. Public Policy Instit. of CA.

Hastie, T J, and R Tibshirani. 1990. *Generalized Additive Models*. Chapman and Hall.

He, Minxue, Michael Anderson, Andrew Schwarz, Tapash Das, Elissa Lynn, Jamie Anderson, Armin Munévar, Jordi Vasquez, and Wyatt Arnold. 2019. "Potential Changes in Runoff of California's Major Water Supply Watersheds in the 21st Century." *Water* 11 (1651).

Henriksen, By James A, John Heasley, Jonathan G Kennen, and Steven Nieswand. 2006. "Users' Manual for the Hydroecological Integrity Assessment Process Software (Including the New Jersey Assessment Tools)."

Hillman, E J, S G Bigelow, G M Samuelson, P W Herzog, T A Hurly, and S B Rood. 2016. "Increasing River Flow Expands Riparian Habitat: Influences of Flow Augmentation on Channel Form, Riparian Vegetation and Birds Along the Little Bow River, Alberta." *River Research and Applications* 32: 1687–97. https://doi.org/10.1002/rra.

Holmes, R L. 1983. "Computer-Assisted Quality Control in Tree-Ring Dating and Measurement." *Tree-Ring Bulliten* 43: 69–78.

Horton, Gary. 1997. "Truckee River Chronology: A Chronological History of Lake Tahoe and the Truckee River and Related Water Issues." Carson City.

Horton, Robert E. 1941. "An Approach toward a Physical Interpretation of Infiltration-Capacity 1." *Soil Science Society of America Journal* 5 (C): 399–417.

Huang, Wei, Shinichiro Yano, Jianmin Zhang, and Yurong Wang. 2013. "Application of Analytic Hierarchy Process in Selecting a Biological Indicator for a River Flow Restoration." *Ecological Indicators* 25: 180–83. https://doi.org/10.1016/j.ecolind.2012.09.017.

Hultine, K R, S E Bush, and J R Ehleringer. 2010. "Ecophysiology of Riparian Cottonwood and Willow before, during, and after Two Years of Soil Water Removal." *Ecological Applications* 20 (2): 347–61.

IPCC. 2015. "Climate Change 2014: Synthesis Report. Contribution of Working Groups I, II and

III to the Fifth Assessment Report of the Intergovernmental Panel on Climate Change." [Core Writing Team; R.K. Pachauri and L.A. Meyer (eds.)]. IPCC, Geneva, Switzerland.

Jacobson, R B. 2013. "Riverine Habitat Dynamics." In *Treatise on Geomorphology*, edited by J J Shroder, D Butler, and C Hupp, 6–19. San Diego, CA: Academic Press. https://doi.org/10.1016/B978-0-12-374739-6.00318-3.

Janert, Philipp K. 2010. *Data Analysis with Open Source Tools*. 1st ed. O'Reilly Media, Inc.

Jones, E, T Oliphant, and P Peterson. 2001. "SciPy: Open Source Scientific Tools for Python." Online; accessed 2017-09-21. http://www.scipy.org/.

Junk, Wolfgang J, Peter B Bayley, and Richard E Sparks. 1989. "The Flood Pulse Concept in River-Floodplain Systems." *Canadian Special Publication Fisheries and Aquatic Sciences* 106: 110–27. https://doi.org/citeulike-article-id:3662134.

Kakouei, Karan, Jens Kiesel, Sami Domisch, Katie S Irving, Sonja C Jähnig, and Jochem Kail. 2018. "Projected Effects of Climate-Change-Induced Flow Alterations on Stream Macroinvertebrate Abundances." *Ecology and Evolution* 8: 3393–3409. https://doi.org/10.1002/ece3.3907.

Keefer, Matthew L, Christopher A Peery, and Christopher C Caudill. 2008. "Migration Timing of Columbia River Spring Chinook Salmon: Effects of Temperature, River Discharge, and Ocean Environment." *Transactions of the American Fisheries Society* 137 (4): 1120–33. https://doi.org/10.1577/T07-008.1.

Kennard, Mark J, Stephen J Mackay, Bradley J Pusey, Julian D Olden, and Marsh Nick. 2010. "Quantifying Uncertainty in Estimation of Hydrologic Metrics for Ecohydrological Studies." *River Research and Applications* 26: 137–56. https://doi.org/10.1002/rra.1249.

Kimball, B. A. 1976. "Smoothing Data with Cubic Splines." *Agronomy Journal* 68: 126–29.

Koczot, K.M., J.C. Risley, J.M. Gronberg, J.M. Donovan, and K.R. McPherson. 2021. "Precipitation-Runoff Processes in the Merced River Basin Central California, with Prospects for Streamflow Predictability, Water Years 1952 – 2013: U.S. Geologic Survey Scientific Investigations Report 2020 – 5150." https://doi.org/10.3133/ sir20205150.

Kondolf, G Mathias, Kristen Podolak, and Theodore E Grantham. 2013. "Restoring Mediterranean-Climate Rivers." *Hydrobiologia* 719: 527–45. https://doi.org/10.1007/s10750-012-1363-y.

Konrad, Christopher P, Julian D Olden, David A Lytle, Theodore S Melis, John C Schmidt, Erin N Bray, Mary C Freeman, et al. 2011. “Large-Scale Flow Experiments for Managing River Systems.” *BioScience* 61 (12): 948–59. https://doi.org/10.1525/bio.2011.61.12.5.

Kormos, Patrick R, Charles H Luce, Seth J Wegner, and Wouter R Berghuijs. 2016. “Trends and Sensitivities of Low Streamflow Extremes to Discharge Timing and Magnitude in Pacific Northwest Mountain Streams.” *Water Resources Research* 52: 4990–5007. https://doi.org/10.1002/2015WR018125.Received.

Kramer, John. 1988. “Lake Tahoe, the Truckee River, and Pyramid Lake: The Past, Present, and Future of Interstate Water Issues.” *Pacific Law Journal* 19 (4): 1339–90.

Kusche, J, R Schmidt, S Petrovic, and R Rietbroek. 2009. “Decorrelated GRACE Time-Variable Gravity Solutions by GFZ, and Their Validation Using a Hydrological Model.” *Journal of Geodesy* 83: 903–13. https://doi.org/10.1007/s00190-009-0308-3.

Ladochy, Steve, Richard Medina, and William Patzert. 2007. “Recent California Climate Variability: Spatial and Temporal Patterns in Temperature Trends.” *Climate Research* 33: 159–69.

Lane, Belize A., Helen E. Dahlke, Gregory B. Pasternack, and Samuel Sandoval-Solis. 2017. “Revealing the Diversity of Natural Hydrologic Regimes in California with Relevance for Environmental Flows Applications.” *Journal of the American Water Resources Association* 53 (2): 411–30. https://doi.org/10.1111/1752-1688.12504.

Lane, Belize A, Samuel Sandoval-solis, Eric D Stein, Sarah M Yarnell, Gregory B Pasternack, and Helen E Dahlke. 2018. “Beyond Metrics? The Role of Hydrologic Baseline Archetypes in Environmental Water Management.” *Environmental Management* 62 (4): 678–93. https://doi.org/10.1007/s00267-018-1077-7.

Leavitt, Steven W. 2010. “Tree-Ring C–H–O Isotope Variability and Sampling.” *Science of the Total Environment* 408: 5244–53. https://doi.org/10.1016/j.scitotenv.2010.07.057.

Leavitt, Steven W, and S R Danzer. 1993. “Method for Batch Processing Small Wood Samples to Holocellulose for Stable Isotope Analysis.” *Analytical Chemistry* 65: 87–89.

Letcher, R. A., S. Yu Schreider, A. J. Jakeman, B. P. Neal, and R. J. Nathan. 2001. “Methods for the Analysis of Trends in Streamflow Response Due to Changes in Catchment Condition.” *Environmetrics* 12 (7): 613–30. https://doi.org/10.1002/env.486.

Liang, Wei, Dan Bai, Zhao Jin, Yuchi You, Jiaxing Li, and Yuting Yang. 2015. "A Study on the Streamflow Change and Its Relationship with Climate Change and Ecological Restoration Measures in a Sediment Concentrated Region in the Loess Plateau, China." *Water Resources Management* 29: 4045–60. https://doi.org/10.1007/s11269-015-1044-5.

Liu, Dedi, Yao Xu, Shenglian Guo, Lihua Xiong, Pan Liu, and Qin Zhao. 2018. "Stream Temperature Response to Climate Change and Water Diversion Activities." *Stochastic Environmental Research and Risk Assessment* 32: 1397–1413. https://doi.org/10.1007/s00477-017-1487-8.

Liu, Zhu, Jonathan D Herman, Guobiao Huang, Tariq Kadir, and Helen E Dahlke. 2021. "Identifying Climate Change Impacts on Surface Water Supply in the Southern Central Valley, California." *Science of the Total Environment* 759: 1–14. https://doi.org/10.1016/j.scitotenv.2020.143429.

Livneh, B, T J Bohn, D S Pierce, F Munoz-Ariola, B Nijssen, R Vose, D Cayan, and L D Brekke. 2015. "A Spatially Comprehensive, Hydrometeorological Data Set for Mexico, the U.S., and Southern Canada 1950-2013." *Nature Scientific Data* 5 (150042). https://doi.org/doi:10.1038/sdata.2015.42.

Lohmann, D, E Raschke, B Nijssen, and D P Lettenmaier. 1998. "Regional Scale Hydrology: I . Formulation of the VIC-2L Model Coupled to a Routing Model." *Hydrological Sciences Journal* 43 (1): 131–41. https://doi.org/10.1080/02626669809492107.

Lundquist, Jessica D., Paul J. Neiman, Brooks Martner, Allen B. White, Daniel J. Gottas, and F. Martin Ralph. 2008. "Rain versus Snow in the Sierra Nevada, California: Comparing Doppler Profiling Radar and Surface Observations of Melting Level." *Journal of Hydrometeorology* 9 (2): 194–211. https://doi.org/10.1175/2007jhm853.1.

Lundquist, Jessica D, Daniel R Cayan, and Michael D Dettinger. 2004. "Spring Onset in the Sierra Nevada: When Is Snowmelt Independent of Elevation?" *Journal of Hydrometeorology* 5: 327–42.

Lundquist, Jessica D, Michael D Dettinger, Iris T Stewart, and Daniel R Cayan. 2009. "Variability and Trends in Spring Runoff in the Western United States." In *Climate Warming in Western North America—Evidence and Environmental Effects*, edited by F Wagner, 63–76. University of Utah Press.

Luo, Lifeng, Deanna Apps, Samuel Arcand, Huating Xu, Ming Pan, and Martin Hoerling. 2017. "Contribution of Temperature and Precipitation Anomalies to the California Drought during 2012 – 2015." *Geophysical Research Letters* 44: 3184–92. https://doi.org/10.1002/2016GL072027.

Lytle, David A., and N. Le Roy Poff. 2004. "Adaptation to Natural Flow Regimes." *Trends in Ecology and Evolution* 19 (2): 94–100. https://doi.org/10.1016/j.tree.2003.10.002.

Maavara, Taylor, Qiuwen Chen, Kimberly Van Meter, Lee E Brown, Jianyun Zhang, Jinren Ni, and Christiane Zarfl. 2020. "River Dam Impacts on Biogeochemical Cycling." *Nature Reviews Earth & Environment* 1: 103–16. https://doi.org/10.1038/s43017-019-0019-0.

Madej, M A. 2010. "Analysis of Trends in Climate, Streamflow, and Stream Temperature in North Coastal California." *Proceedings of the Fourth Interagency Conference on Research in the Watersheds*, no. March: 40–45.

Magilligan, Francis J, and Keith H Nislow. 2005. "Changes in Hydrologic Regime by Dams." *Geomorphology* 71: 61–78. https://doi.org/10.1016/j.geomorph.2004.08.017.

Mahoney, John M., and Stewart B. Rood. 1998. "Streamflow Requirements for Cottonwood Seedling Recruitment-An Integrative Model." *Wetlands* 18 (4): 634–45. https://doi.org/10.1007/BF03161678.

Mallakpour, Iman, Mojtaba Sadegh, and Amir Aghakouchak. 2018. "A New Normal for Stream Flow in California in a Warming Climate: Wetter Wet Seasons and Drier Dry Seasons." *Journal of Hydrology* 567: 203–11. https://doi.org/10.1016/j.jhydrol.2018.10.023.

Mamo, Thewodros G. 2015. "Evaluation of the Potential Impact of Rainfall Intensity Variation Due to Climate Change on Existing Drainage Infrastructure." *Journal of Irrigation and Drainage Engineering* 141 (10): 1–7. https://doi.org/10.1061/(ASCE)IR.1943-4774.0000887.

Mann, Michael E. 2004. "On Smoothing Potentially Non-Stationary Climate Time Series." *Geophysical Research Letters* 31 (January): 18–21. https://doi.org/10.1029/2004GL019569.

Mao, Yixin, Bart Nijssen, and Dennis P Lettenmaier. 2015. "Is Climate Change Implicated in the 2013–2014 California Drought? A Hydrologic Perspective." *Geophysical Research Letters* 42: 2805–13. https://doi.org/10.1002/2015GL063456.Received.

Martinez, Sandra, Stefanie Kralisch, Oscar Escolero, and Maria Perevochtchikova. 2015.

"Vulnerability of Mexico City's Water Supply Sources in the Context of Climate Change." *Journal of Water and Climate Change* 6 (3): 518–33. https://doi.org/10.2166/wcc.2015.083.

Mazor, Raphael D., Jason T. May, Ashmita Sengupta, Kenneth S. McCune, Brian P. Bledsoe, and Eric D. Stein. 2017. "Tools for Managing Hydrologic Alteration on a Regional Scale: Setting Targets to Protect Stream Health." *Freshwater Biology*, 786–803. https://doi.org/10.1111/fwb.13062.

McElreath, Richard. 2020. *Statistical Rethinking: A Bayesian Course with Examples in R and Stan*. Chapman and Hall/CR.

McNamara, J.P., Chandler, D., Seyfried, M. and Achet, S. (2005), Soil moisture states, lateral flow, and streamflow generation in a semi-arid, snowmelt-driven catchment. Hydrol. Process., 19: 4023-4038. https://doi.org/10.1002/hyp.5869

Meko, David M, Jonathan M Friedman, Ramzi Touchan, Jesse R Edmondson, Eleanor R Griffin, and Julian A Scott. 2015. "Alternative Standardization Approaches to Improving Streamflow Reconstructions with Ring-Width Indices of Riparian Trees." *The Holocene* 25 (7): 1–9. https://doi.org/10.1177/0959683615580181.

Mittal, Neha, Ajay Gajanan Bhave, Ashok Mishra, and Rajendra Singh. 2016. "Impact of Human Intervention and Climate Change on Natural Flow Regime." *Water Resources Management* 30: 685–99. https://doi.org/10.1007/s11269-015-1185-6.

Moore, G.W., Jones, J.A. and Bond, B.J. (2011), How soil moisture mediates the influence of transpiration on streamflow at hourly to interannual scales in a forested catchment. Hydrol. Process., 25: 3701-3710. https://doi.org/10.1002/hyp.8095

Mote, Philip W, Sihan Li, Dennis P Lettenmaier, Mu Xiao, and Ruth Engel. 2018. "Dramatic Declines in Snowpack in the Western US." *Npj Climate and Atmospheric Science* 1 (2): 1–6. https://doi.org/10.1038/s41612-018-0012-1.

Mount, Jeffrey F. 1995. *California Rivers and Streams: The Conflict Between Fluvial Process and Land Use*. Berkeley: University of California Press.

Moyle, Peter B, Jacob V E Katz, and Rebecca M Quiñones. 2011. "Rapid Decline of California' s Native Inland Fishes: A Status Assessment." *Biological Conservation* 144: 2414–23. https://doi.org/10.1016/j.biocon.2011.06.002.

Moyle, Peter B, Joseph D Kiernan, Patrick K Crain, and Rebecca M Quiñones. 2013. "Climate Change Vulnerability of Native and Alien Freshwater Fishes of California: A Systematic Assessment Approach." *PLoS ONE* 8 (5): 1–12. https://doi.org/10.1371/journal.pone.0063883.

Moyle, Peter, Rebecca M Quiñones, Jacob V E Katz, and J Weaver. 2015. *Fish Species of Special Concern in California (3rd Ed.)*. Sacramento, CA: California Department of Fish and Wildlife.

Musselman, Keith N, Nans Addor, Julie A Vano, and Noah P Molotch. 2021. "Winter Melt Trends Portend Widespread Declines in Snow Water Resources." *Nature Climate Change*. https://doi.org/10.1038/s41558-021-01014-9.

Norris, Richard H, and Martin C Thoms. 1999. "What Is River Health?" *Freshwater Biology* 41: 197–209.

Null, Sarah E, Joshua H Viers, Michael L Deas, Stacy K Tanaka, and Jeffrey F Mount. 2013. "Stream Temperature Sensitivity to Climate Warming in California's Sierra Nevada: Impacts to Coldwater Habitat." *Climatic Change* 116: 149–70. https://doi.org/10.1007/s10584-012-0459-8.

O'Briain, Rossa. 2019. "Climate Change and European Rivers: An Eco-hydromorphological Perspective." *Ecohydrology* 12: 1–18. https://doi.org/10.1002/eco.2099.

Olden, Julian D., and N. L. Poff. 2003. "Redundancy and the Choice of Hydrologic Indices for Characterizing Streamflow Regimes." *River Research and Applications* 19 (2): 101–21. https://doi.org/10.1002/rra.700.

Olden, Julian D, Christopher P Konrad, Theodore S Melis, Mark J Kennard, Mary C Freeman, Meryl C Mims, Erin N Bray, et al. 2014. "Are Large-Scale Flow Experiments Informing the Science and Management of Freshwater Ecosystems?" *Frontiers in Ecology and the Environment* 12 (3): 176–85. https://doi.org/10.1890/130076.

Ortiz-Partida, J. P., Sam Sandoval-Solis, J Arellano-Gonzalez, J Medellín-Azuara, and J E Taylor. 2019. "Managing Water Differently: Integrated Water Resources Management as a Framework for Adaptation to Climate Change in Mexico." In *Integrated Water Resource Management*, edited by E Vieira, Samuel Sandoval-Solis, V Pedrosa, and J. Pablo Ortiz-Partida. Springer, Cham. https://doi.org/https://doi.org/10.1007/978-3-030-16565-9_6.

Paetzold, A, C Yoshimura, and K Tockner. 2008. “Riparian Arthropod Responses to Flow Regulation and River Channelization.” *Journal of Applied Ecology* 45.

Palmer, Margaret, and Albert Ruhi. 2019. “Linkages between Flow Regime, Biota, and Ecosystem Processes: Implications for River Restoration.” *Science* 365 (September). https://doi.org/10.1126/science.aaw2087.

Palshikar, Girish. 2009. “Simple Algorithms for Peak Detection in Time- Series Simple Algorithms for Peak Detection in Time-Series.” In *Proc. 1st Int. Conf. Advanced Data Analysis, Business Analytics and Intelligence*.

Pasternack, Gregory B, and Linda A Hinnov. 2003. “Hydrometeorological Controls on Water Level in a Vegetated Chesapeake Bay Tidal Freshwater Delta” 58: 367–87. https://doi.org/10.1016/S0272-7714(03)00106-9.

Patterson, Noelle K, Belize A Lane, Samuel Sandoval-solis, Gregory B Pasternack, Sarah M Yarnell, and Yexuan Qiu. 2020. “A Hydrologic Feature Detection Algorithm to Quantify Seasonal Components of Flow Regimes.” *Journal of Hydrology* 585: 1–12. https://doi.org/10.1016/j.jhydrol.2020.124787.

Paul, Sahana, and Huang-Hsiung Hsu. 2012. “Comparative Study of Performance of CMIP3 GCMs in Simulating the East Asian Monsoon Variability.” *Terrestrial, Atmospheric and Oceanic Sciences* 23 (4): 377–95. https://doi.org/10.3319/TAO.2012.02.01.01(A)1.

Pepin, N, R S Bradley, H. F. Diaz, M. Baraer, E. B. Caceres, N. Forsythe, H. Fowler, et al. 2015. “Elevation-Dependent Warming in Mountain Regions of the World.” *Nature Cl* 5. https://doi.org/10.1038/nclimate2563.

Persad, Geeta G, Daniel L Swain, Claire Kouba, and J. Pablo Ortiz-Partida. 2020. “Inter-Model Agreement on Projected Shifts in California Hydroclimate Characteristics Critical to Water Management.” *Climatic Change* 162: 1493–1513.

Peternel-staggs, Karin, Laurel Saito, and Christian H Fritsen. 2008. “Evaluation of a Modeling Approach to Assess Nitrogen Assimilative Capacity Due to River Restoration.” *Journal of Water Resources Planning and Management* 134 (5). https://doi.org/10.1061/(ASCE)0733-9496(2008)134.

Phelan, Colleen A, David W Pearce, and Stewart B Rood. 2022. “Thirsty Trees: Even with Continuous River Flow Riparian Cottonwoods Are Constrained by Water Availability.”

Trees, 1–14. https://doi.org/10.1007/s00468-022-02285-1.

Pierce, David W, Daniel R Cayan, and Laurel DeHann. 2016. "Creating Climate Projections to Support the 4 Th California Climate Assessment." La Jolla, California, USA.

Pierce, David W, Daniel R Cayan, and Bridget L Thrasher. 2014. "Statistical Downscaling Using Localized Constructed Analogs (LOCA)." *Journal of Hydrometeorology* 15: 2558–85. https://doi.org/10.1175/JHM-D-14-0082.1.

Pierce, David W, Julie F Kalansky, and Daniel R Cayan. 2018. "Climate, Drought, and Sea Level Rise Scenarios for the Fourth California Climate Assessment."

Plummer, M. 2003. "A Program for Analysis of Bayesian Graphical Models Using Gibbs Sampling." In *Proceedings of the 3rd International Workshop on Distributed Statistical Computing (DSC 2003)*, 1–10. Vienna.

Poff, N. LeRoy, and J. V. Ward. 1989. "Implications of Streamflow Variability and Predictability for Lotic Community Structure: A Regional Analysis of Streamflow Patterns." *Canadian Journal of Fisheries and Aquatic Sciences* 46 (10): 1805–18. https://doi.org/10.1139/f89-228.

Poff, N. Leroy, and Julie K.H. Zimmerman. 2010. "Ecological Responses to Altered Flow Regimes: A Literature Review to Inform the Science and Management of Environmental Flows." *Freshwater Biology* 55 (1): 194–205. https://doi.org/10.1111/j.1365-2427.2009.02272.x.

Poff, N L, J David Allan, Mark B Bain, J R Karr, K L Prestegaard, B D Richter, R E Sparks, and J C Stromberg. 1997. "The Natural Flow Regime." *Bioscience* 47 (11): 769–84. https://doi.org/Doi 10.2307/1313099.

Poff, N Leroy, Julian D Olden, David M Merritt, and David M Pepin. 2007. "Homogenization of Regional River Dynamics by Dams and Global Biodiversity Implications." *PNAS* 104 (14): 5732–37.

Poff, N Leroy, and J V Ward. 1990. "Physical Habitat Template of Lotic Systems: Recovery in the Context of Historical Pattern of Spatiotemporal Heterogeneity." *Environmental Management* 14 (5): 629–45.

Pollock, D S G. 1999. *A Handbook of Time-Series Analysis, Signal Processing and Dynamics*. London: The Academic Press. https://doi.org/https://doi.org/10.1016/B978-0-12-560990-

6.X5000-3.

Postel, S, and Brian Richter. 2003. *Rivers for Life: Managing Water for People and Nature*. Washington, DC: Island Press.

Press, William H., and Saul A. Teukolsky. 1990. "Savitzky-Golay Smoothing Filters." *Computers in Physics* 4 (669). https://doi.org/10.1063/1.4822961.

Puijalon, S, and G Bornette. 2013. "Multi-Scale Macrophyte Responses to Hydrodynamic Stress and Disturbances: Adaptive Strategies and Biodiversity Patterns." *Ecohydraulics*, 261–73.

Ragozin, David L. 1983. "Error Bounds for Derivative Estimates Based on Spline Smoothing of Exact or Noisy Data." *Journal of Approximation Theory* 37 (4): 335–55. https://doi.org/10.1016/0021-9045(83)90042-4.

Regonda, Satish K, Balaji Rajagopalan, Martyn Clark, and John Pitlick. 2005. "Seasonal Cycle Shifts in Hydroclimatology over the Western United States." *Journal of Climate* 18: 372–84.

Richter, Brian D., Jeffrey V. Baumgartner, Jennifer Powell, and David P. Braun. 1996. "A Method for Assessing Hydrologic Alteration within Ecosystems." *Conservation Biology* 10 (4).

Rinne, K T, T Boettger, N J Loader, I Robertson, V R Switsur, and J S Waterhouse. 2005. "On the Purification of A-Cellulose from Resinous Wood for Stable Isotope (H, C and O) Analysis." *Chemical Geology* 222: 75–82.

Rood, S. B., C. R. Gourley, E.M. Ammon, L. G. Heki, J. R. Klotz, M. L. Morrison, D. Mosley, G. G. Scoppettoone, S. Swanson, and P. L. Wagner. 2003. "Flows for Floodplain Forests: A Successful Riparian Restoration." *BioScience* 53 (7): 647–56. https://doi.org/10.1641/0006-3568(2003)053[0647:ffffas]2.0.co;2.

Rood, Stewart B., S Kaluthota, Karen M. Gill, E J Hillman, S. G. Wooodman, D W Pearce, and John M. Mahoney. 2016. "A Twofold Strategy for Riparian Restoration: Combining a Functional Flow Regime and Direct Seeding to Re-establish Cottonwoods." *River Research and Applications* 32: 836–44. https://doi.org/10.1002/rra.

Rood, Stewart B, Sarah G Bigelow, and Alexis A Hall. 2011. "Root Architecture of Riparian Trees: River Cut-Banks Provide Natural Hydraulic Excavation, Revealing That Cottonwoods Are Facultative Phreatophytes." *Trees* 25: 907–17.

https://doi.org/10.1007/s00468-011-0565-7.

Rood, Stewart B, Jeffrey H Braatne, and Francine M R Hughes. 2003. "Ecophysiology of Riparian Cottonwoods: Stream Flow Dependency, Water Relations and Restoration." *Tree Physiology* 23: 1113–24. https://doi.org/10.1093/treephys/23.16.1113.

Rood, Stewart B, Glenda M Samuelson, Jeffrey H Braatne, Chad R Gourley, Francine M R Hughes, John M Mahoney, and Francine Hughes. 2005. "Managing River Flows to Restore Floodplain Forests." *Frontiers in Ecology and the Environment* 3 (4): 193–201.

Rood, Stewart, Deborah J Ball, Karen M Gill, Sobadini Kaluthota, Matthew G Letts, and David W Pearce. 2013. "Hydrologic Linkages between a Climate Oscillation, River Flows, Growth, and Wood D13C of Male and Female Cottonwood Trees." *Plant, Cell & Environment* 36: 984–93. https://doi.org/10.1111/pce.12031.

Sabo, John L, Kevin E McCluney, Yevgeniy Marusenko, Andrew Keller, and Candan U Soykan. 2008. "Greenfall Links Groundwater to Aboveground Food Webs in Desert River Floodplains." *Ecological Monographs* 78 (4): 615–31.

Salmaso, Francesca, Livia Servanzi, Giuseppe Crosa, Silvia Quadroni, and Paolo Espa. 2021. "Assessing the Impacts of Hydropeaking on River Benthic Macroinvertebrates: A State-of-the-Art Methodological Overview." *Environments* 8 (67): 1–14. https://doi.org/10.3390/environments8070067.

Sang, Yan Fang. 2013. "A Review on the Applications of Wavelet Transform in Hydrology Time Series Analysis." *Atmospheric Research* 122: 8–15. https://doi.org/10.1016/j.atmosres.2012.11.003.

Sawaske, Spencer R., and David L. Freyberg. 2014. "An Analysis of Trends in Baseflow Recession and Low-Flows in Rain-Dominated Coastal Streams of the Pacific Coast." *Journal of Hydrology* 519 (PA): 599–610. https://doi.org/10.1016/j.jhydrol.2014.07.046.

Schneider, Roger. 2011. "Survey of Peaks/Valleys Identification in Time Series."

Scholkmann, Felix, Jens Boss, and Martin Wolf. 2012. "An Efficient Algorithm for Automatic Peak Detection in Noisy Periodic and Quasi-Periodic Signals." *Algorithms* 5: 588–603. https://doi.org/10.3390/a5040588.

Schook, D M, E A Carlson, J S Sholtes, and D J Cooper. 2016. "Effects of Moderate and Extreme Flow Regulation on Populus Growth along the Green and Yampa Rivers, Colorado

and Utah." *River Research and Applications* 32: 1698–1708. https://doi.org/10.1002/rra.

Schook, Derek M, Jonathan M Friedman, Jamie D Hoover, Steven E Rice, Richard D Thaxton, and David J Cooper. 2022. "Riparian Forest Productivity Decline Initiated by Streamflow Diversion Then Amplified by Atmospheric Drought 40 Years Later." *Ecohydrology* 15: 1–14. https://doi.org/10.1002/eco.2408.

Schook, Derek M, Jonathan M Friedman, Craig A Stricker, Adam Z Csank, and David J Cooper. 2020. "Short- and Long-Term Responses of Riparian Cottonwoods (Populus Spp.) to Flow Diversion: Analysis of Tree-Ring Radial Growth and Stable Carbon Isotopes." *Science of the Total Environment* 735: 139523. https://doi.org/10.1016/j.scitotenv.2020.139523.

Schwarz, Andrew, Patrick A Ray, Sungwook Wi, Casey Brown, Minxue He, and Matthew Correa. 2018. "Climate Change Risks Faced by the California Central Valley Water Resource System."

Schwarz, Andrew, Patrick Ray, and Wyatt Arnold. 2019. "Decision Scaling Evaluation of Climate Change Driven Hydrologic Risk to the State Water Project." Sacramento, CA.

Scott, Michael L, Patrick B Shafroth, and Gregor T Auble. 1999. "Responses of Riparian Cottonwoods to Alluvial Water Table Declines." *Environmental Management* 23 (3): 347–58.

Serreze, Mark C., Martyn P. Clark, Richard L. Armstrong, David A. McGinnis, and Roger S. Pulwarty. 1999. "Characteristics of the Western United States Snowpack from Snowpack Telemetry (SNOTEL) Data." *Water Resources Research* 35 (7): 2145–60. https://doi.org/10.1029/1999wr900090.

Shafroth, Patrick B., Karen J. Schlatter, Martha Gomez-Sapiens, Erick Lundgren, Matthew R. Grabau, Jorge Ramírez-Hernández, J. Eliana Rodríguez-Burgueño, and Karl W. Flessa. 2017. "A Large-Scale Environmental Flow Experiment for Riparian Restoration in the Colorado River Delta." *Ecological Engineering* 106: 645–60. https://doi.org/10.1016/j.ecoleng.2017.02.016.

Sherman, Bradford, Charles R Todd, D Koehn, and Tom Ryan. 2007. "MODELLING THE IMPACT AND POTENTIAL Modelling the Impact and Potential Mitigation of Cold Water Pollution on Murray Cod Populations Downstream of Hume Dam, Australia." *River Research and Applications* 23: 377–89. https://doi.org/10.1002/rra.

Siirila-Woodburn, Erica R, Alan M Rhoades, Benjamin J Hatchett, Laurie S Huning, Julia Szinai, Christina Tague, Peter S Nico, et al. 2021. "A Low-to-No Snow Future and Its Impacts on Water Resources in the Western United States." *Nature Reviews: Earth & Environment* 2 (November): 800–819. https://doi.org/10.1038/s43017-021-00219-y.

Simon, Andrew, and Massimo Rinaldi. 2006. "Disturbance, Stream Incision, and Channel Evolution: The Roles of Excess Transport Capacity and Boundary Materials in Controlling Channel Response." *Geomorphology* 79: 361–83. https://doi.org/10.1016/j.geomorph.2006.06.037.

Smith, Brennan, and Stuart Schwartz. 2017. "Automating Recession Curve Displacement Recharge Estimation." *Groundwater* 55 (1): 81–87. https://doi.org/10.1111/gwat.12439.

Snyder, Keirith A, and David G Williams. 2000. "Water Sources Used by Riparian Trees Varies among Stream Types on the San Pedro River, Arizona." *Agriculture and Forest Meteorology* 105: 227–40.

Steel, Anna E., Ryan A. Peek, Robert A. Lusardi, and Sarah M. Yarnell. 2018. "Associating Metrics of Hydrologic Variability with Benthic Macroinvertebrate Communities in Regulated and Unregulated Snowmelt-Dominated Rivers." *Freshwater Biology* 63 (8): 844–58. https://doi.org/10.1111/fwb.12994.

Stella, John C, Jess Riddle, Hervé Piégay, Matthieu Gagnage, and Marie-Laure Trémélo. 2013. "Geomorphology Climate and Local Geomorphic Interactions Drive Patterns of Riparian Forest Decline along a Mediterranean Basin River." *Geomorphology* 202: 101–14. https://doi.org/10.1016/j.geomorph.2013.01.013.

Stewart, Iris T. 2008. "Changes in Snowpack and Snowmelt Runoff for Key Mountain Regions." *Hydrological Processes* 23 (1): 78–94. https://doi.org/10.1002/hyp.7128.

Stewart, Iris T, Daniel R Cayan, and Michael D Dettinger. 2005. "Changes toward Earlier Streamflow Timing across Western North America." *Journal of Climate* 18: 1136–55.

Stewart, Iris T, Darren L Ficklin, Carlos A Carrillo, and Russell Mcintosh. 2015. "21st Century Increases in the Likelihood of Extreme Hydrologic Conditions for the Mountainous Basins of the Southwestern United States." *Journal of Hydrology* 529: 340–53. https://doi.org/10.1016/j.jhydrol.2015.07.043.

Stokes, M A, and T L Smiley. 1968. *An Introduction to Tree-Ring Dating*. Chicago, USA:

University of Chicago Press.

Stromberg, Julie C, and Duncan T Patten. 1990. “Riparian Vegetation Instream Flow Requirements: A Case Study from a Diverted Stream in the Eastern Sierra Nevada, California, USA.” *Environmental Management* 14 (2): 185–94.

Su, Guohuan, Maxime Logez, Jun Xu, Shengli Tao, Sébastien Villéger, and Sébastien Brosse. 2021. “Human Impacts on Global Freshwater Fish Biodiversity.” *Science* 371: 835–38.

Sultana, Rebeka, and Molan Choi. 2018. “Sensitivity of Streamflow Response in the Snow-Dominated Sierra Nevada Watershed Using Projected CMIP5 Data.” *Journal of Hydrologic Engineering* 23 (8): 1–12. https://doi.org/10.1061/(ASCE)HE.1943-5584.0001640.

Swain, Daniel L, Baird Langenbrunner, J David Neelin, and Alex Hall. 2018. “Increasing Precipitation Volatility in Twenty-First- Century California.” *Nature Climate Change* 8: 427–33. https://doi.org/10.1038/s41558-018-0140-y.

Thomas, Brian F., Richard M. Vogel, and James S. Famiglietti. 2015. “Objective Hydrograph Baseflow Recession Analysis.” *Journal of Hydrology* 525: 102–12. https://doi.org/10.1016/j.jhydrol.2015.03.028.

UNESCO. 2009. “Water in a Changing World. The United Nations World Water Development Report 3.” World Water Assessment Programme. Water in a Changing World. The United Nations World Water Development Report 3 (UNESCO, 2009).

US Army Corps of Engineers. 1995. Lower Truckee River Reconnaissance Report, issued 1995.

Verveer, P. J. 2003. “SciPy Reference Guide: Multi-Dimensional Image Processing - ‘Gaussian Filter1d’ and ‘Gaussian Filter.’”

Vorosmarty, C. J., Christian Leveque, Carmen Revenga, Robert Bos, Chris Caudill, and John Chilton. 2005. “Fresh Water.” In *Millennium Ecosystem Assessment*, 165–207. Island Press.

Vorosmarty, C J, P B Mcintyre, M O Gessner, D Dudgeon, A Prusevich, P Green, S Glidden, et al. 2010. “Global Threats to Human Water Security and River Biodiversity.” *Nature* 467: 555–61. https://doi.org/10.1038/nature09440.

Wahba, Grace. 1978. “Improper Priors, Spline Smoothing and the Problem of Guarding Against Model Errors in Regression.” *Journal of the Royal Statistical Society. Series B (Methodological).* 40 (3): 364–72.

Walling, Des E. 2012. “The Role of Dams in the Global Sediment Budget.” In *Erosion and*

Sediment Yields in the Changing Environment (Proceedings of a Symposium Held at the Institute of Mountain Hazards and Environment, CAS-Chengdu, China, 11–15 October 2012), 3–11. IAHS Publ. 356.

Williams, Christopher A., and David J. Cooper. 2005. "Mechanisms of Riparian Cottonwood Decline along Regulated Rivers." *Ecosystems* 8 (4): 382–95. https://doi.org/10.1007/s10021-003-0072-9.

Willms, Chad R, David W Pearce, and Stewart B Rood. 2006. "Growth of Riparian Cottonwoods: A Developmental Pattern and the Influence of Geomorphic Context." *Trees* 20: 210–18. https://doi.org/10.1007/s00468-005-0027-1.

Wohl, Ellen, B P Bledsoe, R B Jacobson, N L Poff, S L Rathburn, D M Walters, and A C Wilcox. 2015. "The Natural Sediment Regime in Rivers: Broadening the Foundation for Ecosystem Management." *BioScience* 65 (4): 358–71. https://doi.org/10.1093/biosci/biv002.

Yarnell, Sarah M., Geoffrey E. Petts, John C. Schmidt, Alison A. Whipple, Erin E. Beller, Clifford N. Dahm, Peter Goodwin, and Joshua H. Viers. 2015. "Functional Flows in Modified Riverscapes: Hydrographs, Habitats and Opportunities." *BioScience* 65 (10): 963–72. https://doi.org/10.1093/biosci/biv102.

Yarnell, Sarah M, Eric D Stein, J Angus Webb, Theodore Grantham, Rob A Lusardi, Julie Zimmerman, Ryan A Peek, Belize A Lane, Jeanette Howard, and Samuel Sandoval-Solis. 2020. "A Functional Flows Approach to Selecting Ecologically Relevant Flow Metrics for Environmental Flow Applications." *River Research and Applications* 36 (2): 1–7. https://doi.org/10.1002/rra.3575.

Yarnell, Sarah M, Joshua H Viers, and Jeffrey F Mount. 2010. "Ecology and Management of the Spring Snowmelt Recession." *BioScience* 60 (2): 114–27. https://doi.org/10.1525/bio.2010.60.2.6.

Zarri, Liam J, Eric M Danner, Miles E Daniels, and E P Palkovacs. 2019. "Managing Hydropower Dam Releases for Water Users and Imperiled Fishes with Contrasting Thermal Habitat Requirements." *Journal of Applied Ecology* 56: 2423–30. https://doi.org/10.1111/1365-2664.13478.

Zhang, Hongbo, Qiang Huang, Qiang Zhang, Lei Gu, Keyu Chen, and Qijun Yu. 2016.

"Changes in the Long-Term Hydrological Regimes and the Impacts of Human Activities in the Main Wei River, China." *Hydrological Sciences Journal* 61 (6): 1054–68. https://doi.org/10.1080/02626667.2015.1027708.

Zimmerman, Julie K H, Daren M Carlisle, Jason T May, Kirk R Klausmeyer, Theodore E Grantham, Larry R Brown, and Jeanette K Howard. 2017. "Patterns and Magnitude of Flow Alteration in California , USA." *Freshwater Biology*, 859–73. https://doi.org/10.1111/fwb.13058.

———. 2018. "Patterns and Magnitude of Flow Alteration in California, USA." *Freshwater Biology* 63: 859–73. https://doi.org/10.1111/fwb.13058.

Appendix 1

Supplementary Materials for:

A hydrologic feature detection algorithm to quantify seasonal components of flow regimes

Noelle K. Patterson[1], Belize A. Lane[2], Samuel Sandoval-Solis[1], Gregory B. Pasternack[1], Sarah M. Yarnell[3], Yexuan Qiu[1]

1. Department of Land, Air and Water Resources, University of California, Davis
2. Department of Civil and Environmental Engineering, Utah State University
3. Center for Watershed Sciences, University of California, Davis

Software Availability

Name: Functional Flows Calculator

Developers: Yexuan Qiu (primary) and Noelle Patterson

Available from: https://github.com/leogoesger/func-flow

Programming language: Python 3.6

Interactive website and documentation: https://eflows.ucdavis.edu/

Contact: https://github.com/leogoesger/func-flow/issues

Software requirements: Python3 and compatible text editor

First year available: 2017

Cost: Free

1. Functional Flow Calculations

Four distinct applications of the Seasonal Flows Detection Algorithm (SFDA) are used to calculate the start timing of functional flows in California: (1) fall pulse flow timing, (2) wet season start timing, (3) spring recession start timing, and (4) dry season start timing (Figure A1-1). The general steps for SFDA calculation are also included for reference in Figure A1-2.

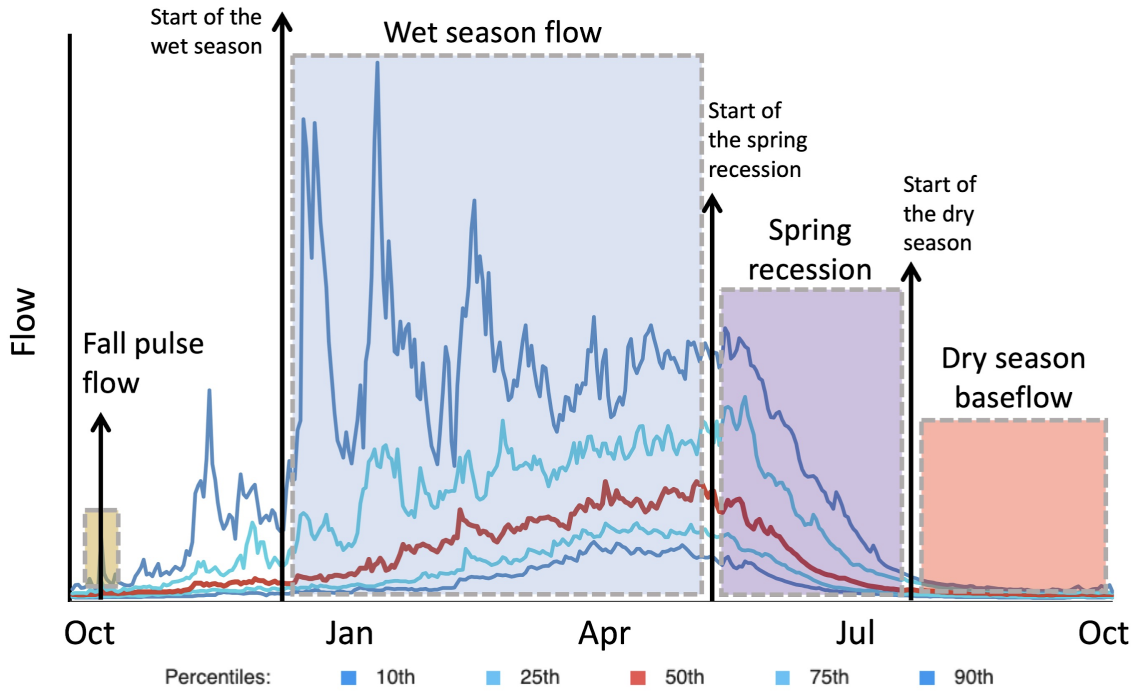

Figure A1-1. Identification of the start timing of four functional flows identified for California (Yarnell et al. 2015) using the proposed signal processing algorithm. The timing of flow transitions identified by the algorithm are marked with arrows. Hydrographs indicate the 10th, 25th, 50th, 75th, and 90th percentiles of flow in a mixed rain-snow river system (modified from Yarnell et al. in review). A water year in California is defined as October 1 to September 30.

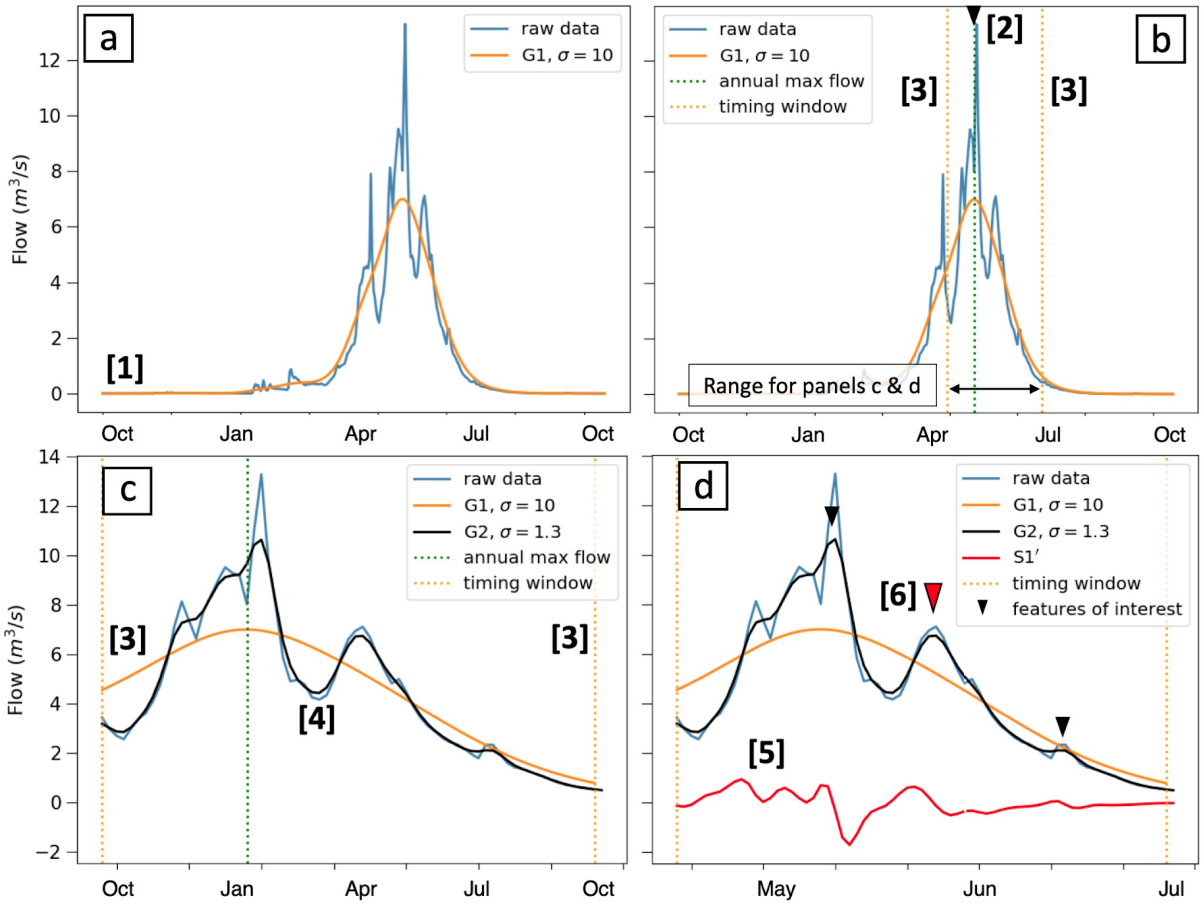

Figure A2-2. Six general steps of the SFDA. (a) Step 1: observed data is smoothed with a Gaussian filter (G1). (b) Step 2: a hydrologic feature of interest is detected from G1. Step 3: a search window is set around the hydrologic feature. (c) Step 4: a second, lower standard deviation Gaussian filter (G2) is applied to observed data to detect finer resolution peaks. (d) Step 5: the slope of the smoothed data G2 is detected using the derivative of a spline curve (S1'). Step 6: peak features of interest are identified based on magnitude or slope characteristics.

2.1 Fall Pulse Flow Timing

The fall pulse flow is the first significant flow event of the water year, signaling the transition from the dry season to the wet season, and its calculation requires one iteration of the SFDA steps (Figure A1-3). Within each water year, a low standard deviation Gaussian filter (G1, σ=0.2) is applied to daily streamflow time series in the windowed range from the start of the water year to the start of the wet season, which is calculated previously. The derivative of a spline function is used to identify all local peaks in the windowed period based on a sign change

in the derivative from positive to negative (triangles, Figure A1-3). Searching forward through time from the start of the water year, the first local peak meeting the following requirements is selected as the fall pulse flow: (1) magnitude exceeds 200% of previous dry season median baseflow magnitude; (2) duration of the peak's rising limb is less than 20 days; and (3) maximum peak magnitude is at least 30% higher than the valleys on either side of the peak. This event does not occur in all water years in California, particularly dry water years with limited fall-season rainfall.

There are two exceptions to the relative magnitude requirement described above. First, if the previous dry season median magnitude was relatively high (above 0.7 cms), the relative magnitude threshold was set as 150% of the previous dry season baseflow instead of 200%; this prevented the magnitude threshold from being set too high. Second, 0.08 cms is set as the minimum allowable magnitude threshold based on expert judgment that lower flows would not be ecologically significant across most gaged streams in California.

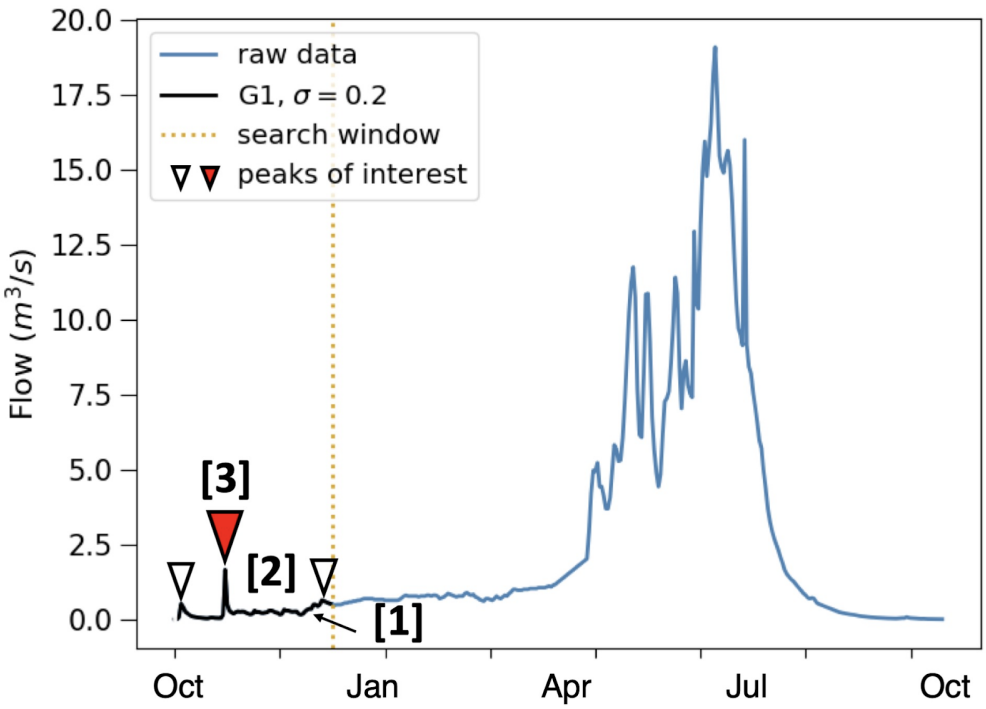

Figure A1-3. SFDA steps to calculate the fall pulse flow timing metric. Step 1: observed data is smoothed from the start of the water year until the identified start of the wet season with a low standard deviation Gaussian filter (G1). Step 2: peaks of interest are identified using the derivative of a spine function. Step 3: the fall pulse flow is identified based on magnitude and rate of change requirements.

2.2 Wet Season Start Timing

Wet season start timing delineates the peak magnitude portion of the water year during which streams receive the greatest inputs from storm runoff or snowmelt. This calculation uses one iteration of the SFDA steps (Figure A1-4), similar to the calculation of dry season start timing. Within each water year, a high standard deviation Gaussian filter (G1, σ=10) is applied to detect the water year's global peak (P1) and preceding global valley (V1). A relative magnitude threshold M1 is then set based on the magnitude of P1 and V1 as an upper limit (M1=γ*(P1-V1), where γ=0.2), to ensure that wet season start timing is not set after flows have already increased during the water year. A spline curve is then fit to G1 so that its derivative can be used as a hydrologic requirement in the final feature detection step. Finally, searching backwards in time

from P1, the date that discharge first falls below M1 and below a rate of change equaling (δ*P1, where δ=0.002) is selected as the wet season start timing. Similarly, the values for γ and δ were defined based on expert opinion of the co-authors to achieve functional flow identification as illustrated conceptually in Figure 1.

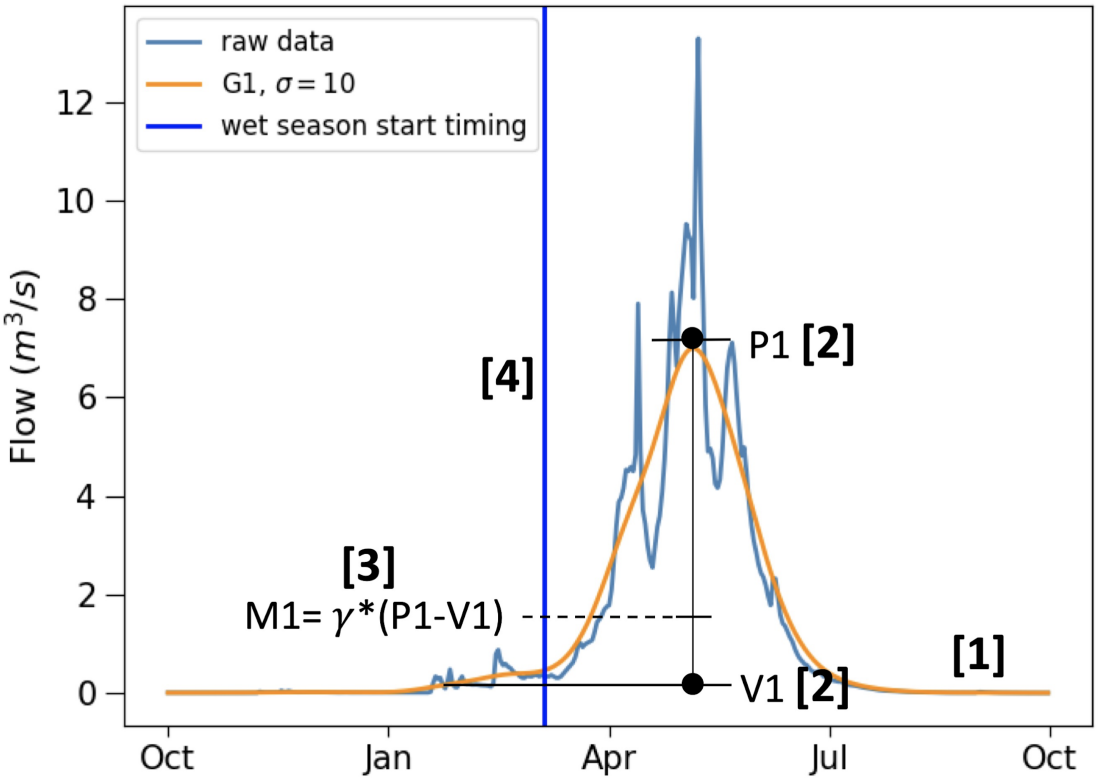

Figure A1-4. SFDA steps to calculate the wet season start timing metric. Step 1: observed data is smoothed with a Gaussian filter (G1). Step 2: the global peak and previous global valley are identified from G1. Step 3: the magnitude threshold M1 is set based on the relative difference of P1 and V1. Step 4: wet season start timing is set based on magnitude and rate of change requirements.

2.3 Spring Recession Start Timing

The spring recession represents the seasonal transition from wet season high flows to persistent and low-variability dry season flows. To apply the SFDA to this flow component, two iterations of the SFDA are performed, beginning with the general SDFA steps described in

Figure A1-2. Within each water year, a high standard deviation Gaussian filter (G1, σ=10) is applied to the raw daily streamflow time series to detect major wet and dry seasons (Figure A1-2a, step 1). The peak flow of the wet season is then identified from G1 to determine the subsequent high to low flow transition (Figure A1- 2b, step 2). A 70-day search window (20 days before and 50 days after) is applied around the peak flow date to constrain further analysis (Figure A1- 2b, step 3). Within the search window, a second low standard deviation Gaussian filter (G2, σ=1.3, Figure A1- 2c, step 4) is applied to the raw time series and the derivative of a spline function (S1') is used to detect individual storm events within the windowed range based on the occurrence of sign reversals in S1' from positive to negative (Figure A1- 2d, step 5). The algorithm then searches through the identified peaks moving backward in time (arrows, Figure A1- 1d) until it detects a peak feature exceeding a magnitude threshold of 50% of the smoothed maximum flow, and a rate of change threshold based on a percentage (0.02-0.08%) of the water year's maximum slope. These hydrologic requirements are intended to distinguish the last major storm event of the wet season (red arrow, Figure A1- 2d), when the hydrograph transitions from wet season flow to a gradual baseflow recession that occurs as the catchment drains.

Once the last storm event feature is identified, a second, partial iteration of the SFDA is applied to a relatively narrow time window to more precisely identify spring recession start timing (Figure A1- 5). A narrow search window of four days before to seven days after (black dotted lines, step 6, Figure A1- 5) is set around the final identified peak from the first iteration of calculation steps (black dashed line, Figure A1- 5), and the peak flow value within this window is identified from the raw daily streamflow time series (black dashed line, step 7, Figure A1-5). Finally, the spring recession start timing is set as four days following this peak flow value (red line, step 8, Figure A1- 5) to limit the effects of individual storm events on the spring recession

timing and subsequent flow metric calculations. The parameter values used in this algorithm were selected based on expert opinion of the co-authors to achieve functional flow identification as illustrated conceptually in Figure A1-1.

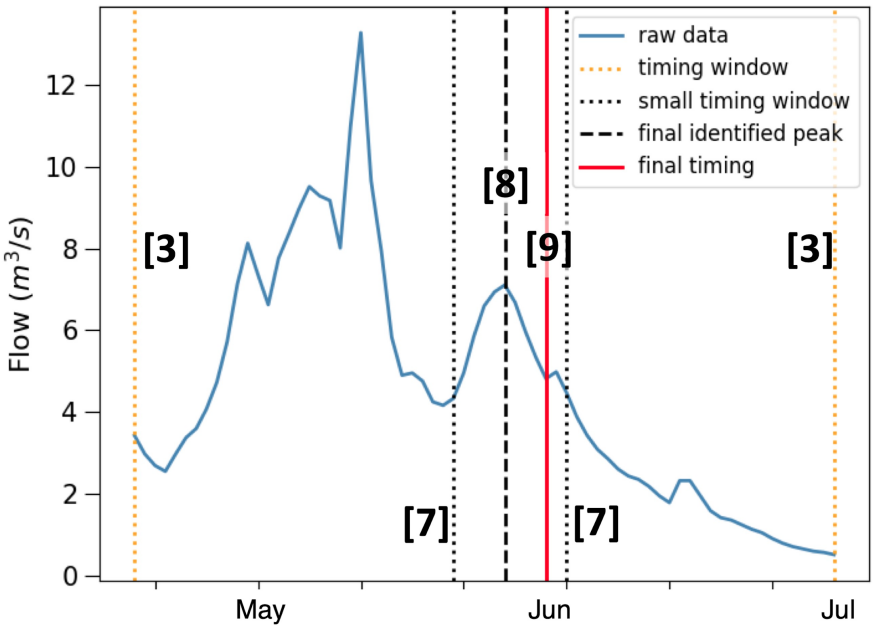

Figure A1-5. Second iteration of SFDA steps used for calculating spring recession start timing. Previous steps for the spring recession calculation are described by Fig. 2. Step 7: A small timing window is set around the final identified peak. Step 8: The max flow within the small timing window is identified. Step 9: The final spring recession timing is set four days after the max flow from step 8.

2.4 Dry Season Baseflow Start Timing

Dry season baseflow refers to the low magnitude, low variability portion of the water year in California's seasonally dry Mediterranean climate. This calculation requires only one iteration of SFDA steps (Figure A1-6). Within each water year, a high standard deviation Gaussian filter (G1, σ=7) is applied to detect the water year's global peak (P1) and subsequent global valley (V1). A relative magnitude upper threshold M1 is then set based on the magnitude

of P1 and V1 (M1=α*(P1-V1), where α=0.125), to ensure that the magnitude at the dry season start is sufficiently below seasonal peak flows. A spline curve is then fit to G1 so that its derivative can be used as a hydrologic requirement in the final feature detection step. Finally, G1 is searched moving forward in time to identify the first date that flow falls below magnitude M1 and below a rate of change threshold equaling (β*P1, where β=0.001). The values for α and β were defined based on expert opinion of the co-authors to achieve functional flow identification as illustrated conceptually in Figure A1-1.

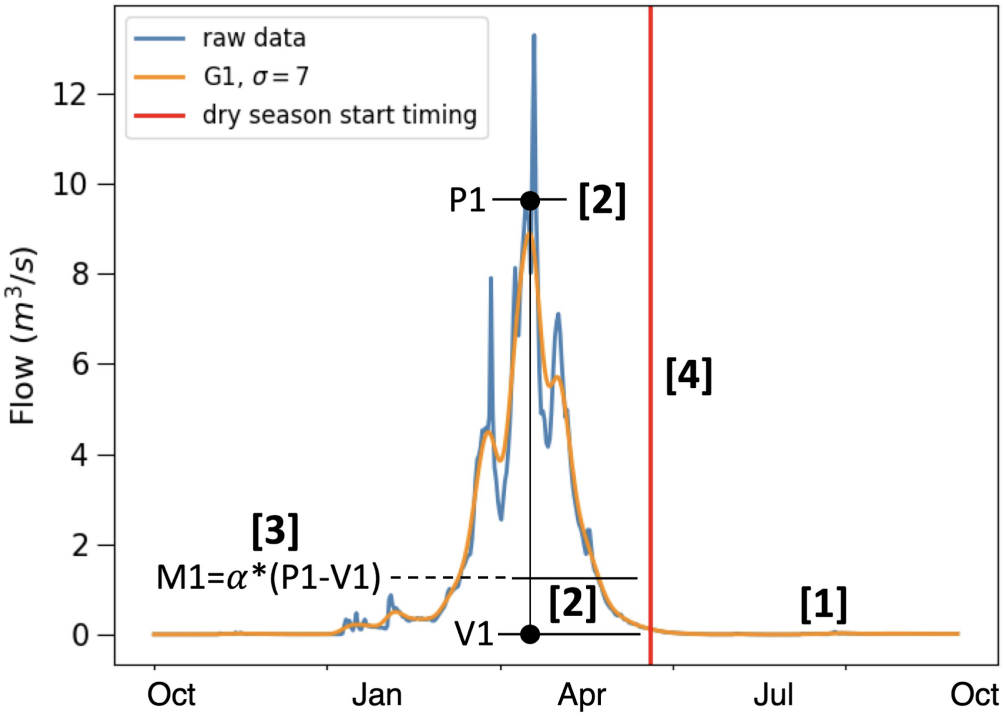

Figure A1-6. SFDA steps to calculate dry season start timing. Step 1: observed data is smoothed with a Gaussian filter (G1). Step 2: the global peak and subsequent global valley are identified from G1. Step 3: the magnitude threshold M1 is set based on the relative difference between P1 and V1. Step 4: dry season start timing (red line) is set based on magnitude and rate of change requirements.

2. Seasonal Flow Detection Algorithm Development

3.1 Data Smoothing

Data smoothing is a type of filtering in which low-frequency components are retained while high-frequency components are attenuated, enabling detection of features of interest at different frequencies or time-scales (Press and Teukolsky 1990). In the case of daily streamflow data, low-frequency components can include seasonal to annual fluctuations or secular (non-cyclical) interannual trends, while high-frequency components include daily to sub-seasonal fluctuations. Common finite-difference smoothing techniques include simple running averages, weighted moving averages, and exponential filters (Janert 2010). The simple running average (Eq. A1-1) calculates the average value within a set window k of data points and attributes that average to the centermost value within the window.

$$S_i = \frac{1}{2k\ +\ 1} \sum_{j=-k}^{k} x_{i+j}$$

[A1-1]

where $\{x_i\}$ are the data points, k is the time window, and the smoothed value at position i is s_i.

While the running average is the simplest presented method to calculate, it can cause distortion of the filtered time series whenever spikes in the raw data are encountered (Press and Teukolsky 1990, Janert 2010). The weighted moving average method (Eq. A1-2) seeks to address this issue by placing less weight on values at the ends of the smoothing window and more weight towards the center, smoothing abrupt distortions and better retaining local maxima in the output function.

$$S_i = \sum_{j=-k}^{k} w_j x_{i+j}$$

[A1-2]

where w_j are weighting factors, and all weighting factors equal to 1.

3.2. Valley location adjustment

A limitation of the proposed feature detection algorithm is that features of interest occurring between a local valley and a peak, such as the precise start of a stormflow event, may not be readily detected under low flow conditions with consecutive observations of the same discharge value, due to the effect of smoothing filters. In this case, a valley location adjustment was applied to identify a more hydrologically relevant valley location for flow metric calculations. Consider the daily streamflow time series from x=1 to 10 in Figure A1-7. Basic valley detection on G1 would identify the local valley location as the middle of the trough (V1/2) between the two peaks, P1 and P2 (yellow dots, Figure A1- 7). However, a hydrologic valley may be better described as the last baseflow observation before a storm event than as the observation exactly between two storms. A sensitivity factor Z is applied to identify a superior valley location (V2') between V1/2 and the local peak (P2) based on the relative magnitude of daily streamflow observations at these two locations (red dots, Figure A1- 7). Z is calculated by solving for Z in the following equation X=(V1/2 - P2)*Z such that the first value in the G1 series with a magnitude greater or equal to X (searching from the initial valley V1/2) is set as the adjusted valley location (red triangle, Figure A1- 7). In certain cases, a slope requirement is applied in conjunction with the relative magnitude requirement to more accurately identify valley location.

This method was used in the SDFA application to California functional flows to determine the duration of the fall pulse flow.

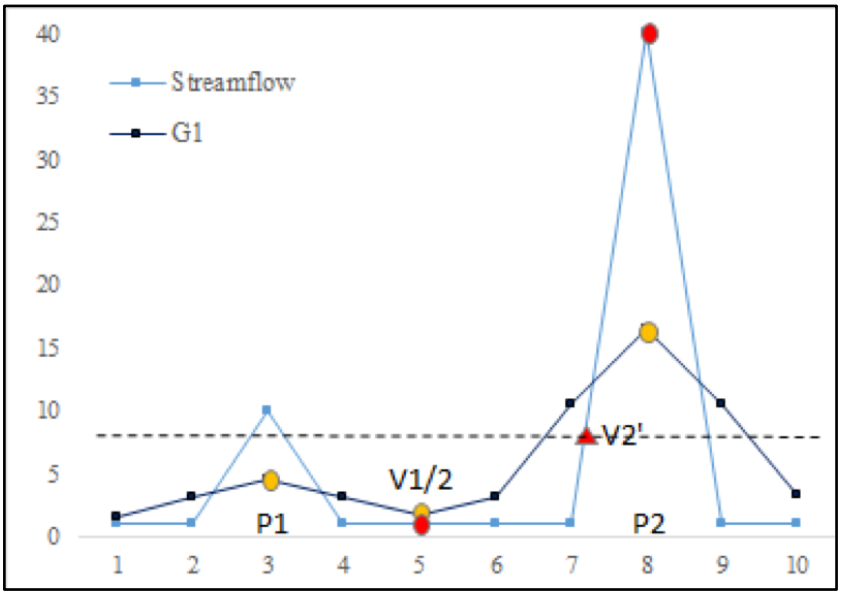

Figure A1-7. Illustration of the valley location adjustment algorithm for theoretical streamflow data.

References

Janert, P. K. (2010). *Data Analysis with Open Source Tools* (1st ed.). O'Reilly Media, Inc.

Press, W. H., & Teukolsky, S. A. (1990). Savitzky-Golay Smoothing Filters. *Computers in Physics*, *4*(669). https://doi.org/10.1063/1.4822961

Yarnell, S. M., Petts, G. E., Schmidt, J. C., Whipple, A. A., Beller, E. E., Dahm, C. N., … Viers, J. H. (2015). Functional Flows in Modified Riverscapes: Hydrographs, Habitats and Opportunities. *BioScience*, *65*(10), 963–972. https://doi.org/10.1093/biosci/biv102

Appendix 2

Supplementary Materials for:

Projected Effects of Temperature and Precipitation Variability Change on Streamflow Patterns Using a Functional Flows Approach

Noelle K. Patterson[1], Belize A. Lane[2], Samuel Sandoval-Solis[1], Geeta G. Persad[3], and J. Pablo Ortiz-Partida[4]

[1]Department of Land, Air and Water Resources, University of California, Davis, CA, USA

[2]Department of Civil and Environmental Engineering, Utah State University, Logan, UT, USA

[3]Department of Geological Sciences, University of Texas at Austin, Austin, TX, USA

[4]Union of Concerned Scientists, Oakland, CA, USA

1. Figures for GCM-based streamflow at RCP4.5 emissions levels.

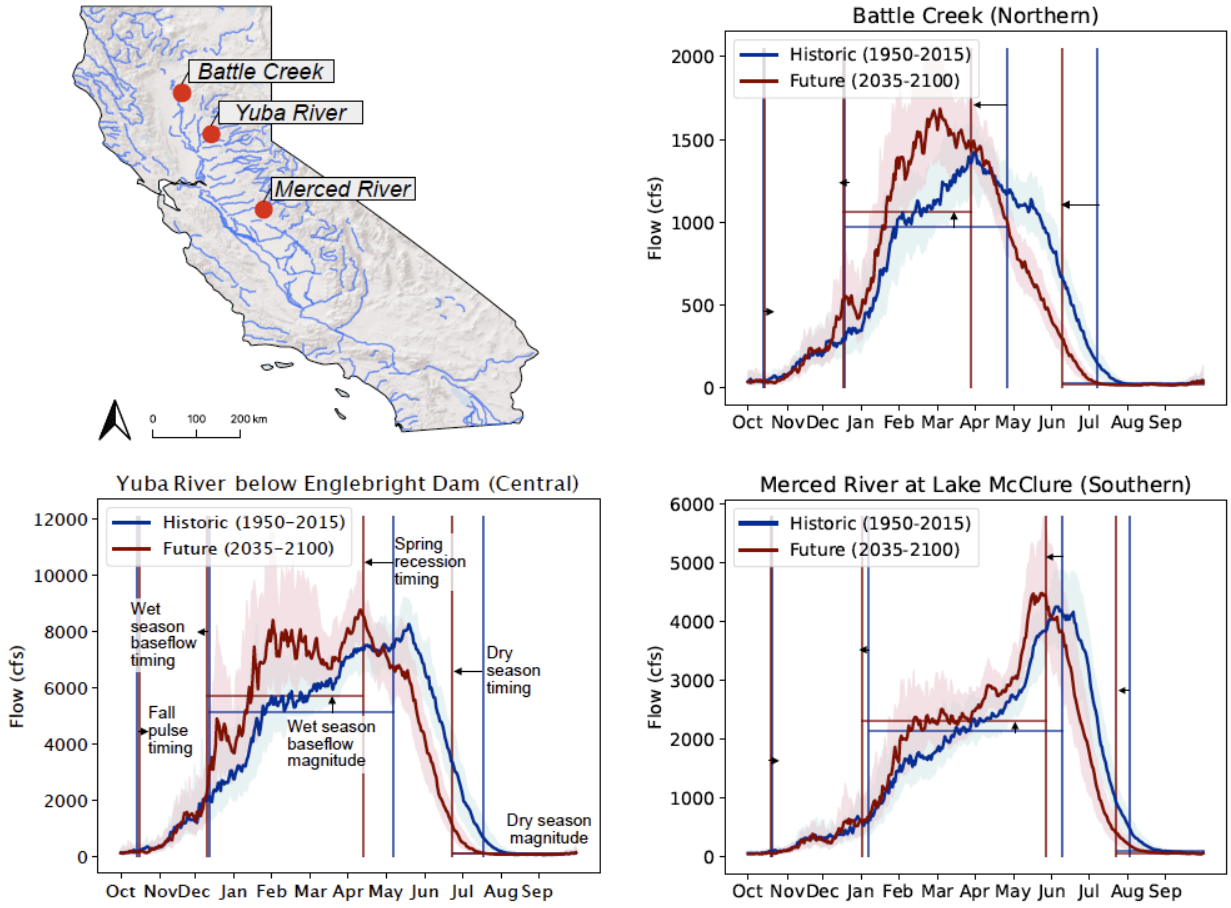

Figure A2-1. Historic (1950-2015) and future (2035-2100) simulated daily streamflow for three sites in California, aggregated over ten RCP4.5 GCMs (RCP8.5 in main text). Shifts in calculated functional flow metrics for the historic and future time periods are marked with arrows.

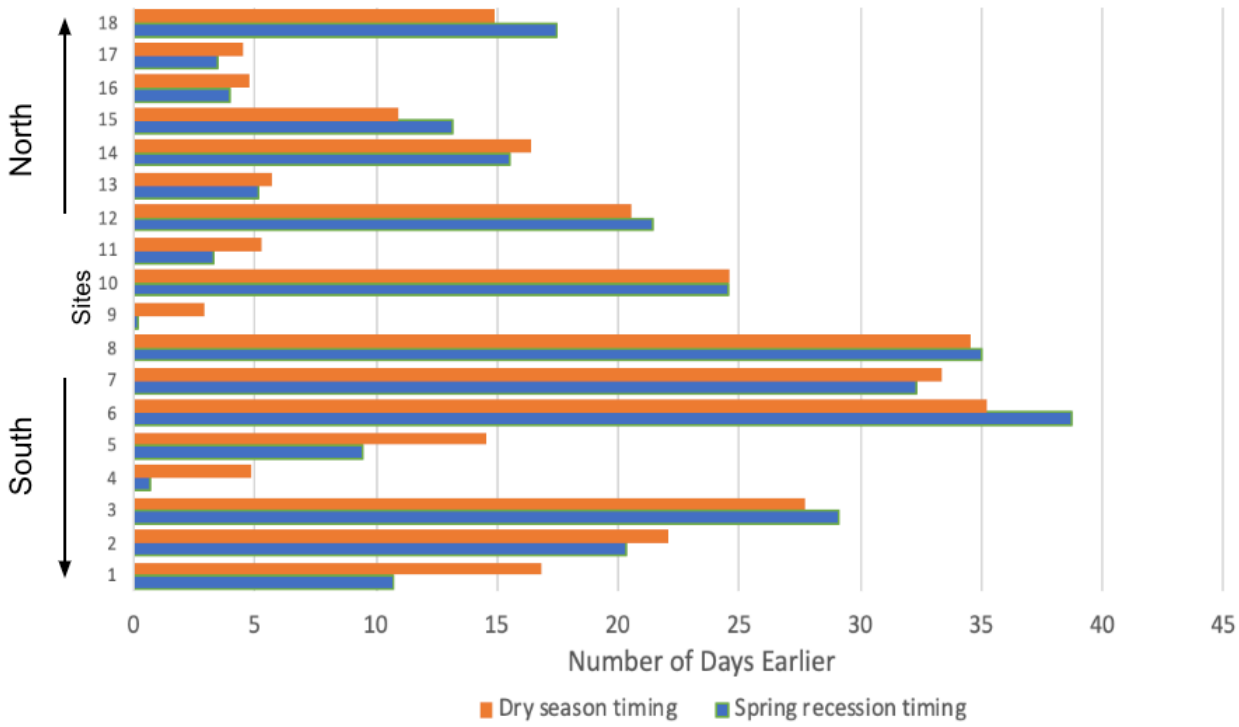

Fig A2-2. Timing shifts in dry season and spring recession functional flow metrics across all study catchments at the RCP4.5 emissions level scenario illustrate the variability of shifts across the Sierra Nevada study region. All sites exhibit a shift towards earlier timing to varying amounts.

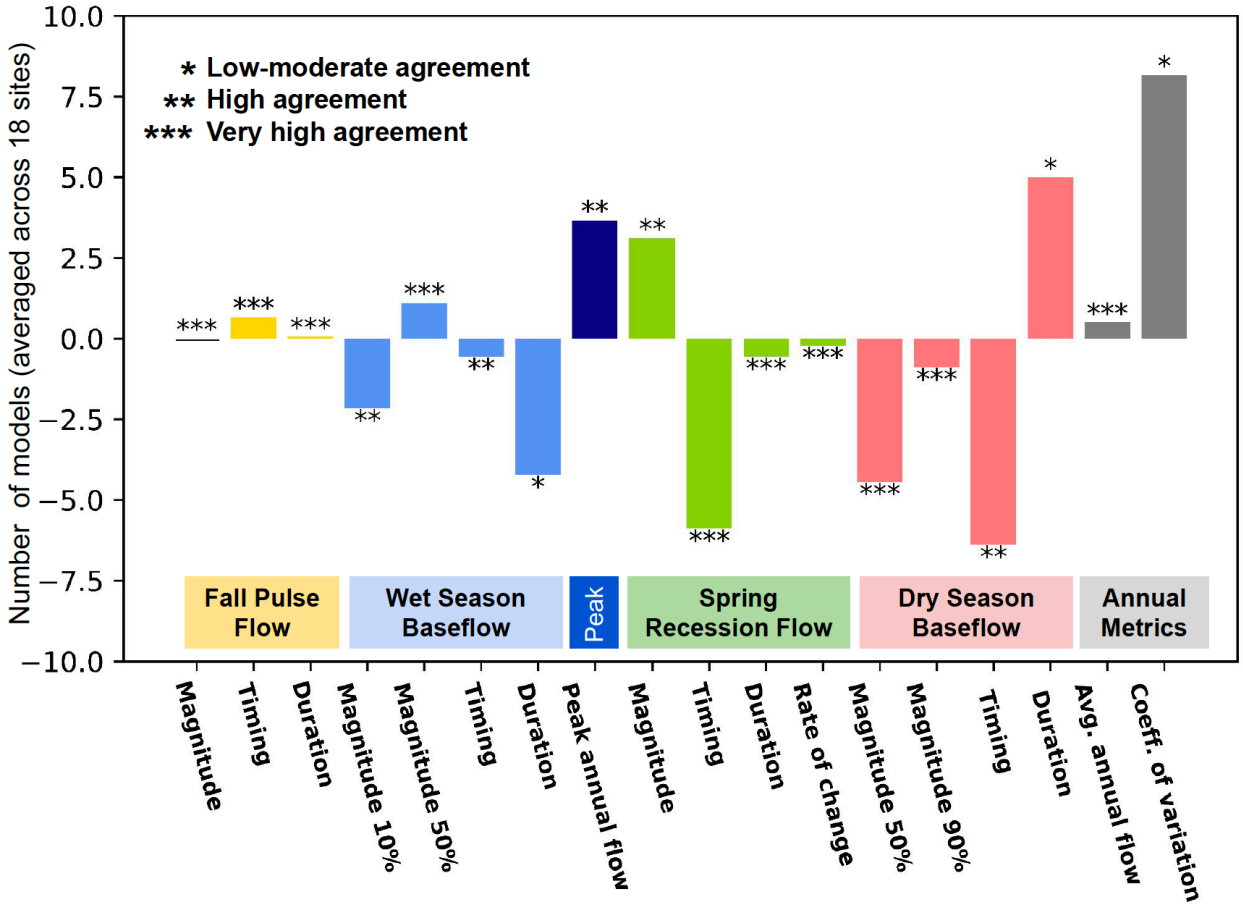

Figure A2-3. Results for RCP 4.5 trends in functional flow metrics, showing the number of models experiencing significant change (out of 10 total), averaged across the 18 total sites, where the direction of the bar indicates positive or negative change. Stars above the bars indicate model agreement according to the Gini index, where index values of 0-25% get one star, 25-50% get two stars, and 50-100% get three stars.

2. Calculation of Gini Index for measurement of agreement

The Gini index is a common measurement of purity or homogeneity, and was used in this study to test for agreement in functional flow metric trends across the 18 sites in the study area and the 10 models employed at each site (10 models each for RCP4.5 and RCP8.5 emissions scenarios). For each functional flow metric at a given site and given model, its trend was calculated across the 150-year period of record and recorded as either: 1) increasing, 2)

decreasing, or 3) no-change. The Gini index was used to determine the level of agreement in trend outcome across the ten models at each site, according to the Gini purity formula:

$$G = 1 - \sum_{i=1}^{n} (P_i)^2 \quad (1)$$

Where Gini Index G is calculated based on a deduction of the sum of the square of each category's probability of occurrence, Pi, from one. Pi is calculated for each of the three trend outcomes (increasing, decreasing, or no-change) as the number of occurrences out of ten, the total number of models. In a case such as this with three categories, the maximum value of G is one, indicating maximum purity. Maximum impurity, when values are spread equally across all three categories, is 2/3. To translate this Gini Index into a percentage ranging from 0-100%, the following equation is used for Gini purity with three categories:

$$Gini\ Percent = 100\left(1 - G\left(\frac{3}{2}\right)\right) \quad (2)$$

When translated to the Gini percent, a score of 100 indicates that all outcomes are in a single category and agreement is at 100%, such as if trend outcomes at a site were increasing across all ten models. A Gini percent closer to 0 would indicate trend outcomes were more evenly split between increasing, decreasing, and no-change outcomes. In Figure A2-2 of the SM, or Figure 2-5 of the main text, the stars over the trend outcome bars indicate ranges of the Gini percent score, where 0-25% is given one star, 25-50% is two stars, and 50-100% is three stars. In the outcomes

of this study, the Gini score never reached 100% for any single site, and three stars were infrequently reached. The ranges to use for the stars were therefore based on the relative instances of agreement instead of three equal splits between 0-100%.

3. Decision scaling climate modeling on the Merced River

The 42 scenarios used for the Merced River decision scaling analysis consist of combinations of climate parameters that are shifted according to the strategy described in Table A2-1. The five parameters and their notations in Table A2-1 are: temperature (DT), precipitation volume (DP), precipitation event intensity (DI-E), seasonal precipitation variability (DI-S), and interannual precipitation variability (DI-I). The ranges listed out for each parameter represent that parameter's full range: for temperature (DT), 1-5 describes Celsius degrees, for precipitation volume (DP), -30-30 represents percentages of shift in volume from a 30% decrease to a 30% increase, and for precipitation intensity (DI), 1-5 represents scaled values of precipitation variability where 1 is the low end of the range and 5 is the highest. The exact values for DI parameters are listed in Table 0. Scenarios are grouped into three broad categories in the Name column of Table 1: OAT (one-at-a-time), Extremes, and Mid-range. OAT scenarios feature climate parameters which are shifted one at a time in increments across their full range. The three climate parameters describing attributes of precipitation variability (DI-S, DI-E, DI-I) are shifted individually in the OAT scenarios but are shifted together in the mid-range and extreme scenarios. There are ten extreme scenarios, which shift either one, two, or all climate parameters together to the end of their range. For temperature and precipitation variability metrics there is only one extreme end of the range (hottest or most variable, respectively), but precipitation

volume is shifted to both ends of its range (driest and wettest) in the extreme scenarios. There are 8 mid-range scenarios, in which each climate parameter is increased by either 1/3 or 2/3 of its full range. Three models overlap between the OAT and extreme scenarios, but they are listed out redundantly in Table 1 in order to fully describe each scenario group (numbering is until 45 in Table 1 but with overlap there are just 42 models total). Baseline climate data for the Merced River Basin consisting of daily air temperature and precipitation was generated by Livneh et al. (2013) by detrending historic data from 1950-2013. This data represents historic climate conditions and was perturbed with the decision scaling framework to develop subsequent climate scenarios.

The ecological exceedance analysis was then performed to determine the frequency that decision scaling climate scenarios exceeded historic ranges of functional flow metrics, i.e. the relative frequency, in percentage, that a given scenario exceeded historic metric ranges. "Eco-exceedance" was calculated for each functional flow metric as the percentage years (out of 64 annual values) that the metric exceeded the (a) full range and (b) 10th to 90th percentile range of values in the control scenario. Eco-exceedance values are summarized across all scenarios and group by functional flow components in Table A2-5. Table A2-6 reports actual functional flow metric values for each scenario, averaged across the period of record.

Table A2-1. List of scenarios for decision scaling on the Merced River, which include One-at-a-time (OAT), Mid-range, and Extreme scenario categories.

Name	DT (1-5)	DP (-30- 30)	DI-S (1-5)	DI-E (1-5)	DI-I (1-5)	Label
1. Control	0	0	0	0	0	T0P0S0E0I0

2. DT-OAT	1	0	0	0	0	T1P0S0E0I0
3. DT-OAT	2	0	0	0	0	T2P0S0E0I0
4. DT-OAT	3	0	0	0	0	T3P0S0E0I0
5. DT-OAT	4	0	0	0	0	T4P0S0E0I0
6. DT-OAT	5	0	0	0	0	T5P0S0E0I0
7. DP-OAT	0	-30	0	0	0	T0P-30S0E0I0
8. DP-OAT	0	-20	0	0	0	T0P-20S0E0I0
9. DP-OAT	0	-10	0	0	0	T0P-10S0E0I0
10. DP-OAT	0	10	0	0	0	T0P10S0E0I0
11. DP-OAT	0	20	0	0	0	T0P20S0E0I0
12. DP-OAT	0	30	0	0	0	T0P30S0E0I0
13. DI-S-OAT	0	0	1	0	0	T0P0S1E0I0
14. DI-S-OAT	0	0	2	0	0	T0P0S2E0I0
15. DI-S-OAT	0	0	3	0	0	T0P0S3E0I0
16. DI-S-OAT	0	0	4	0	0	T0P0S4E0I0
17. DI-S-OAT	0	0	5	0	0	T0P0S5E0I0
18. DI-E-OAT	0	0	0	1	0	T0P0S0E1I0

19.	DI-E-OAT	0	0	0	2	0	T0P0S0E2I0
20.	DI-E-OAT	0	0	0	3	0	T0P0S0E3I0
21.	DI-E-OAT	0	0	0	4	0	T0P0S0E4I0
22.	DI-E-OAT	0	0	0	5	0	T0P0S0E5I0
23.	DI-I-OAT	0	0	0	0	1	T0P0S0E0I1
24.	DI-I-OAT	0	0	0	0	2	T0P0S0E0I2
25.	DI-I-OAT	0	0	0	0	3	T0P0S0E0I3
26.	DI-I-OAT	0	0	0	0	4	T0P0S0E0I4
27.	DI-I-OAT	0	0	0	0	5	T0P0S0E0I5
28.	Extremes - T	5	0	0	0	0	In OAT
29.	Extremes - P dry	0	-30	0	0	0	In OAT
30.	Extremes - P wet	0	30	0	0	0	In OAT
31.	Extremes - I	0	0	5	5	5	T0P0S5E5I5
32.	Extremes - TP	5	-30	0	0	0	T5P-30S0E0I0
33.	Extremes - TI	5	0	5	5	5	T5P0S5E5I5
34.	Extremes - PI	0	30	5	5	5	T0P30S5E5I5
35.	Extremes - PI	0	-30	5	5	5	T0P-30S5E5I5

36.	Extremes - all wet	5	30	5	5	5	T5P30S5E5I5
37.	Extremes - all dry	5	-30	5	5	5	T0P-30S5E5I5
38.	Mid-range	1.7	1.7	1.7	1.7	1.7	T1.7P1.7I1.7
39.	Mid-range	1.7	1.7	3.4	3.4	3.4	T1.7P1.7I3.4
40.	Mid-range	1.7	3.4	1.7	1.7	1.7	T1.7P3.4I1.7
41.	Mid-range	3.4	1.7	1.7	1.7	1.7	T3.4P1.7I1.7
42.	Mid-range	1.7	3.4	3.4	3.4	3.4	T1.7P3.4I3.4
43.	Mid-range	3.4	3.4	1.7	1.7	1.7	T3.4P3.4I1.7
44.	Mid-range	3.4	1.7	3.4	3.4	3.4	T3.4P1.7I3.4
45.	Mid-range	3.4	3.4	3.4	3.4	3.4	T3.4P3.4I3.4

The full range of values used for each climate parameter is listed in Table A2-2. Ranges for each parameter were informed by Global Climate Models (GCMs) so that decision scaling scenarios would represent actual expected outcomes for future conditions. The range of values for the three precipitation variability metrics were calculated from daily precipitation data from 10 GCMs at both RCP 4.5 and 8.5 emissions scenarios by Persad et al (2020). The values represent change between present-day (2006-2035) and end-of-century (2075-2099) conditions for each variability metric. The 10 GCMs used to define precipitation variability ranges (Table A2-3) are identified by the California Climate Change Technical Advisory Group as having the

best performance for California (Pierce et al. 2018), and are the same models used for other parts of this study. For each precipitation variability parameter calculated from GCM outputs, the lowest and highest values across all models were used as the range for decision scaling analysis (Table A2-2). In some cases, the sign differed between high and low model outcomes, meaning some models predicted a lowering of precipitation variability (usually at RCP4.5 levels) while others predicted an increase. The calculation method used to apply each precipitation variability parameter to the detrended 1950-2013 daily precipitation timeseries is described in Table A2-4.

Table A2-2. Full range of each climate parameter used for decision scaling on the Merced River.

Parameter name	Units	Low	High	Notes
Temperature	C	0	5	Shift applied uniformly across daily values as addition to original temperature value
Precipitation volume	Percentage	-30	30	Shift applied uniformly across daily values as a multiplier
Event scale precipitation intensity	Percentage	-21.25	70.35	Scale highest 3 days in each year by multiplier
Seasonal scale precipitation variability	Percentage	-3.76	12.10	Scale days in wet season months by multiplier, and adjust dry season months to achieve net zero difference
Interannual variability – shift in lowest 5% values	Percentage	20.17 (wetter)	29.10 (drier)	Driest 5% of water years are scaled by a multiplier to either get drier or wetter
Interannual variability – shift in highest 5% values	Percentage	13.89 (drier)	28.89 (wetter)	Wettest 5% of water years are scaled by a multiplier to either get wetter or drier
Interannual variability – shift in 20th percentile years	Percentage	7.81 (wetter)	8.10 (drier)	Water years in the 20th percentile (driest 20% of years) are scaled by a multiplier to get drier or wetter
Interannual variability – shift in 80th percentile years	Percentage	9.56 (drier)	34.09 (wetter)	Water years above the 80th percentile (wettest 20% of years) are scaled by a multiplier to get wetter or drier

Table A2-3: Global climate models used in this study.

Number	Model name
1	ACCESS1
2	CanESM2
3	CCSM4
4	CESM1-BGC
5	CMCC-CMS
6	CNRM-CM5
7	GFDL-CM3
8	HadGEM2-CC
9	HadGEM2-ES
10	MIROC5

Table A2-4. Precipitation variability parameters implemented in the decision scaling framework and modeled with the SAC-SMA-DS model on the Merced River.

Metric	Description	Implementation
Event Intensity	Proportion of annual precipitation occurring in the three wettest days of the year.	The three wettest days of the year are scaled with a multiplier, and dry season precipitation is adjusted with a multiplier to achieve net zero difference in annual precipitation.
Seasonal Variability	Proportion of annual precipitation occurring in the wet (November-	Precipitation in all days of the wet season months is scaled with a

	March) and dry (April-October) season months.	multiplier to adjust. Precipitation in the dry season is then adjusted with a multiplier to account for the change in the wet season, to achieve net zero difference in annual precipitation.
Interannual Variability	This metric incorporates two measures of interannual intensity: 1) The number of years in the POR that occur under the 20th percentile or above the 80th percentile of annual precipitation, and 2) The percentile of total annual precipitation of the wettest and driest years on records.	Two adjustments take place: 1) Years under (over) the 80th (20th) percentile of annual precipitation are scaled with a multiplier enough to reach the level of the 80th (20th) percentile of annual precipitation, pre-adjustment. 2) The wettest (driest) year on record is scaled with a multiplier.

Table A2-5. Eco-exceedance results for decision scaling on the Merced River. See Table A2-1 for a description of each scenario. Eco-exceedance is calculated as the percent of functional flow metrics for each scenario that exceeds the range in the control scenario, reported as a total for each functional flow component.

Scenario name	Scenario type	Total exceedance	Annual metrics	Fall pulse	Wet season	Peak flows	Spring recession	Dry season
SACSMA_T0P0S0E0I0	Control	0	0	0	0	0	0	0
SACSMA_T1P0S0E0I0	DT-OAT	2.8	2.4	1.1	2.4	4.8	3.6	3.6
SACSMA_T2P0S0E0I0	DT-OAT	4.1	4	1.1	3.6	3.2	5.6	6
SACSMA_T3P0S0E0I0	DT-OAT	6.3	3.2	1.6	4	6.3	13.5	6.3
SACSMA_T4P0S0E0I0	DT-OAT	9.8	4.8	1.6	4.8	6.3	21	13.1
SACSMA_T5P0S0E0I0	DT-OAT	13.9	5.6	1.6	6.7	6.3	31	19.4
SACSMA_T0P-30S0E0I0	DP-OAT	5.8	7.9	1.6	6.3	11.1	3.6	8.3
SACSMA_T0P-20S0E0I0	DP-OAT	3.2	3.2	1.1	3.6	3.2	2.4	5.2
SACSMA_T0P-10S0E0I0	DP-OAT	1.6	3.2	0.5	2	3.2	0.8	1.6
SACSMA_T0P10S0E0I0	DP-OAT	2.8	2.4	1.1	2.4	1.6	1.2	6.7
SACSMA_T0P20S0E0I0	DP-OAT	4.6	4	2.1	6.3	1.6	1.2	9.1
SACSMA_T0P30S0E0I0	DP-OAT	6.6	5.6	2.1	7.9	7.9	1.2	14.3
SACSMA_T0P0S1E0I0	DI-S-OAT	1.8	1.6	1.1	2.4	3.2	1.6	1.6
SACSMA_T0P0S2E0I0	DI-S-OAT	0.9	1.6	0	0.4	3.2	0.8	1.2
SACSMA_T0P0S3E0I0	DI-S-OAT	1.3	1.6	0	1.2	1.6	0.8	2.8
SACSMA_T0P0S4E0I0	DI-S-OAT	1.5	1.6	0	2	1.6	1.2	2.4
SACSMA_T0P0S5E0I0	DI-S-OAT	1.7	1.6	0	2.4	1.6	1.6	2.4
SACSMA_T0P0S0E1I0	DI-E-OAT	0.7	0.8	0	0.4	0	0.4	2
SACSMA_T0P0S0E2I0	DI-E-OAT	1.6	2.4	1.1	1.6	3.2	1.2	1.6
SACSMA_T0P0S0E3I0	DI-E-OAT	2.2	3.2	2.1	2.4	3.2	1.2	2.4
SACSMA_T0P0S0E4I0	DI-E-OAT	2.2	4	2.1	2	4.8	1.2	2
SACSMA_T0P0S0E5I0	DI-E-OAT	3.1	4	2.1	2.8	9.5	1.6	3.6
SACSMA_T0P0S0E0I1	DI-I-OAT	1.2	2.4	0.5	0.8	3.2	0.8	1.6
SACSMA_T0P0S0E0I2	DI-I-OAT	1.7	3.2	1.1	1.6	4.8	1.2	1.2
SACSMA_T0P0S0E0I3	DI-I-OAT	1.1	2.4	0.5	0.8	1.6	0.4	1.6
SACSMA_T0P0S0E0I4	DI-I-OAT	3.4	2.4	1.1	1.6	3.2	3.2	7.5
SACSMA_T0P0S0E0I5	DI-I-OAT	4	5.6	1.1	3.6	1.6	2.8	7.5
SACSMA_T0P0S5E5I5	Extremes	4.8	6.3	2.6	2.8	7.9	2.4	9.1
SACSMA_T0P-30S0E0I0	Extremes	5.8	7.9	1.6	6.3	11.1	3.6	8.3
SACSMA_T0P-30S5E5I5	Extremes	8.9	15.9	1.1	7.5	15.9	5.6	14.3
SACSMA_T0P30S5E5I5	Extremes	9	11.9	2.6	8.7	15.9	2.4	17.5
SACSMA_T5P-30S0E0I0	Extremes	19.6	16.7	0.5	15.1	14.3	29	31.7
SACSMA_T5P0S5E5I5	Extremes	19.1	11.1	3.2	12.7	15.9	35.3	26.2
SACSMA_T5P-30S5E5I5	Extremes	24.6	24.6	3.2	14.3	15.9	39.3	38.5
SACSMA_T5P30S5E5I5	Extremes	21.3	16.7	4.2	13.9	33.3	38.5	23.4
SACSMA_T1.7P1.7I1.7	Mid-range	4.3	4	0.5	4.4	4.8	5.6	6
SACSMA_T1.7P1.7I3.4	Mid-range	6.7	5.6	2.1	4.4	11.1	8.7	9.9
SACSMA_T1.7P3.4I1.7	Mid-range	4.2	3.2	1.6	4	7.9	5.2	5.2
SACSMA_T1.7P3.4I3.4	Mid-range	6.3	5.6	1.6	3.6	12.7	8.3	9.5
SACSMA_T3.4P1.7I1.7	Mid-range	7.8	4.8	1.6	4.8	4.8	15.9	9.9
SACSMA_T3.4P1.7I3.4	Mid-range	10.6	7.1	2.1	6.7	11.1	19	13.9
SACSMA_T3.4P3.4I1.7	Mid-range	7.9	4.8	1.6	4	11.1	15.9	9.5
SACSMA_T3.4P3.4I3.4	Mid-range	9.2	6.3	1.6	4.8	14.3	16.7	11.9

Table A2-6. Functional flow metric values for each decision scaling scenario in the Merced River case study, averaged across the period of record (1950-2013). Table is split into two parts to improve readability.

		Fall Pulse			Wet Season Baseflow				Peak Flow
Model	Scenario type	Magnitude	Timing	Duration	Magnitude 10th percentile	Magnitude 50th percentile	Timing	Duration	Annual Peak Magnitude
SACSMA_CTR_T0P0S0E0I0	Control	12254.7	6.0	5.0	2130.8	4976.5	102.3	90.8	22062.3
SACSMA_OATT_T1P0S0E0I0	DT-OAT	13480.7	3.3	5.0	1904.7	4323.6	99.0	89.3	24516.2
SACSMA_OATT_T2P0S0E0I0	DT-OAT	10224.5	3.3	4.8	1566.6	3391.8	34.5	120.3	27184.3
SACSMA_OATT_T3P0S0E0I0	DT-OAT	11352.1	3.3	4.8	1759.6	4899.7	34.5	79.8	31060.9
SACSMA_OATT_T4P0S0E0I0	DT-OAT	15102.5	4.3	4.7	1685.9	5722.6	35.3	38.7	35712.3
SACSMA_OATT_T5P0S0E0I0	DT-OAT	16212.2	4.3	5.0	1786.4	6257.8	35.3	38.7	38170.4
SACSMA_OATP_T0P-10S0E0I0	DP-OAT	10930.2	4.8	5.2	1701.0	4309.3	105.4	84.0	17469.8
SACSMA_OATP_T0P-20S0E0I0	DP-OAT	8412.1	4.8	5.2	1653.4	4174.3	127.4	60.4	13614.2
SACSMA_OATP_T0P-30S0E0I0	DP-OAT	5164.1	4.0	4.3	1509.7	3559.4	128.7	59.0	9770.9
SACSMA_OATP_T0P10S0E0I0	DP-OAT	14805.0	6.0	4.8	2917.3	6130.8	112.3	83.8	26194.5
SACSMA_OATP_T0P20S0E0I0	DP-OAT	17426.9	6.0	4.8	3128.6	6473.5	112.3	84.0	30329.9
SACSMA_OATP_T0P30S0E0I0	DP-OAT	20047.0	6.0	4.8	3416.1	7710.6	112.8	88.5	34396.8
SACSMA_OATS_T0P0S1E0I0	DI-S-OAT	12193.3	6.0	5.0	2268.0	5273.9	106.8	86.3	21905.8
SACSMA_OATS_T0P0S2E0I0	DI-S-OAT	12259.1	6.0	5.0	2116.4	4963.8	102.3	90.8	22064.8
SACSMA_OATS_T0P0S3E0I0	DI-S-OAT	12306.2	6.0	4.8	2248.0	4841.4	103.5	89.8	22214.5
SACSMA_OATS_T0P0S4E0I0	DI-S-OAT	12336.2	6.0	4.5	2343.5	5131.6	111.0	84.5	22341.0
SACSMA_OATS_T0P0S5E0I0	DI-S-OAT	13567.8	4.8	5.0	1960.3	5446.7	114.8	81.8	21649.5
SACSMA_OATE_T0P0S0E1I0	DI-E-OAT	8998.4	4.8	4.4	2202.4	5046.5	108.0	84.0	18330.7
SACSMA_OATE_T0P0S0E2I0	DI-E-OAT	12382.6	6.0	5.0	2133.7	4974.4	102.3	90.8	22335.4
SACSMA_OATE_T0P0S0E3I0	DI-E-OAT	14278.0	3.3	6.0	1698.1	4366.9	99.3	92.5	26219.1
SACSMA_OATE_T0P0S0E4I0	DI-E-OAT	16292.4	3.3	5.3	1682.5	4307.9	99.3	92.3	30233.1
SACSMA_OATE_T0P0S0E5I0	DI-E-OAT	18354.9	3.3	5.3	1692.5	4305.8	99.5	94.5	34305.0
SACSMA_OATI_T0P0S0E0I1	DI-I-OAT	11860.8	3.3	5.8	1644.5	4234.2	99.3	92.0	21108.1
SACSMA_OATI_T0P0S0E0I2	DI-I-OAT	12126.3	6.0	5.0	2116.6	4942.1	102.3	90.8	21804.4
SACSMA_OATI_T0P0S0E0I3	DI-I-OAT	12822.7	6.0	5.0	2420.9	5419.8	110.8	82.5	23336.6
SACSMA_OATI_T0P0S0E0I4	DI-I-OAT	11606.7	4.8	4.4	2549.6	5821.5	115.0	80.2	24287.2
SACSMA_OATI_T0P0S0E0I5	DI-I-OAT	12149.6	4.8	4.4	2959.1	6449.4	119.0	78.4	25844.4
SACSMA_EXT_T0P-30S5E5I5	Extremes	11030.2	4.8	5.0	1291.3	3337.4	112.6	77.6	19887.2
SACSMA_EXT_T0P30S5E5I5	Extremes	32012.0	6.3	5.3	2763.2	6749.4	92.8	116.8	61455.7
SACSMA_EXT_T0P0S5E5I5	Extremes	20598.6	6.3	5.3	1981.7	4629.0	89.5	109.3	41146.0
SACSMA_EXT_T5P-30S0E0I0	Extremes	6066.6	3.3	4.5	990.2	2879.0	34.5	45.8	18578.9
SACSMA_EXT_T5P-30S5E5I5	Extremes	13406.2	4.3	5.3	967.6	3554.6	33.7	26.3	39173.8
SACSMA_EXT_T5P0S5E5I5	Extremes	8344.5	3.5	5.5	1479.8	6551.6	36.0	29.0	78176.9
SACSMA_EXT_T5P30S5E5I5	Extremes	14374.3	3.5	5.5	2328.1	10498.1	39.0	26.0	114045.7
SACSMA_MID_T1.7P1.7I1.7	Mid-range	12758.9	3.3	5.3	1175.6	2401.2	29.8	151.3	23890.3
SACSMA_MID_T1.7P1.7I3.4	Mid-range	14014.9	4.3	4.3	1290.1	4607.7	35.3	58.3	35707.6
SACSMA_MID_T1.7P3.4I1.7	Mid-range	15780.5	4.3	4.3	1690.6	5676.6	35.3	60.7	36250.7
SACSMA_MID_T1.7P3.4I3.4	Mid-range	20400.8	4.3	4.3	1799.4	6516.1	35.3	60.0	49835.6
SACSMA_MID_T3.4P1.7I1.7	Mid-range	12577.2	4.3	4.7	1469.2	4572.0	35.0	57.7	30737.2
SACSMA_MID_T3.4P1.7I3.4	Mid-range	16642.0	4.3	4.7	1241.7	6378.4	35.3	24.3	43049.5
SACSMA_MID_T3.4P3.4I1.7	Mid-range	18635.3	4.3	5.0	1872.1	7071.4	35.3	38.3	43343.3
SACSMA_MID_T3.4P3.4I3.4	Mid-range	23986.1	4.3	5.0	1770.0	8962.7	35.3	24.3	59507.4

		Spring Recession				Dry Season				Annual Metrics	
Model	Scenario type	Magnitude	Timing	Duration	Recession rate of change	Magnitude 50th percentile	Magnitude 90th percentile	Timing	Duration	Average annual flow	Coefficient of variation
SACSMA_CTR_T0P0S0E0I0	Control	10601.5	193.0	62.0	0.0325	270.1	1258.5	255.0	159.8	2842.2	1.3
SACSMA_OATT_T1P0S0E0I0	DT-OAT	7469.7	188.3	57.8	0.0314	309.0	1413.4	246.0	166.5	2429.8	1.4
SACSMA_OATT_T2P0S0E0I0	DT-OAT	9488.2	154.8	83.3	0.0341	325.8	1304.9	238.0	140.3	2702.0	1.4
SACSMA_OATT_T3P0S0E0I0	DT-OAT	11466.0	114.3	114.5	0.0351	333.5	1256.8	228.8	151.0	2680.0	1.5
SACSMA_OATT_T4P0S0E0I0	DT-OAT	15963.9	74.0	144.0	0.0365	83.9	375.7	218.0	164.0	2568.6	1.8
SACSMA_OATT_T5P0S0E0I0	DT-OAT	16982.8	74.0	70.0	0.0340	152.7	1477.1	144.0	237.7	2532.5	2.0
SACSMA_OATP_T0P-10S0E0I0	DP-OAT	8642.6	189.4	64.6	0.0325	348.6	1482.8	254.0	180.0	2241.8	1.3
SACSMA_OATP_T0P-20S0E0I0	DP-OAT	7592.6	187.8	64.8	0.0318	286.8	1107.3	252.6	181.2	1848.2	1.3
SACSMA_OATP_T0P-30S0E0I0	DP-OAT	6073.0	187.7	62.5	0.0320	193.3	753.1	250.2	166.5	1483.3	1.2
SACSMA_OATP_T0P10S0E0I0	DP-OAT	11776.2	196.0	59.5	0.0325	318.3	1457.5	255.5	155.8	3273.3	1.3
SACSMA_OATP_T0P20S0E0I0	DP-OAT	12662.2	196.3	60.5	0.0351	362.0	1736.4	256.8	156.5	3704.0	1.3
SACSMA_OATP_T0P30S0E0I0	DP-OAT	13374.7	201.3	57.3	0.0348	413.1	2020.2	258.5	155.0	4135.2	1.3
SACSMA_OATS_T0P0S1E0I0	DI-S-OAT	10434.0	193.0	61.3	0.0330	278.9	1204.0	254.3	158.0	2848.2	1.2
SACSMA_OATS_T0P0S2E0I0	DI-S-OAT	10610.3	193.0	62.0	0.0326	270.6	1262.0	255.0	159.8	2841.6	1.3
SACSMA_OATS_T0P0S3E0I0	DI-S-OAT	10753.6	193.3	62.3	0.0323	272.8	1247.7	255.5	158.3	2838.9	1.3
SACSMA_OATS_T0P0S4E0I0	DI-S-OAT	10892.9	195.5	61.3	0.0312	277.2	1282.4	256.8	157.0	2840.8	1.3
SACSMA_OATS_T0P0S5E0I0	DI-S-OAT	10080.7	196.6	60.4	0.0306	470.0	1881.4	257.0	176.4	2647.3	1.3
SACSMA_OATE_T0P0S0E1I0	DI-E-OAT	10097.5	192.0	61.0	0.0345	405.1	1890.2	253.0	154.6	2866.0	1.1
SACSMA_OATE_T0P0S0E2I0	DI-E-OAT	10606.0	193.0	61.8	0.0327	270.5	1260.6	254.8	160.0	2844.6	1.3
SACSMA_OATE_T0P0S0E3I0	DI-E-OAT	8961.7	191.8	61.5	0.0327	338.2	1421.3	253.3	163.0	2497.5	1.4
SACSMA_OATE_T0P0S0E4I0	DI-E-OAT	8986.4	191.5	60.5	0.0330	313.7	1404.0	252.0	164.3	2528.6	1.5
SACSMA_OATE_T0P0S0E5I0	DI-E-OAT	8645.4	194.0	56.8	0.0325	143.6	507.4	250.8	130.0	2558.9	1.5
SACSMA_OATI_T0P0S0E0I1	DI-I-OAT	8674.0	191.3	64.0	0.0320	361.6	1389.1	255.3	161.0	2385.5	1.3
SACSMA_OATI_T0P0S0E0I2	DI-I-OAT	10501.0	193.0	62.0	0.0317	267.3	1243.9	255.0	159.8	2816.3	1.3
SACSMA_OATI_T0P0S0E0I3	DI-I-OAT	11011.4	193.3	62.0	0.0327	291.4	1430.2	255.3	157.0	2963.9	1.3
SACSMA_OATI_T0P0S0E0I4	DI-I-OAT	10888.8	195.2	58.6	0.0374	509.2	2527.8	253.8	150.6	3255.2	1.2
SACSMA_OATI_T0P0S0E0I5	DI-I-OAT	11153.3	197.4	57.0	0.0364	565.3	2897.4	254.4	151.6	3438.9	1.2
SACSMA_EXT_T0P-30S5E5I5	Extremes	7227.4	190.2	63.6	0.0310	179.9	822.9	253.8	170.0	1775.4	1.5
SACSMA_EXT_T0P30S5E5I5	Extremes	14127.9	209.5	53.8	0.0422	533.8	2656.5	263.3	149.0	4798.5	1.5
SACSMA_EXT_T0P0S5E5I5	Extremes	11741.9	198.8	58.3	0.0340	352.0	1747.8	257.0	156.3	3358.4	1.5
SACSMA_EXT_T5P-30S0E0I0	Extremes	10764.2	80.3	80.0	0.0342	117.8	1044.8	160.3	219.5	1374.7	1.7
SACSMA_EXT_T5P-30S5E5I5	Extremes	16499.6	60.0	107.7	0.0311	81.9	746.9	167.7	209.7	1698.8	2.5
SACSMA_EXT_T5P0S5E5I5	Extremes	46252.0	65.0	86.0	0.0298	288.6	1852.3	151.0	232.5	3296.8	2.5
SACSMA_EXT_T5P30S5E5I5	Extremes	67558.2	65.0	89.0	0.0308	498.9	2595.8	154.0	229.5	4844.6	2.6
SACSMA_MID_T1.7P1.7I1.7	Mid-range	6485.5	181.0	57.5	0.0328	221.5	1175.5	238.5	173.5	2059.5	1.5
SACSMA_MID_T1.7P1.7I3.4	Mid-range	14248.6	93.7	144.3	0.0324	116.8	458.2	238.0	142.0	2499.5	1.7
SACSMA_MID_T1.7P3.4I1.7	Mid-range	14673.5	96.0	145.7	0.0350	133.7	514.7	241.7	140.0	3068.6	1.5
SACSMA_MID_T1.7P3.4I3.4	Mid-range	24036.4	95.3	145.0	0.0372	177.3	596.9	240.3	141.0	3387.6	1.7
SACSMA_MID_T3.4P1.7I1.7	Mid-range	11606.9	92.7	130.0	0.0361	81.4	352.1	222.7	159.0	2199.7	1.7
SACSMA_MID_T3.4P1.7I3.4	Mid-range	18843.7	59.7	162.0	0.0395	101.5	404.6	221.7	160.0	2463.6	2.0
SACSMA_MID_T3.4P3.4I1.7	Mid-range	19985.0	73.7	151.7	0.0366	120.9	456.8	225.3	156.3	3025.8	1.8
SACSMA_MID_T3.4P3.4I3.4	Mid-range	31660.5	59.7	165.3	0.0389	131.7	522.3	225.0	156.7	3361.1	2.0

Appendix 3

Supplementary Materials for:

Dendrochronology reveals the response of a riparian forest to water management policies in an arid basin

Noelle K. Patterson[1], Samuel Sandoval-Solis[1], Belize A. Lane[2], Xiaoli Dong[3], Adam Z. Csank[4]

[1]Department of Land, Air and Water Resources, University of California, Davis, CA, USA

[2]Department of Civil and Environmental Engineering, Utah State University, Logan, UT, USA

[3]Department of Environmental Science and Policy, University of California, Davis, CA, USA

[4]University of Nevada, Department of Geography, 1664 N. Virginia St., Reno, NV 89557, USA

1. Regime shift analysis on functional flow metrics

Table A3-1. Regime shift analysis results for functional flow metrics of streamflow above and below Derby Dam. The year of the greatest shift is reported, along with the magnitude and percent change in each metric.

		Downstream flow			Upstream flow		
Metric	**Units**	**Years**	**Percent Difference**	**Magnitude of difference**	**Years**	**Percent Difference**	**Magnitude of difference**
Fall pulse flow magnitude	cms	1952	317.7	374.2	1985	7.0	79.4
Fall pulse flow timing	timing (date)	1954	16.6	3.0	1978	25.3	7.7
Wet season baseflow median magnitude	cms	1959	31.3	234.8	1988	-9.2	-114.7
Wet season baseflow timing	timing (date)	1960	-22.9	-27.0	1986	16.0	14.1
Wet season baseflow duration	days	1957	29.9	31.3	1985	-9.7	-12.9
Peak magnitude	cms	1988	-3.9	-124.5	1988	-17.5	-705.8
Spring recession magnitude	cms	1988	-3.9	-78.1	1988	-16.6	-439.7
Spring recession timing	timing (date)	1989	5.8	12.9	1989	1.4	2.9
Spring recession duration	days	1966	13.4	13.4	1964	46.0	26.6
Spring recession rate of change	percent	1959	-59.9	-0.109	1961	-23.8	-0.022
Dry season median magnitude	cms	1972	726.5	132.2	1988	-14.0	-43.4
Dry season magnitude (90th percentile)	cms	1974	306.6	208.3	1987	-17.9	-91.6
Dry season timing	timing (date)	1949	11.4	21.4	1989	4.7	19.9
Dry season duration	days	1955	-27.8	-50.3	1985	2.0	-20.0
Average annual flow	cms	1970	76.6	240.8	1988	-10.0	-78.8
Coefficient of variation	percent	1965	-45.0	-0.883	1961	-10.2	-0.080

2. Water Surface Level Plots

Water surface level plots represent periodic surface water level monitoring that was performed at each field site 2020 – 2021. The purpose of these measurements was to develop a partial flow-rating curve, relating surface water level changes at the field sites to the surface water levels recorded at the nearest USGS gage site. These rating curves were used to ensure that water level measured at long-term gaging stations would be a reasonable representation of

conditions at each study site. They also revealed the differences in water surface – flow relationships among field sites.

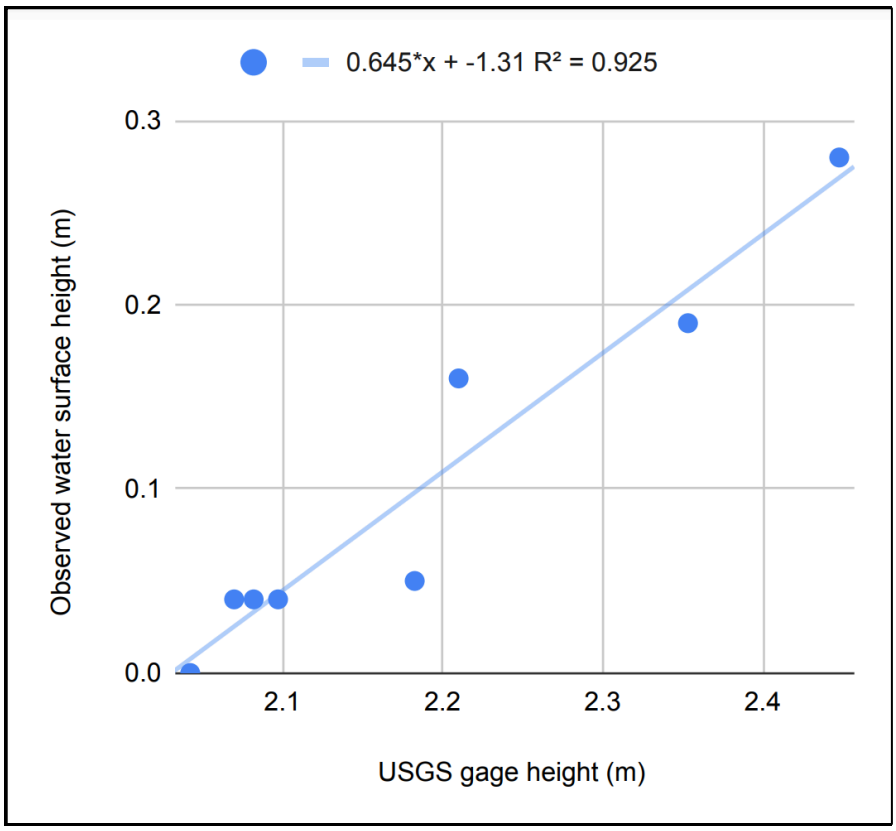

Figure A3-1. Water surface level rating curve between field site US-1 and USGS gage #10350000. Observed water surface height is reported as heights above the lowest recorded level.

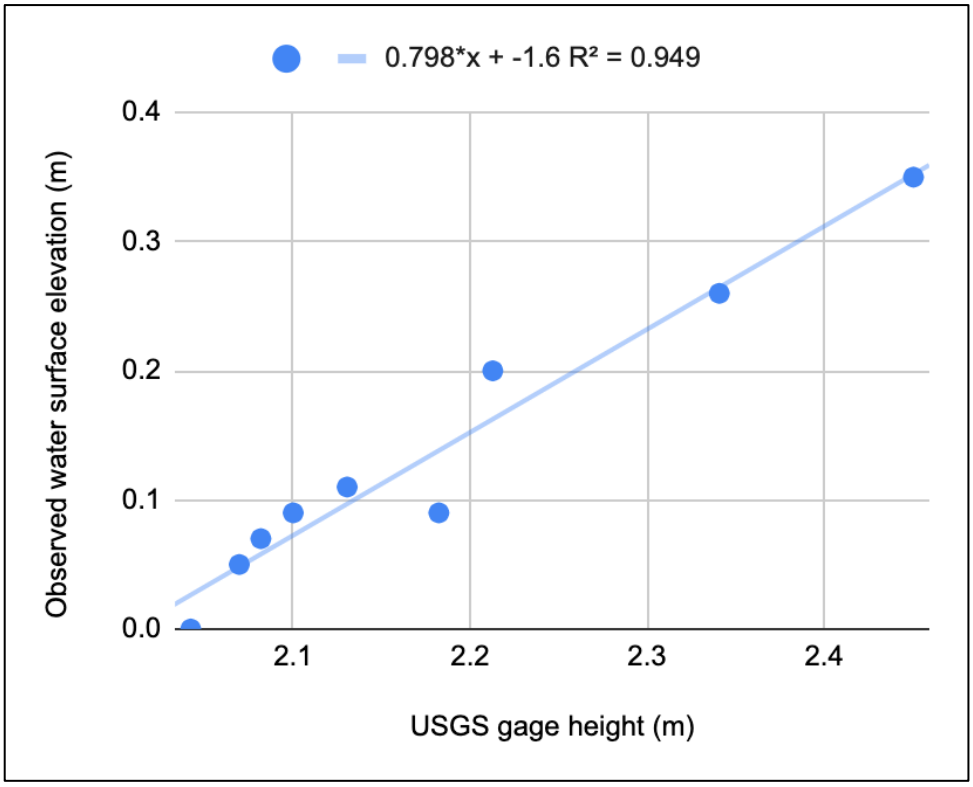

Figure A3-2. Water surface level rating curve between field site US-2 and USGS gage #10350000. Observed water surface height is reported as heights above the lowest recorded level.

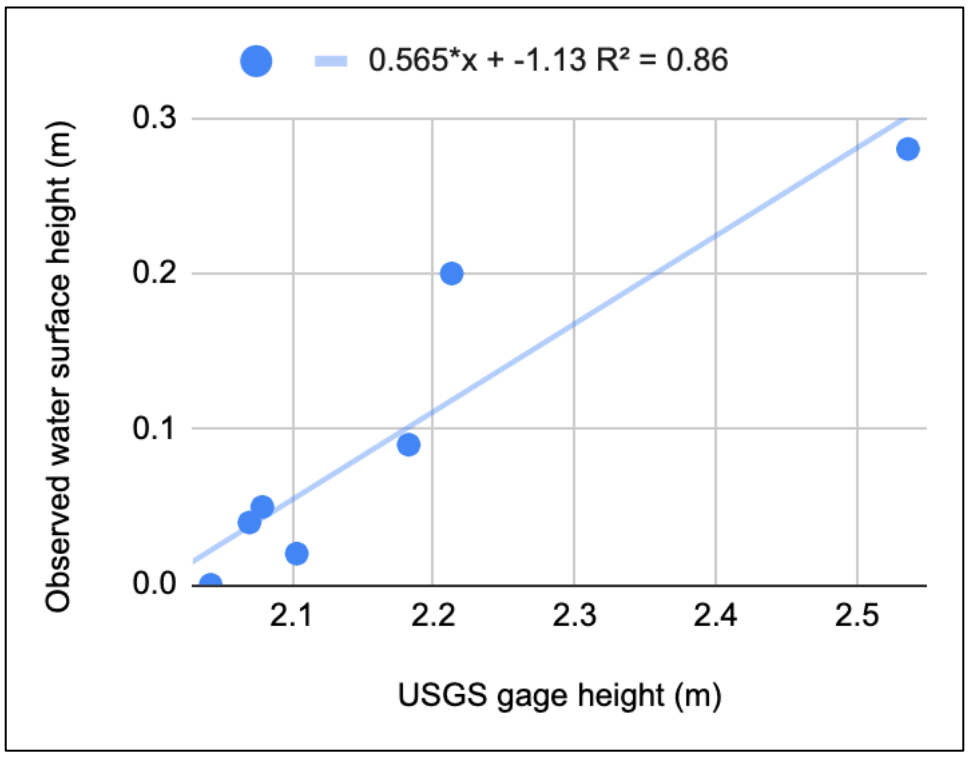

Figure A3-4. Water surface level rating curve between field site US-3 and USGS gage #10350000. Observed water surface height is reported as heights above the lowest recorded level.

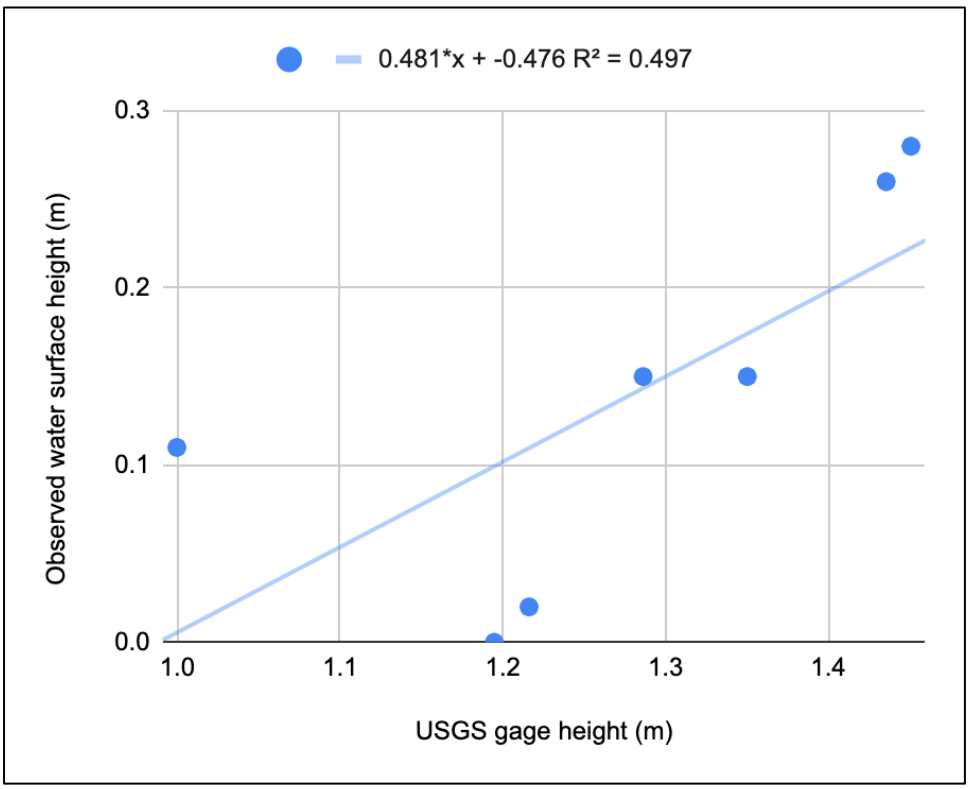

Figure A3-5. Water surface level rating curve between field site DS-1 and USGS gage #10350000. Observed water surface height is reported as heights above the lowest recorded level.

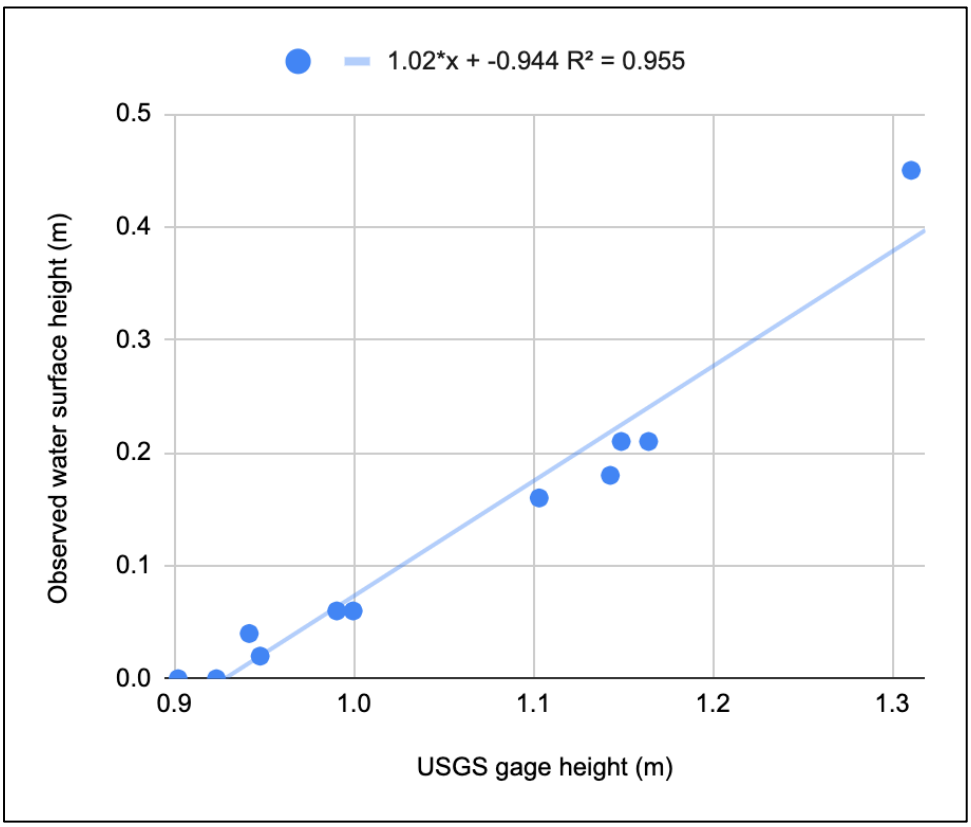

Figure A3-6. Water surface level rating curve between field site DS-2 and USGS gage #10350000. Observed water surface height is reported as heights above the lowest recorded level.

3. Shallow Groundwater Monitoring Plots

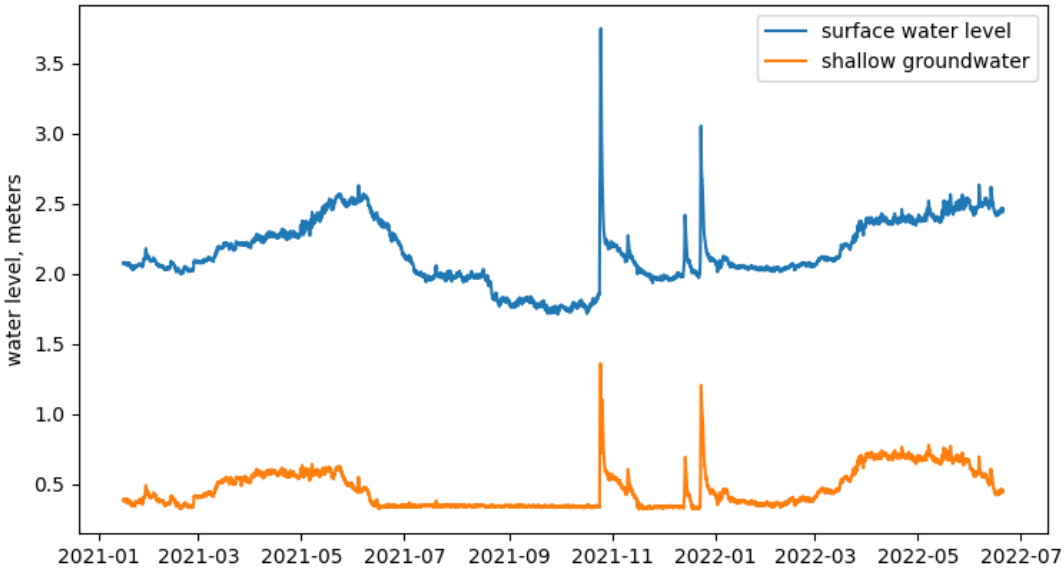

Figure A3-7. Shallow groundwater at Site US-2 reported at hourly intervals, along with hourly surface water from the nearest USGS gage on the Truckee River at Tracy (# 10350340). The y-axis scale is relative and adjusted to allow comparison between the two data sources. Note the flat-line period in the shallow groundwater plot between 06/2021 – 10/2021 is due to groundwater falling below the sensor depth.

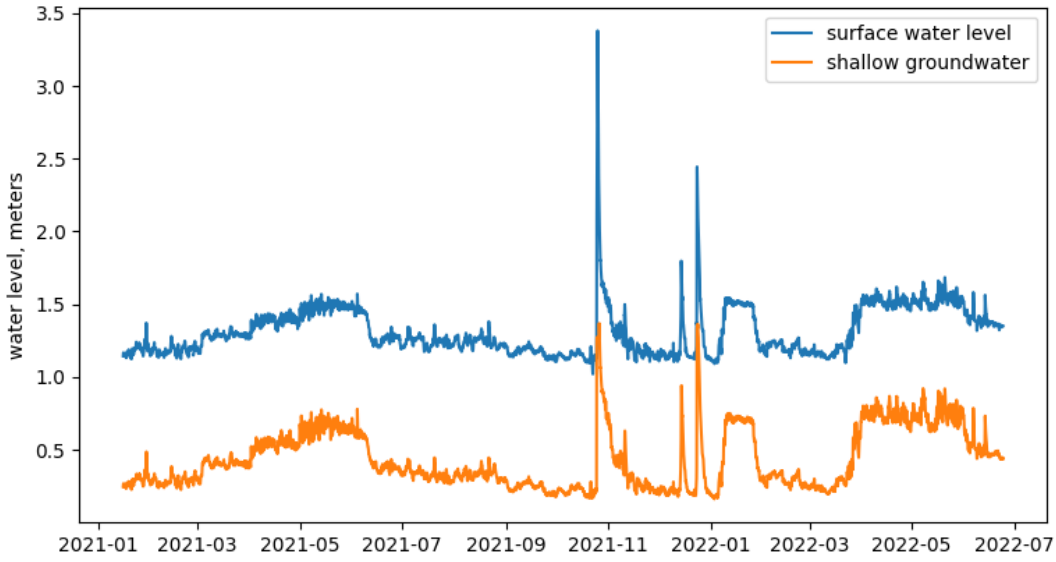

Figure A3-8. Shallow groundwater at Site DS-1 reported at hourly intervals, along with hourly surface water from the nearest USGS gage on the Truckee River at Wadsworth (# 10351650). The y-axis scale is relative and adjusted to allow comparison between the two data sources.

4. Tukey's HSD results for all trees

Table A3-2. Tukey's Honestly Significant Difference (HSD) outcomes for all trees with records beginning at or before 1967 for upstream trees and 1958 for downstream trees. A score of TRUE indicates significance between groups (growth before or after 1973 (1983) for downstream (upstream) trees at a $p<0.05$ level. The average change in growth between groups is also presented, for individual trees and as a group average.

Site	Tree ID	Tukey HSD 1973	Mean change BAI 1973 (mm2)	Percent change 1973	Tukey HSD 1982	Mean change BAI 1982 (mm2)	Percent change 1982
US-1	11				TRUE	-6278	-48
US-1	13				TRUE	4831	94
US-1	16				FALSE	1204	20
US-1	23				TRUE	1693	308
US-1	4				FALSE	2662	25
US-1	6				TRUE	4277	286
US-1	7				TRUE	3461	149
US-3	1				TRUE	2741	83
US-3	13				TRUE	3046	63
US-3	15				FALSE	-152	-8
US-3	16				FALSE	-734	-6
US-3	17				TRUE	1244	46
US-3	2				TRUE	11492	227
US-3	20				FALSE	-462	-16
US-3	6				FALSE	-926	-16

US-3	7				TRUE	-2091	-37
US total						1626	73
DS-1	11	TRUE	2285	35			
DS-1	18	TRUE	2414	65			
DS-1	5	TRUE	4099	123			
DS-2	13	TRUE	4961	372			
DS-2	14	FALSE	848	15			
DS-2	15	FALSE	-962	-10			
DS-2	16	TRUE	704	70			
DS-2	17	TRUE	-1129	-17			
DS-2	18	TRUE	1609	74			
DS-2	19	FALSE	1050	12			
DS-2	20	TRUE	1575	34			
DS-2	5	TRUE	5672	170			
DS-2	6	TRUE	10103	445			
DS-2	7	TRUE	8639	391			
DS total			2991	127			

5. Bayesian Statistical Modeling

Table A3-3. Primary and alternate versions of the Bayesian statistical model using different combinations of parameters are presented and implemented as a sensitivity analysis.

		Model									
Functional flow component	parameter	All parameters	Growing season precipitation	Spring recession	Dry season baseflow	Wet season baseflow	Peak flow	Fall pulse	No VPD	No temperature	Average flow
Annual	Average annual flow	X	X						X	X	X
	Coefficient of variation	X	X	X	X	X		X			
Fall Pulse Flow	Magnitude	X	X					X			
	Timing	X	X					X			
Wet Season Baseflow	Duration	X	X			X					
	Start timing	X	X			X					
	Median magnitude					X					
Peak flow	Magnitude	X	X				X				
Spring Recession Flow	Peak magnitude	X	X	X							
	Rate of Change	X	X	X							
	Timing	X	X	X							
Dry Season Baseflow	Duration	X	X		X						
	Median magnitude	X	X		X						
	Magnitude (90th)	X	X		X						
	Start timing	X	X		X						
Climate	Annual mean temperature	X	X	X	X	X		X	X		X
	Annual max vapor pressure deficit	X	X	X	X	X		X		X	X
	Annual precipitation	X		X	X	X		X	X	X	X
	Growing season precipitation		X								

Table A3-4. Widely Applicable Information Criterion (WAIC) scores for the primary Bayesian model and all alternate models. A lower WAIC score indicates a better predictive performance of the model, balanced against the number of model parameters. The SE columns represents standard error. Since the primary model has the lowest WAIC score, it is considered the best performing model.

Model	**WAIC**	**SE**
All parameters (primary model)	6689	3.76
All parameters (growing season precipitation)	6733	3.79
Spring reccesion	7410	3.81
Dry season baseflow	7227	3.78
Wet season baseflow	7243	3.80
Peak flow	7656	3.71
Fall pulse	7653	3.65
No VPD	7654	3.79
No temperature	7664	3.81
Average flow	7607	3.80